NASA TECHNICAL NOTE

FAN AND WING FORCE DATA FROM WIND-TUNNEL INVESTIGATION OF A 0.38-METER (15-IN.) DIAMETER VTOL MODEL LIFT FAN INSTALLED IN A TWO-DIMENSIONAL WING

by Joseph A. Yuska and James H. Diedrich

Lewis Research Center
Cleveland, Ohio 44135

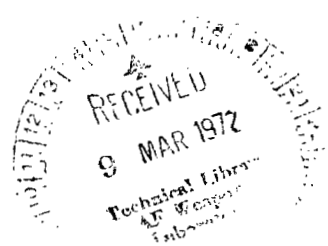

NATIONAL AERONAUTICS AND SPACE ADMINISTRATION • WASHINGTON, D. C. • MARCH 1972

1. Report No. NASA TN D-6654	2. Government Accession No.
3. Recipien.	
4 Title and Subtitle FAN AND WING FORCE DATA FROM WIND-TUNNEL INVESTIGATION OF A 0.38-METER (15-IN.) DIAMETER VTOL MODEL LIFT FAN INSTALLED IN A TWO-DIMENSIONAL WING	5. Report Date March 1972
	6. Performing Organization Code
7. Author(s) Joseph A. Yuska and James H. Diedrich	8. Performing Organization Report No. E-6607
	10. Work Unit No. 764-72
9. Performing Organization Name and Address Lewis Research Center National Aeronautics and Space Administration Cleveland, Ohio 44135	11. Contract or Grant No.
	13. Type of Report and Period Covered Technical Note
12. Sponsoring Agency Name and Address National Aeronautics and Space Administration Washington, D. C. 20546	14. Sponsoring Agency Code
15. Supplementary Notes	

16. Abstract

Test data are presented for a 38-cm (15-in.) diameter, 1.28-pressure-ratio model VTOL lift fan installed in a two-dimensional wing and tested in a 2.74- by 4.58-meter (9- by 15-ft)V/STOL wind tunnel. Tests were run with and without exit louvers over a wide range of crossflow velocities and wing angle of attack. Tests were also performed with annular-inlet vanes, inlet bellmouth surface discontinuities, and fences to induce fan windmilling. The report presents data on the axial force of the fan assembly and overall wing forces and moments as measured on force balances for various static and crossflow test conditions. Midspan wing surface pressure coefficient data are also presented.

17. Key Words (Suggested by Author(s)) Vtol Propulsion Lift fan-in-wing Wind tunnel	18. Distribution Statement Unclassified - unlimited		
19. Security Classif. (of this report) Unclassified	20. Security Classif. (of this page) Unclassified	21. No. of Pages 101	22. Price* $3.00

* For sale by the National Technical Information Service, Springfield, Virginia 22151

FAN AND WING FORCE DATA FROM WIND-TUNNEL INVESTIGATION OF A 0.38-METER (15-IN.) DIAMETER VTOL MODEL LIFT FAN INSTALLED IN A TWO-DIMENSIONAL WING

by Joseph A. Yuska and James H. Diedrich

Lewis Research Center

SUMMARY

This report presents fan-assembly and wing-force data obtained from static and crossflow tests of a 38-centimeter (15-in.) diameter lift fan installed in a two-dimensional wing in a 2.74- by 4.58-meter (9- by 15-ft) V/STOL wind tunnel. The basic objective of the investigation was to determine lift fan behavior in the crossflow environment and to define the principal factors affecting fan performance. The fan stage was designed for a pressure ratio of 1.28 at a corrected tip speed of 299 meters per second (980 ft/sec). A compact, two-stage, air-driven turbine contained within the hub section of the fan powered the lift fan. With this arrangement, the turbine and fan exhaust flows were coaxial. Tests were run with and without exit louvers over a wide range of tunnel air speeds (crossflow velocities) from 21 to 73 m/sec (70 to 240 ft/sec) and a wing angle of attack of $\pm 15^{\circ}$. Other tests were conducted with annular inlet vanes, discontinuities on the surface of the inlet bellmouth, and fences to induce fan windmilling.

The data presented include fan-assembly axial force and wing overall forces and moments as measured on separate force balances, and wing-surface pressure coefficients at midspan. The results indicated that, over the range of crossflow velocities tested, the axial force of the fan assembly with louvers on or off remained at roughly the same level at design rotational speed; and increased slightly at 70 percent of design speed. The annular inlet vanes and the bellmouth surface discontinuities had little effect on fan static and crossflow force variation. Positive windmill rotation of 2.5 percent of design speed was obtained with a startup fence installed at the rear of the fan inlet.

INTRODUCTION

Design studies have indicated the feasibility of vertical-takeoff-and-landing (VTOL)

civilian transport aircraft using lift-fan propulsion systems (e.g., refs. 1 to 4). Experimental investigations have demonstrated the feasibility of lift-fan performance (e.g., refs. 5 to 8). However, the design of economically viable VTOL transport aircraft will require advanced lift-fan system technology. Considerable research and development is therefore indicated in the areas of engine component design, lift-fan design, system integration, and lift-fan transition performance (refs. 9 and 10).

One of the major requirements for VTOL transport aircraft design is detailed data on the performance of advanced-concept lift fans in the transition speed range from vertical to normal wing-supported flight. Crossflow inlet distortion encountered during transition has an adverse affect on lift-fan performance and noise generation. There is also the interference effect of the interaction of the fan flow and external airflow.

The NASA Lewis Research Center recently embarked on a research program to generate detailed design and performance data on advanced lift-fan concepts. An initial experimental test project measured the detailed crossflow performance of a 38-centimeter (15-in.) diameter model lift fan installed in a two-dimensional wing. The fan-in-wing model tests were conducted in a 2.74- by 4.58-meter (9- by 15-ft)V/STOL wind tunnel (ref. 11).

The fan design pressure ratio was 1.28 at a corrected tip speed of 299 meters per second (980 ft/sec). A compact two-stage air-driven turbine contained within the hub section of the fan powered the model lift fan. High-pressure air was supplied to the drive turbine through six struts spanning the fan passage. With this arrangement, the turbine and fan exhaust flows were coaxial.

A wing load cell balance measured the lift, drag, and pitching moment of the combined fan-in-wing model. A separate load cell balance contained within the wing measured only the fan axial force. Pressure and temperature instrumentation installed in the fan passage provided measurements of fan performance and detailed data on the internal flow distributions.

The test conditions covered the transition speed range from 21 to 73 meters per second (70 to 240 ft/sec). The model lift fan was operated over a speed range from 70 to 110 percent of design rotational speed. The wing angle of attack was varied $\pm 15^{\circ}$. Flow deflecting louvers were installed at the fan exit, and louver position was varied from 3° forward deflection to 40° aft deflection.

This report presents the measured fan axial force data obtained from static and crossflow tests of the described fan-in-wing installation with and without flow deflecting louvers at the fan exit, as well as the overall aerodynamic characteristics of the fan-in-wing configuration with power on and power off. The aerodynamic characteristics of the basic wing configuration, including midspan surface pressure coefficient data, are also included. To obtain an indication of fan flow-induced forces, the wing and fan force components are discussed. Investigations of fan windmill characteristics, and the effect of annular inlet vanes and inlet surface discontinuities on fan axial force are included.

SYMBOLS

A	fan frontal area, 0.117 m^2 (1.263 ft^2)
c	wing chord, m (ft)
C_D	drag coefficient, D/qS
C_L	lift coefficient, L/qS
C_M	pitching-moment coefficient about the wing quarter chord, M/qSc
C_p	wing surface pressure coefficient, $(p_s - p)/q$
D	drag, N (lbf)
F	axial force, N (lbf)
F/δA	axial force loading, N/m^2 (lbf/ft^2)
F_D	component of axial force in drag direction, N (lbf)
F_L	component of axial force in lift direction, N (lbf)
L	lift, N (lbf)
M	pitching moment about the wing quarter chord, m-N (ft-lbf)
N	angular velocity, radians/sec (rpm)
$N/\sqrt{\theta}$	corrected angular velocity, radians/sec (rpm)
p	free-stream dynamic pressure, N/m^2 (lbf/ft^2)
p_s	wing surface static pressure, N/m^2 (lbf/ft^2)
q	free-stream dynamic pressure, N/m^2 (lbf/ft^2)
R	resultant force, $(L^2 + D^2)^{1/2}$, N (lbf)
S	wing planform area, m^2 (ft^2)
T	free-stream total temperature, K (^oR)
U_T	fan tip speed, m/sec (ft/sec)
$U_T/\sqrt{\theta}$	corrected fan tip speed, m/sec (ft/sec)
V	crossflow velocity, m/sec (ft/sec)
X,Y	inlet vane mean line coordinates, cm (in.)
x	distance along airfoil chord from leading-edge, m (ft)
x/c	chord ratio
y	airfoil ordinate, m (ft)

α	wing angle of attack, deg
β_L	exit louver position, deg
δ	ratio of inlet total pressure to standard sea-level pressure of 1.01325×10^5 N/m^2 (2116.22 lb/ft^2)
θ	ratio of inlet total temperature to standard sea-level temperature of 288.2 K (518.7° R)
φ	resultant force angle, $\tan^{-1}$ (D/L), deg

MODEL AND APPARATUS

Wing and Wing Balance

A photograph of the fan-in-wing model installed in the 2.74-by 4.58-meter (9- by 15-ft) V/STOL test section is shown in figure 1. The wing spanned the 2.7-meter (9-ft) height of the test section and had a 1.4-meter (4.5-ft) chord. The wing has a constant airfoil section along the span except in the fan area. The lower surface of the wing around the fan exit was modified by a fairing that covered the fan exit instrumentation. The fairing increased the local wing thickness ratio from 17 to 17.7 percent. Dimensions including the fairing and coordinates for the modified NACA 65_3 A(218)-217 airfoil section are shown in figure 2. Twenty-four static pressure taps were placed along the wing chord at mid-span as shown in figure 2.

The wing was constructed entirely of steel. The wing surfaces were formed from 0.318-centimeter (0.125-in.) thick steel plates attached with screws to the load-carrying members. The screw heads were flush or below the surface. Joints between surface plates were flush and smooth with a 0.076-centimeter (0.030-in.) maximum gap between joints. The wing surface tolerance was ±0.038 centimeter (0.015 in.) from the true surface, and the surface waviness was not more than 0.003 unit per unit of surface length.

The fan-in-wing model was attached to a wing balance that measures overall model lift, drag, and pitching moment. Figure 3 is a sketch of the wing balance showing pertinent dimensions. The model was suspended from the upper frame structure and balanced level and true vertical. One end of the load cell links was grounded to the tunnel structure and the active end was attached to the wing structure. Three load cell links were used to measure wing lift and moment, and two load cell links were used to measure wing drag. Supporting the balance from the tunnel produced fluctuating load cell readings caused by wing and tunnel vibrations. Electric filters were used to provide a steady mean value of the load cell output. With the load cell ranges shown in figure 3, the load capacity of the balance is

Lift, N (lbf) . . . . . ±40 034 (±9000)
Drag, N (lbf) . . . . . ±4448 (±1000)
Moment, m-N (ft-lb) . . . . . ±6440 (±4750)

The wing angle of attack was remotely varied over a range of ±15°.

Fan and Drive Turbine Characteristics

The fan-in-wing installation is shown in figure 4. The fan thrust axis was located at the midspan of the wing at the position of maximum thickness (40 percent chord). The fan assembly shown in figure 4 was attached to a balance system within the wing. The fan balance consists of three 2224-newton (500-lbf) load cells equally spaced on a 57.2-centimeter (22.5-in.) diameter circle. The balance measured the combined axial force of the fan and turbine. Drive air was supplied from both sides of the wing. The fan balance was calibrated with the turbine drive air lines pressurized.

Figure 5 shows a cross section of the model lift fan. The fan rotor tip diameter was 38.6 centimeter (15.2 in.), and the stage exit diameter was 37.5 centimeters (14.78 in.). The diameter of the fan inlet bellmouth at the wing junction was 55.9 centimeters (22.0 in.). The fan inlet bellmouth was contoured flush with the wing upper surface. The fan hub protruded from the wing lower surface as shown in figure 5. The inlet and exit flow area of the fan stage were 0.092 square meter (0.990 ft^2) and 0.081 square meter (0.868 ft^2), respectively. The fan rotor had 35 blades which were made from 18 Nickel-200 maraging steel. Two 0.152-centimeter (0.060-in.) diameter damper wires located at 60 percent of the passage height from the hub provided sufficient damping to prevent blade flutter and reduce blade vibration. Six instrumentation rakes equally spaced circumferentially were located behind the rotor and at the duct exit. The fan passage area was adjusted to account for the local blockage presented by the instrumentation. The fan design characteristics are summarized in table I. For the fan design, the inlet total pressure was 1.0132×10^5 newtons per square meter (2116 lb/ft^2), the inlet total temperature was 300 K (540° R), and the exit static pressure was equal to the ambient static pressure.

The fan drive was a compact, two-stage supersonic turbine contained in the fan hub. The turbine was scaled from a previous NASA design reported in references 12 and 13. The turbine had a mean diameter of 13.7 centimeters (5.4 in.) and developed 511 kilowatts (685 hp) to drive the fan at design conditions. The turbine was driven by high-pressure air supplied through six equally spaced struts (12.5 percent thickness ratio) spanning the fan passage (fig. 5). The struts connected the inner and outer 360° plenums. With this arrangement, the fan and turbine exhaust flows were coaxial. The turbine design speed point corresponded to 105 percent of fan design speed. The drive turbine

design characteristics are summarized in table II. At fan design speed, the turbine thrust was 25 percent of the total axial force. For the drive turbine, corrections to standard conditions are based on turbine-inlet conditions.

For some tests, exit louvers were mounted on the wing as shown in figure 6. For this installation, the louver forces appeared only on the wing balance and not on the fan balance. The exit louvers covered both the fan and drive turbine exhaust. The exit louvers were capable of remotely vectoring the fan and drive turbine thrust from 3° forward (negative louver angle of attack) to 40° aft (positive louver angle of attack). Figure 7 is a sketch of the exit louvers including installation details and airfoil section coordinates.

TESTS

Procedures

The general test procedure was to first bring the tunnel up to speed and set the desired level of dynamic pressure in the test section. The tunnel was allowed to stabilize for several minutes while the desired values of wing angle of attack, fan speed, and louver position were established. The time to acquire data for a single test point was typically about 25 seconds. During the data acquisition period, test conditions were stabilized through the individual control systems for each of the preceding parameters. The fan speed generally fluctuated somewhat during the data acquisition time. Over the speed range, the variation was ±5.24 radians per second (±50 rpm) which was only a ±0.3 percent variation of the design speed.

Static performance tests on the model lift fan were generally performed with the fan axis parallel to the tunnel axis and the inlet of the fan facing upstream. This orientation was used to achieve the least distortion of flow at the fan inlet. The tunnel circuit was vented to the atmosphere during static testing to minimize recirculation of the fan exhaust.

Tests were performed at tunnel dynamic pressures ranging from 287 to 2870 newtons per square meter (6 to 60 lb/ft^2), at wing angles of attack between $\pm 15^{\circ}$, at louver positions from -3° to $+40^{\circ}$, and over the range of fan speeds from 70 to 110 percent design speed.

Data Accuracy and Repeatability

Table III lists the accuracy values obtained from calibration tests. Repeat tests with

essentially identical conditions also indicated that the data were repeatable within the same range of values.

The force data presented in this report were not corrected for tunnel wall interference because the tunnel walls were slotted to minimize wall interference effects (ref. 11).

RESULTS AND DISCUSSION

The results obtained from the tests are presented in four main sections. The first deals with the axial force characteristics of the fan assembly in static and crossflow conditions. The second section presents overall aerodynamic results, forces, and moments of the basic wing and the fan-in-wing configuration. The third section contains force comparisons between the fan and wing measurements. Additional investigations conducted with inlet vanes, inlet surface discontinuities and in-flight startup devices are discussed in the fourth section. The wing surface pressure coefficients are presented in the appendix.

Fan Characteristics

This section of the report presents the axial force data obtained from the fan balance measurements (fig. 4) for the fan-in-wing configuration with and without louvers. For the static tests of the louvers-off configuration, the fan balance measured a force that was around 5.5 percent less than the true thrust of the entire fan assembly. This difference was due to fan-generated lift forces that act on the upper wing surface not attached to the fan balance. For the louvers-on configuration, the louvers were not attached to the fan balance; hence, the balance measurement continued to be proportional to fan gross thrust (the thrust losses introduced by the louvers did not appear on the fan balance). Therefore, for both configurations, the fan balance axial force measurement was used as the measure of the thrust performance of the fan. Data are presented in terms of a force loading parameter defined as the axial force as measured on the fan balance corrected to standard conditions divided by the fan inlet area based on the rotor tip diameter (38.6 cm (15.2 in.)).

Static conditions. - Figure 8 shows the fan axial force loading with louvers off over a range of fan speeds from 70 to 110 percent of design speed. Tests were conducted with the fan axis both perpendicular and parallel to the tunnel axis. When the fan axis was parallel to the tunnel axis, the fan flow induced tunnel airflow velocities, which reached values as high as 11 meters per second (35 ft/sec). For this case, the axial

force data were corrected for the resulting ram drag force. Both values are very close, and a single curve can be faired through the data for both fan orientations.

Figure 9 presents the fan static axial-force loading with louvers on over the full range of louver positions. Single curves are faired through the data for the fan oriented parallel and perpendicular to the tunnel axis. The data indicate that for this fan design the louvers tend to increase gross thrust at tip speeds above 90 percent of design. It is suspected that the louvers increase the fan exit static pressure, thus changing the fan operating point, which results in the observed increase in fan gross thrust. A 30° louver position at fan design tip speed produced a fan axial-force loading corresponding to the combined fan and turbine design thrust loading of 40.6×10^3 newtons per square meter (848 lb/ft^2).

Figure 10 presents axial force loading as a function of fan speed over the full range of louver positions. This figure was obtained by cross-plotting the data of figure 9 and includes the louvers-off data for comparison.

Crossflow conditions. - The fan axial force loading at various crossflow velocities is presented in figures 11 and 12 for fan speeds of 70 and 100 percent of design tip speed and for three angles of attack (0° and $\pm 10^{\circ}$). Fan axial force loading is again used as the measure of fan gross thrust. However, the relation between axial force measurement and fan gross thrust is more complex for crossflow conditions than for static conditions because of the effects of wing circulation on the forces on the fan surfaces.

Figure 11 presents the louvers-off data. The data show that, at 100 percent of design speed, the axial-force loading tended to decrease slightly with increasing crossflow velocity but, at the highest crossflow velocity of 73 meters per second (240 ft/sec), the axial-force loading approached the same level as that obtained at zero crossflow conditions. At 70 percent of design speed, the axial-force loading increased uniformly with increasing crossflow velocity through the entire range tested. The data show that at both 100 and 70 percent of design speed, the axial-force loading increased as the angle of attack increased from -10° to $+10^{\circ}$. At a crossflow velocity of 73 meters per second (240 ft/sec), the increase due to angle of attack was around 12 to 15 percent.

The effect of exit louvers on axial force loading in crossflow is shown in figure 12 for three wing angles of attack. The data with the exit louvers on at small louver deflection angles showed essentially the same general trends with crossflow velocity as the data with the exit louvers off. Exit louver deflection had a greater effect on the magnitude of axial-force loading at 100 percent of design speed than at 70 percent of design speed at the three angles of attack tested.

Figure 13 shows the effect of exit louver deflection on axial-force loading at a crossflow velocity of 61 meters per second (200 ft/sec) and zero angle of attack. The same variation of axial-force loading shown in figure 13 was observed for static tests (fig. 9), which indicates that the effect of the louvers is similar for both static and crossflow conditions.

Overall Aerodynamic Characteristics

Basic wing configuration. - The basic wing configuration is the fan-in-wing with covers over the fan inlet and exit. This configuration was tested over the angle of attack range $\pm 15^{\circ}$ at various dynamic pressures ranging from 383 to 2870 newtons per square meter (8 to 60 lbf/ft^2). The aerodynamic characteristics of lift, drag, and pitching moment coefficient for the basic wing configuration are shown in figure 14. The basic wing configuration was tested with and without the exit louvers attached to the wing.

As indicated in figures 14(a) and (b), the louvers had a significant effect on the wing characteristics at negative angles of attack. Addition of the louvers decreased lift and increased drag. However, the nose-down pitching moment decreased essentially uniformly over the entire angle of attack range (fig. 14(c)).

Fan-in-wing configuration; power-off. - Power-off tests for the fan-in-wing configuration shown in figure 1 were also conducted with and without exit louvers. In figure 15, lift, drag, and pitching moment coefficient data are compared with the basic wing configuration. Installation of the fan in the basic wing decreased the lift (less C_L at positive α, and more C_L at negative α; fig. 15(a)), increased the drag (fig. 15(b)) and decreased the nose-down pitching moment (fig. 15(c)). The effect of exit louvers on lift, drag, and pitching moment was similar as that noted previously for the basic wing.

The effect of exit louvers on the wing aerodynamic characteristics can be considered similar to the effect of spoilers on the top surface of an airfoil, or dive brakes on the lower surface of an airfoil (ref. 14). Spoiler or dive brake devices affect the airfoil lift by changing the pressure loading (difference in upper- and lower-surface pressures) in front of the devices to reduce the airfoil lift and changes the airfoil pitching moment. Such devices also increase the flow separation downstream, which produces an increase in airfoil drag. This effect on drag was clearly evident in figures 14(b) and 15(b).

Examples of the effect of louvers on the local (midspan) pressure coefficient distribution in crossflow are shown in figures 16 to 18. The exit louvers had a greater effect on the wing pressure coefficient distribution at -10° angle of attack (fig. 16) than at $+10^{\circ}$ angle of attack (fig. 18). The greatest effect was observed on the wing louver surface over the forward 20 percent of the wing chord. This variation of the pressure coefficient with louver position explains the variation of lift and moment coefficients with exit louver position shown in figures 15(a) and (c).

Fan-in-wing configuration; power-on. - Power-on tests of the fan-in-wing configuration without exit louvers and with exit louvers were conducted at various fan tip speeds for static conditions and over the full range of tunnel dynamic pressure.

Static case: The effect of louver position on absolute magnitude of overall wing forces for static tests (zero tunnel velocity) with the fan axis perpendicular to the tunnel axis is shown in figure 19 for a range of fan tip speeds. The data in figure 19(a) show

that the lift decreases with increasing louver angle deflection. Between a louver deflection of 0° and 30°, the overall lift decreased gradually, but the lift decreases rapidly for louver deflection angles greater than 30°. Figure 19(b) shows that the negative drag (horizontal thrust) increases with increasing louver deflection angles. The drag variations occur continuously for all fan speeds. The observed variations are the result of the combined effects of varying thrust components and possible changes in fan operating point with increasing louver position.

Pitching moment characteristics, as shown in figure 19(c), show a uniform change from negative (nose down) to slightly positive (nose up) pitching moment at a 40° louver deflection at all fan speeds. This variation is expected because the fan axis is located at the 40 percent chord position and a negative (nose down) pitching moment is produced about the quarter chord point for zero exit louver deflection. As the louvers vector the jet exhaust aft, the horizontal thrust component produces a positive (nose up) pitching moment. At 40° louver deflection, the moments produced by the horizontal and vertical thrust components were nearly equal and combined to yield slightly positive (nose up) values of pitching moment.

The variations of magnitude and angle of the overall resultant force vector with louver position are shown in figures 19(d) and (e), respectively. The observed variations were due to the combined effects of a number of factors that varied as louver position was changed. These factors were (1) changes in the lift and drag forces of the louver vanes which, respectively, opposed the drag and lift forces of the wing, (2) changes in the operating point and gross thrust of the fan, and (3) changes in the fan-jet-induced flow on the lower wing surface (variation in induced wing lift). The rapid decrease in resultant force after 30° of louver deflection is believed to be due to rapidly increasing louver drag.

Crossflow: The overall power-on aerodynamic coefficient data (lift, drag, and pitching moment) in crossflow for the louvers-off configuration are presented in figure 20 for three angles of attack (0° and $\pm 10^{\circ}$) and two tip speeds (70 and 100 percent of design). The coefficient data are shown as a function of the speed ratio correlating parameter, defined as the ratio of the crossflow velocity V to the fan tip speed U_T. For high values of speed ratio, the data appear to approach an asymptote, which reflects the diminishing effect of the fan thrust. At an infinite speed ratio, the values should approach the power-off values shown in figure 15. At low speed ratio values, the coefficients approached infinity, which corresponds to the static test condition ($V = 0$) where the fan produces all the force. The observed variations are similar to those reported in references 5 to 7.

The variation of overall aerodynamic characteristics with angle of attack at a constant crossflow velocity V of 62.5 meters per second (205 ft/sec) and for the tip speeds of 70 and 100 percent of design speed is shown in figure 21. The power-off fan-in-wing

aerodynamics are also included. The increase in lift coefficient above the power-off lift coefficient was due to fan thrust and induced wing lift. The power-on configuration appeared to approach a stalled condition at around a 13° angle of attack, whereas the power-off configuration did not stall over the entire angle of attack range.

Figure 21(b) shows the increase in drag with fan power at V = 62.5 meters per second (205 ft/sec). The increase in drag over the power-off case was due to fan ram drag and the component of the axial force (F sin α). At positive angles of attack, the axial force component adds to the overall drag, and, at negative angles, it subtracts from the overall drag.

The pitching moment data (fig. 21(c)) showed a change from a nose-down moment (power off) to a nose-up moment (power on), and only a small change in moment with fan tip speed. With the fan thrust axis located at 40 percent chord, the fan thrust alone would be expected to produce a nose-down moment about the quarter chord. However, it is known that in crossflow the resultant lift force on the fan inlet bellmouth moves forward and that a strong interaction effect occurs between the fan and wing flow fields such that a nose-up moment is generated (ref. 15). A comparison of power-off pressure coefficients (figs. 16 to 18) with the corresponding power-on variations (figs. 46 to 51 of the appendix) reveals the marked difference in pressure distribution on the forward part of the wing that resulted from the fan flow.

The effects of exit louvers on the overall power-on aerodynamic characteristics of the fan-in-wing in crossflow are shown in figures 22 to 24. Data are shown for three angles of attack and a complete range of exit louver angles. Louver-off data are also included for comparison.

Figure 22 shows the effect of louver position on overall lift coefficient at three angles of attack. The overall lift coefficient of the fan-in-wing configuration with louvers on ($\beta_L = -3^{\circ}$, -2°, and -0.2°) and louvers off are essentially the same. Deflection of the louvers aft vectors the thrust forward and decreases the overall lift. This effect was shown previously for static conditions in figure 19. The largest affect is at a low speed ratio (low free-stream velocities) where most of the lift is produced by the fan.

Figure 23 shows the effect of exit louvers on the overall drag characteristics of the fan-in-wing configuration. The addition of louvers at $\beta_L = -0.2^{\circ}$ increases the drag slightly over the louvers-off configuration. Deflecting the louvers aft produces forward fan thrust, which acts opposite to the drag of the wing and the ram drag of the fan. Negative drag (net forward thrust) is then obtained at various combinations of louver angle, angle of attack, and speed ratio. For example, at zero angle of attack, the zero-drag condition occurs at speed ratios of 0.21 and 0.27 for $\beta_L = 30^{\circ}$ and 40°, respectively. For low louver deflection angles, the drag is always positive at all angles of attack and speed ratios. The trends for low louver angles are similar to the louvers-off configuration.

Figure 24 shows the effect of exit louvers on the overall pitching moment characteristics. A comparison of figures 24(a), (b), and (c) shows little variation in pitching moment coefficient with angle of attack. Addition of undeflected ($\beta_L = -0.2^o$) louvers slightly increases the nose-down (negative) pitching moment. Vectoring the fan exhaust aft at low speed ratio conditions produces positive (nose-up) pitching moments, which agrees with the results obtained during static test conditions (fig. 19(c)). At high speed ratio values (above 0.24), the louver position has little effect on the overall pitching moment. The wing surface pressure coefficient data for the test conditions shown in figures 22 to 24 are presented in figures 52 to 60 of the appendix.

Wing and Fan Force Components

This section will discuss the overall force acting on the fan-in-wing with louvers off in terms of lift and drag components. A comparison is made between the overall fan-in-wing forces measured on the wing load cells and the axial force of the fan assembly measured on the fan balance load cells. Data were obtained over the range of fan speeds from 70 to 100 percent of design at zero crossflow velocity. In crossflow, data were obtained over a full range of crossflow velocities, three angles of attack (0^o, $\pm 10^o$), and two fan speeds (70 and 100 percent of design).

A comparison of overall lift and fan axial force at zero crossflow velocity and zero angle of attack is shown in figure 25. The fan and turbine design thrust point is also shown. The wing lift is always slightly greater than the fan axial force. At 100 percent of design speed the difference between the two curves is approximately 5.5 percent of the fan axial force. This difference, as mentioned previously, can be attributed to fan flow, which produces lift forces on the upper wing surfaces not attached to the fan balance (see fig. 5).

Figures 26 and 27 present the variation of three lift components in crossflow at 100 and 70 percent of fan design speed, respectively. In each case, variations shown are (1) the overall wing lift force L, (2) the overall lift minus the lift component of the fan axial force $L - F_L$, and (3) wing lift with power off. The difference between the derived lift curve $L - F_L$ and the power-off lift curve is an indication of the induced lift force on the wing caused by the fan flow. The difference between the two curves is greatest at zero angle of attack, and least at $\pm 10^o$. In all cases the derived lift curve $L - F_L$ easily extrapolates to zero at zero crossflow velocity as it should if the axial force measurement is a true measure of the fan gross thrust.

Figures 28 and 29 present the variations of three drag components in crossflow for 100 and 70 percent of fan design speed, respectively. The drag component of the fan axial force F_D is added vectorially to the overall drag force D to represent the aerodynamic drag on the wing. The difference between the derived drag curve and the power-

off drag curve is a measure of the combined effects of the ram (momentum) drag and the interference drag on the wing of the lift fan flow. The largest difference occurs at -10° angle of attack and the smallest difference at $+10^{\circ}$. As with the lift curves, the derived curve $D - F_D$ easily extrapolates to zero at zero crossflow velocity.

Additional Investigations

Additional investigations were conducted to evaluate the effect of possible fan system components on fan performance. Three installation components or effects were investigated: (1) annular inlet vanes, (2) inlet surface discontinuities, and (3) inlet and exit start-up devices.

Inlet vane configurations. - For a fan-in-wing operating in crossflow, flow separation can occur on the forward portion of the fan inlet bellmouth. If separation occurs, a portion of the inlet flow area is blocked and losses in performance result (refs. 16 and 17). The basic fan-in-wing model was fitted with an annular inlet vane. The purpose of the vane was to suppress or delay separation on the forward section of the inlet bellmouth. Two vanes were designed: (1) a 90° arc vane with a constant thickness cross section and (2) a 180° arc vane with an airfoil cross section. Figure 30 is a photograph of the two vanes, and figure 31 shows the 180° arc airfoil vane installed in the model fan inlet. Figures 32 and 33 present the design details of the 90° arc vane and the 180° arc vane, respectively.

The 180° arc airfoil vane was tested with the exit louvers on, under static conditions over fan speeds ranging from 70 to 110 percent of design. Figure 34 indicates that the 180° arc airfoil vane had little effect on the fan static performance over the range of louver positions and fan speeds tested.

Both inlet vanes were tested at 100 percent of fan design speed over the full range of crossflow velocities and at three angles of attack (0°, $\pm 10^{\circ}$). Figure 35 compares the effects of the two vane configurations on the fan axial force loading in crossflow for the conditions noted. The performance of the fan with the vanes installed differed only slightly from the no-vane configuration. Figure 36 compares the effects of the two vane configurations on the fan axial-force loading for various angles of attack at a fixed crossflow velocity. For a louver angle of -2°, both vane configurations improved the fan performance slightly, mostly at positive angles of attack. For a louver angle of $+40^{\circ}$, the axial-thrust loading increased for the 180° airfoil vane but decreased a like amount for the 90° vane. The negligible effect of the inlet vanes on the axial-force loading may indicate that any improvement in boundary-layer condition was counterbalanced by the extra losses added by the presence of the vanes.

Bellmouth surface discontinuities. - When a lift fan system is installed in the airframe, doors will be used to cover the fan opening to reduce the aircraft drag during

cruise. When these doors are opened during lift-fan operation, discontinuities or steps can be present in the surface near the inlet of the fan. Performance losses could result if the discontinuities disturbed the fan flow.

Three types of surface discontinuities were tested using the fan-in-wing model. These were (1) a surface ramp, (2) a wire ring, and (3) a gap. Figures 37 to 39 show installation features and construction details of the three configurations tested. The results of static tests are shown in figure 40, and the crossflow test results at three angles of attack are shown in figure 41. The inlet surface discontinuities produced a slight increase in axial-force loading at high tip speeds at static conditions, and there was a slight reduction in axial-force loading at high free-stream velocities during crossflow testing.

Windmill characteristics. - In-flight startup of lift-fan engines may require an increased torque because of reverse windmilling. External devices can be used to windmill the fan in the proper direction in order to reduce the starting torque requirement (ref. 18). Two such devices were tested: (1) a startup fence on the upper surface of the wing at the aft end of the bellmouth, and (2) a single-exit louver on the lower surface at the forward part of the fan duct of the wing. Installation and construction details are shown in figures 42 to 44. Windmill tests of the fan-in-wing configuration with and without exit louvers were also conducted.

The results are shown in figure 45. The fan power-off rotational speed is shown as a function of angle of attack at a fixed crossflow velocity. The startup devices are compared with the fan-in-wing model with and without exit louvers. In general, the fan rotor rotation was positive at negative angles of attack and was negative at positive angles of attack. The clean inlet configuration with louvers off had the worst negative windmill condition (-173 rad/sec (-1650 rpm)). The addition of exit louvers reduced the magnitude of the negative rotational speed but did not change the direction of rotation at high angles of attack. The single louver and full exit louvers had essentially identical characteristics.

The startup fence without exit louvers sustained a positive windmill rotation of 68 radians per second (650 rpm) or 2.5 percent of design speed up to an angle of attack of 8°. However, the maximum positive windmill speed was not increased using the startup fence.

SUMMARY OF RESULTS

Tests were conducted to determine the forces on a 1.28-pressure-ratio VTOL model lift fan-in-wing installation under static and crossflow conditions. The results are summarized as follows:

1. The addition of the fan (power off) and louvers to the basic wing configurations reduced the aerodynamic performance of the wing (e.g., lift decreased and drag increased).

2. At static conditions, the axial force of the fan assembly increased with increasing louver deflection angle at design tip speed. Design force was attained when the louvers were in the 30° position. The effect of louvers on fan axial force decreased with decreasing fan speed.

3. At design speed, the axial force of the fan assembly without louvers tended to decrease slightly and then increase slightly with increasing crossflow velocity. At 70 percent of design speed, the fan-assembly axial force increased significantly with increasing crossflow velocity. Increasing wing angle of attack from -10° to $+10^{\circ}$ caused an increase in fan-assembly axial force in all cases. At a crossflow velocity of 73 meters per second (240 ft/sec) the increase due to angle of attack was around 12 to 15 percent.

4. At design fan speed and crossflow conditions, exit louvering increased the magnitude of the fan-assembly axial force, as in the static case, but had little effect on the variation with crossflow velocity. At 70 percent of design speed the louvers had little effect on the fan axial force in crossflow.

5. With fan power on, exit louvering changed the overall wing forces as expected: lift decreased, negative drag (horizontal thrust) increased, and the pitching moment about the quarter chord changed significantly from a large negative (nose down) value to a slightly positive (nose up) value.

6. Comparison of power-on and power-off data showed that overall wing lift and drag forces increased and pitching moment became more positive (nose up) as fan power was increased. Induced effects on overall aerodynamics were evident, with magnitude depending on wing angle of attack.

7. The addition of annular inlet vanes to suppress or delay separation on the forward section of the inlet bellmouth had little effect on the fan-assembly axial force in static and crossflow conditions.

8. Discontinuities on the surface of the fan inlet bellmouth (e.g., gap, ring, ramp) had little effect on the axial force of the fan assembly for both static and crossflow conditions.

9. For the external devices used in windmill the fan in the proper direction to aid in-flight starting, the most effective device was a fence on the upper surface of the wing at the aft end of the bellmouth. This device sustained proper rotation to $+8^{\circ}$ angle of attack; however, the maximum windmill speed was only 2.5 percent of design speed.

Lewis Research Center,
National Aeronautics and Space Administration,
Cleveland, Ohio, November 4, 1971,
764-72.

APPENDIX - WING SURFACE PRESSURE COEFFICIENT DATA

This section presents the power-on midspan wing surface static pressure coefficient data obtained during this investigation (figs. 46 to 60). The wing airfoil section dimensions are shown in figure 2 (p. 21). The static pressure taps were located on the wing upper and lower surfaces along the chord at the midspan position of the wing as shown in figure 2.

The fan axis is located at the 40 percent chord position. The fan was installed between the taps located at the 17.22 and 60.93 percent of chord and covered the interval between 20 and 60 percent of the wing chord. Consequently, there were no static-pressure data shown for this interval. The static taps on the lower surface at the x/c = 17.22 and 60.93 percent of chord positions were located near the lower surface fan exit fairing. The presence of the fairing may have had a slight effect on the static pressure readings at those locations. In addition, when the exit louvers were in place (fig. 42), the louver actuator may also have had some effect on the aft lower surface static pressure measurements.

Data are presented for the louvers off and louvers on configurations over a range of fan speeds from 70 to 100 percent of design, a full range of crossflow velocities from 21 to 73 meters per second (70 to 240 ft/sec), and three angles of attack (0°, $\pm 10^{\circ}$). The test data with the louvers on covers the entire louver position range from -3° to 40°. The data figures are grouped as shown in table IV.

The figures for pressure coefficient shown in this appendix were plotted by computer and photographed on microfilm. The data points were connected by straight lines; therefore, the lines between the points at 17.22 and 60.93 percent of chord are not representative of the actual wing pressure coefficient distribution over that interval.

REFERENCES

1. Anon.: Conference on V/STOL and STOL Aircraft. NASA SP-116, 1966, pp. 311-407.
2. Jagger, D. H.; and Kemp, E. D. G.: The Potential and Development of a V/S.T.O.L. Inter-City Airliner. Aircraft Eng., vol. 42, no. 1, Jan. 1970, pp. 6-13.
3. Deckert, Wallace H.; and Hickey, David H.: Summary and Analysis of Feasibility-Study Designs of V/STOL Transport Aircraft. J. Aircraft, vol. 7, no. 1, Jan.-Feb. 1970, pp. 66-72.
4. Brown, D. G.: The Case for V/STOL Aircraft in Short-Haul Transportation. Paper 700333, SAE, Apr. 1970.
5. Kirk, Jerry V.; Hickey, David H.; and Hall, Leo P.: Aerodynamic Characteristics of a Full-Scale Fan-In-Wing Model Including Results in Ground Effect with Nose-Fan Pitch Control. NASA TN D-2368, 1964.
6. Hall, Lee P.; Hickey, David H.; and Kirk, Jerry V.: Aerodynamic Characteristics of a Large-Scale V/STOL Transport Model with Lift and Lift-Cruise Fans. NASA TN D-4093, 1967.
7. Kirk, Jerry V.; Hodder, Brent K.; and Hall, Leo P.: Large-Scale Wind-Tunnel Investigation of a V/STOL Transport Model with Wing-Mounted Lift Fans and Fuselage-Mounted Lift-Cruise Engines for Propulsion. NASA TN D-4233, 1967.
8. Newsom, William A., Jr.; and Moore, Frederick L.: Wind-Tunnel Investigation of a V/STOL Transport Model with Six Wing-Mounted Lift Fans. NASA TN D-5695, 1970.
9. Lieblein, S.: A Review of Lift Fan Propylsion Systems for Civil VTOL Transports. Paper 70-670, AIAA, June 1970.
10. Sanders, Newell D.; Diedrich, James H.; Hassell, James L., Jr.; Hickey, David H.; Luidens, Roger W.; and Stewart, Warner L.: V/STOL Propulsion. Aircraft Propulsion. NASA SP-259, 1971, pp. 135-168.
11. Yuska, Joseph A.; Diedrich, James H.; and Clough, Nestor; Lewis 9-by-15-Foot V/STOL Wind Tunnel. NASA TM X-2305, 1971.
12. Moffitt, Thomas P.: Design and Experimental Investigation of a Single-Stage Turbine with a Rotor Entering Relative Mach Number of 2. NACA RM E58F20a, 1958.

13. Moffitt, Thomas P.; and Klag, Frederick W., Jr.: Experimental Investigation of Partial- and Full-Admission Characteristics of a Two-Stage Velocity-Compounded Turbine. NASA TM X-410, 1960.

14. Hoak, D. E.; Carlson, J. W.; and Malthan, L. V.: USAF Stability and Control Handbook. McGregor & Werner, Inc., Dayton, Ohio, 1960.

15. McKinney, M. O.; and Newsom, W. A.: Fan V/STOL Aircraft. Ann. N.Y. Acad. Sci., vol. 154, art. 2, Nov. 22, 1968, pp. 872-892.

16. Przedpelski, Zygmunt J.: Lift Fan Technology Studies. NASA CR-761, 1967.

17. Hodder, Brent K.; Kirk, Jerry V.; and Hall, Leo P.: Aerodynamic Characteristics of a Large-Scale Model with a Lift Fan Mounted in a 5-Percent-Thick Triangular Wing, Including the Effects of BLC on the Lift-Fan Inlet. NASA TN D-7031, 1970.

18. Tolhurst, William H., Jr.; and Kelley, Mark W.: Characteristics of Two Large-Scale Jet-Lift Propulsion Systems. Conference on V/STOL and STOL Aircraft. NASA SP-116, 1966, pp. 205-228.

TABLE I. - LIFT FAN DESIGN CHARACTERISTICS

Pressure ratio	1.28
Corrected tip speed, m/sec (ft/sec)	299 (980)
Corrected mass flow, kg/sec (lbm/sec)	18.0 (39.8)
Actual thrust, N (lbf)	3620 (815)
Inlet Mach number	0.60
Rotor blade (double circular arc airfoil section):	
Number of blades	35
Tip diameter, cm (in.)	38.6 (15.2)
Aspect ratio	2.7
Hub-tip ratio	0.463
Solidity (tip)	1.25
Stator blade (NACA-65 series airfoil section):	
Number of blades	36
Aspect ratio	3.0
Solidity (tip)	1.0

TABLE II. - DRIVE TURBINE DESIGN CHARACTERISTICS

Inlet pressure, N/m^2 (psi)	6.89×10^6 (1000)
Inlet temperature, K (^{o}R)	350 (630)
Actual weight flow, kg/sec (lbm/sec)	4.41 (9.72)
Corrected speed, rad/sec (rpm)	1520 (14 550)
Actual thrust, N (lbf)	1310 (294)
Overall total efficiency	0.534
Overall corrected enthalpy, J/kg (Btu/lbm)	95 500 (41.0)

TABLE III. - ACCURACY AND REPEATABILITY RANGES

Tunnel dynamic pressure, N/m^2 (lbf/ft^2)	±19.2 (±0.4)
Wing lift, N (lbf)	±17.8 (±4)
Wing drag, N (lbf)	±2.22 (±0.5)
Wing moment, m-N (ft-lbf)	±7.84 (±5.8)
Wing angle of attack, deg	±0.1
Exit louver position, deg	±0.1
Fan axial force, N (lbf)	±13.3 (±3)

TABLE IV. - LIST OF APPENDIX FIGURES

Figure number	Louver configuration	Variable	Angle of attack, α, deg	Crossflow velocity, V		Fan tip speed, U_T, percent of design	Louver position, β_L, deg
				m/sec	ft/sec		
46	Off	V/U_T	0	--	---	---	--
47	↓	V/U_T	10	--	---	---	--
48	↓	V/U_T	-10	--	---	---	--
49	↓	α	---	61	200	100	--
50	↓	α	---	61	200	70	--
51	On	V/U_T	0	--	---	---	-3
52	↓	↓	0	--	---	---	-2
53	↓	↓	0	--	---	---	30
54	↓	↓	0	--	---	---	40
55	↓	↓	10	--	---	---	-2
56	↓	↓	10	--	---	---	30
57	↓	↓	10	--	---	---	40
58	↓	↓	-10	--	---	---	-3
59	↓	↓	-10	--	---	---	30
60	↓	↓	-10	--	---	---	40

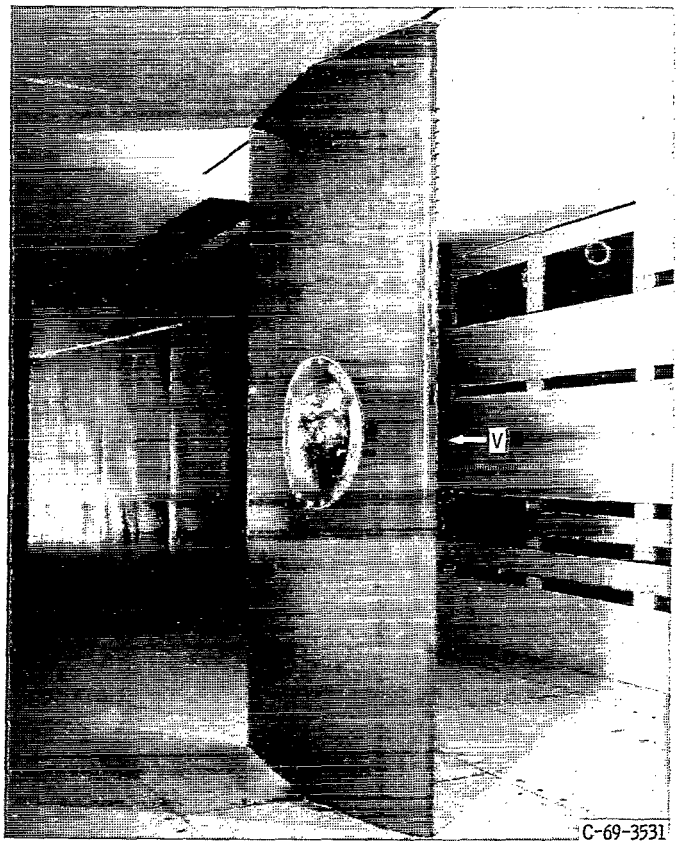

Figure 1. - Fan-in-wing model in 2.74- by 4.58-meter (9- by 15-ft) V/STOL wind tunnel.

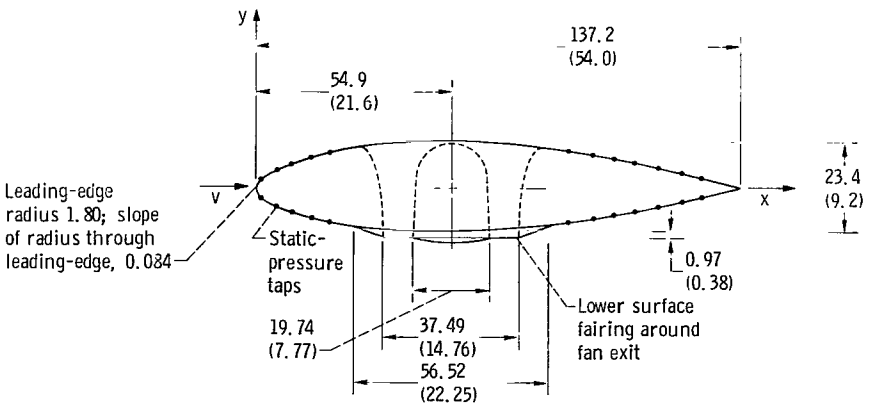

Coordinates of wing airfoil section (NACA 65_3A-(218)-217) in percent of airfoil chord

Station, x/c	Ordinates, y/c	
	Lower	Upper
0	0	0
.926	-1.444	1.815
1.852	-1.981	2.519
2.778	-2.444	3.056
3.704	-2.833	3.500
4.630	-3.167	3.889
5.556	-3.481	4.259
7.407	-3.981	4.889
11.111	-4.852	6.000
12.778	-5.167	6.426
14.815	-5.519	6.870
18.519	-6.074	7.574
22.222	-6.519	8.167
25.926	-6.889	8.648
29.630	-7.167	9.019
33.333	-7.333	9.296
37.037	-7.463	9.444
40.000	-7.481	9.519
42.593	-7.444	9.500
46.296	-7.315	9.389
50.000	-7.056	9.130
53.704	-6.648	8.759
57.407	-6.185	8.259
61.111	-5.667	7.704
64.815	(a)	6.870
65.926		(a)
(a)		
100	0	0

[a]Straight line.

Static-pressure tap locations in percent of airfoil chord

Station, x/c
0.93
3.70
7.41
11.11
17.22
60.93
69.07
73.70
78.33
82.96
87.59
92.22

Figure 2. - Wing airfoil section dimensions and midspan static-pressure tap locations. (All dimensions are in cm (in.).)

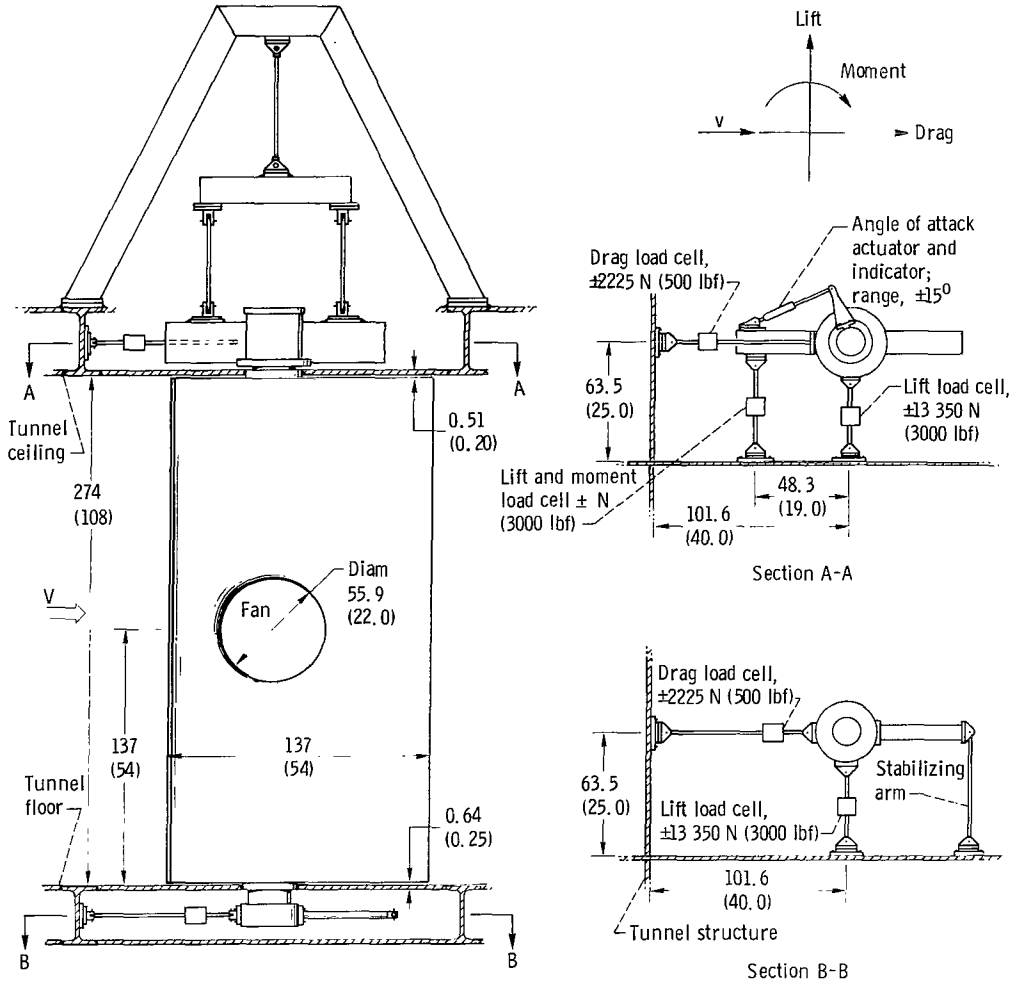

Figure 3. - Wing balance. (All dimensions are in cm (in.).)

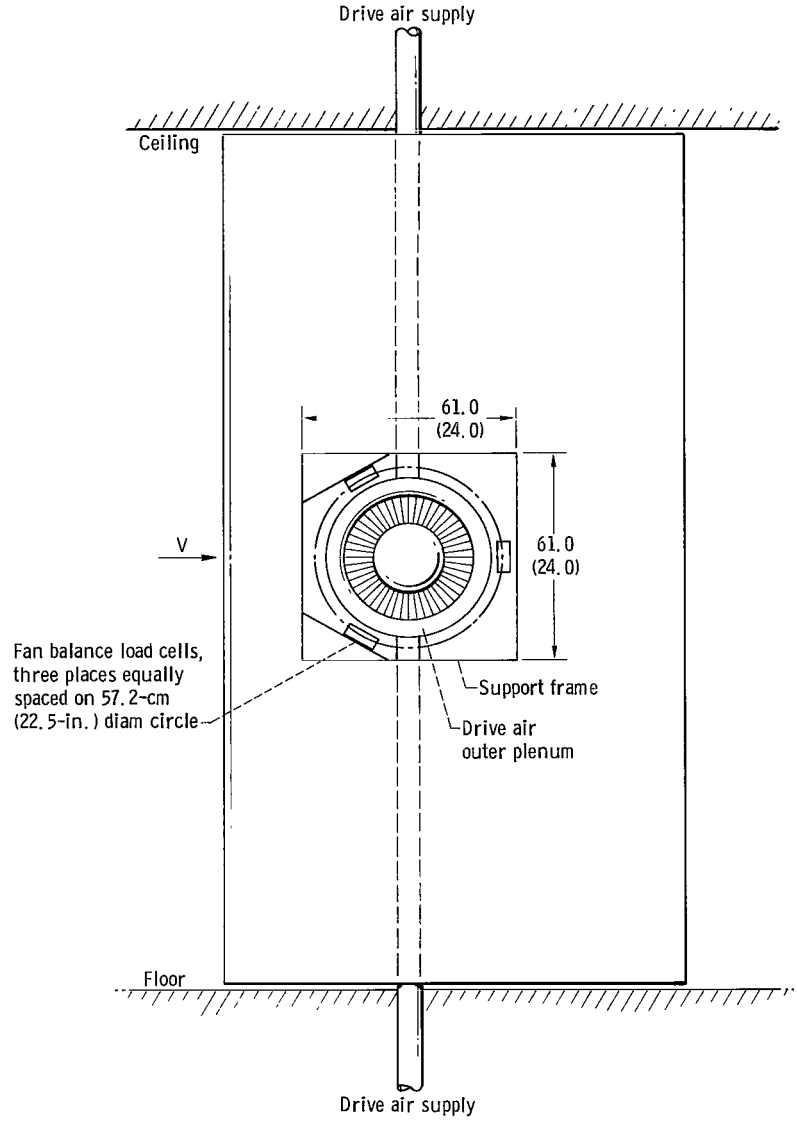

Figure 4. - Fan-in-wing installation on fan balance. (All dimensions are in cm (in.).)

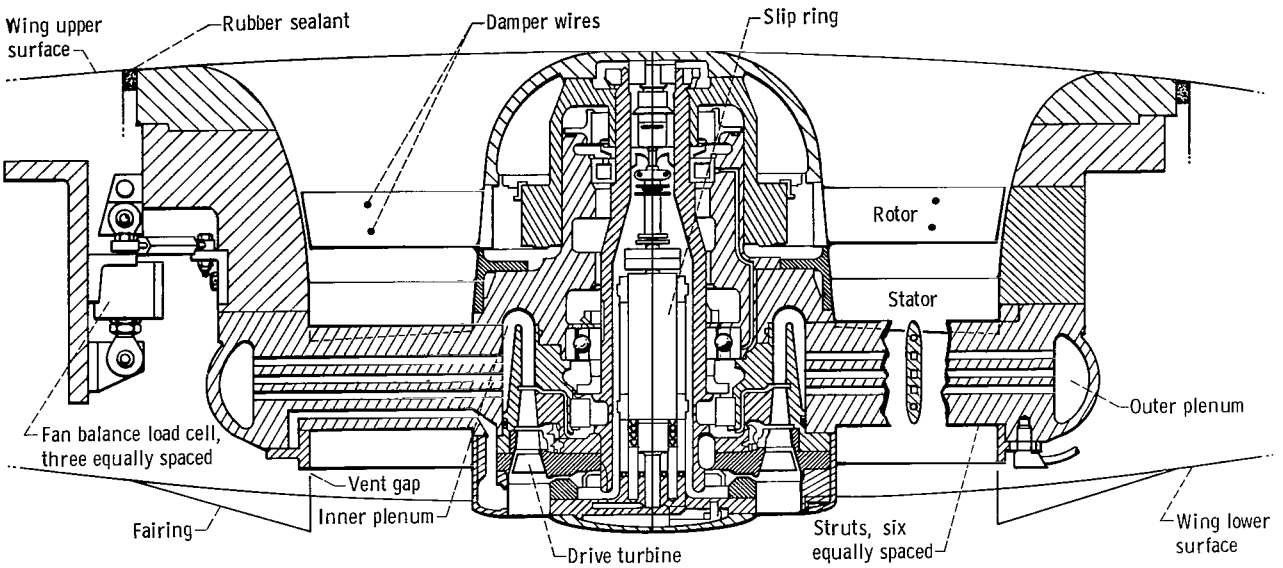

Figure 5. - Cross-section of model lift fan.

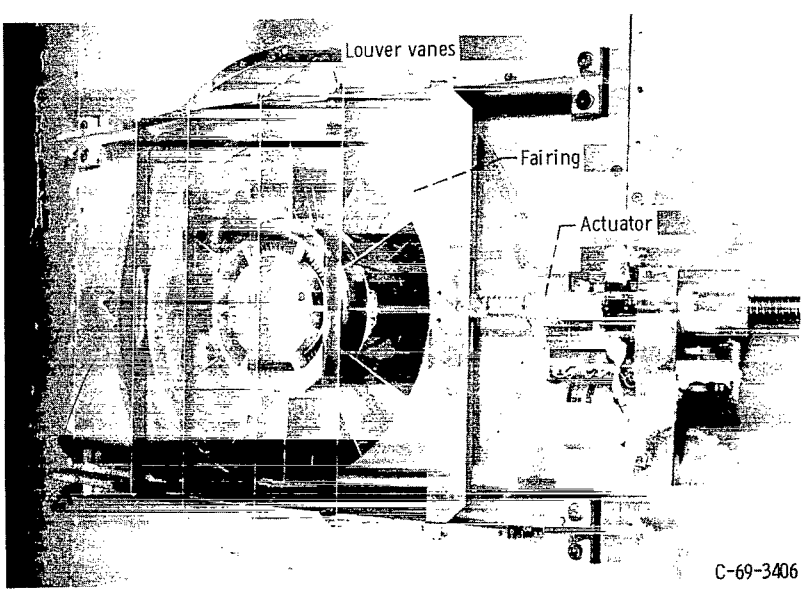

Figure 6. - Exit louver installation.

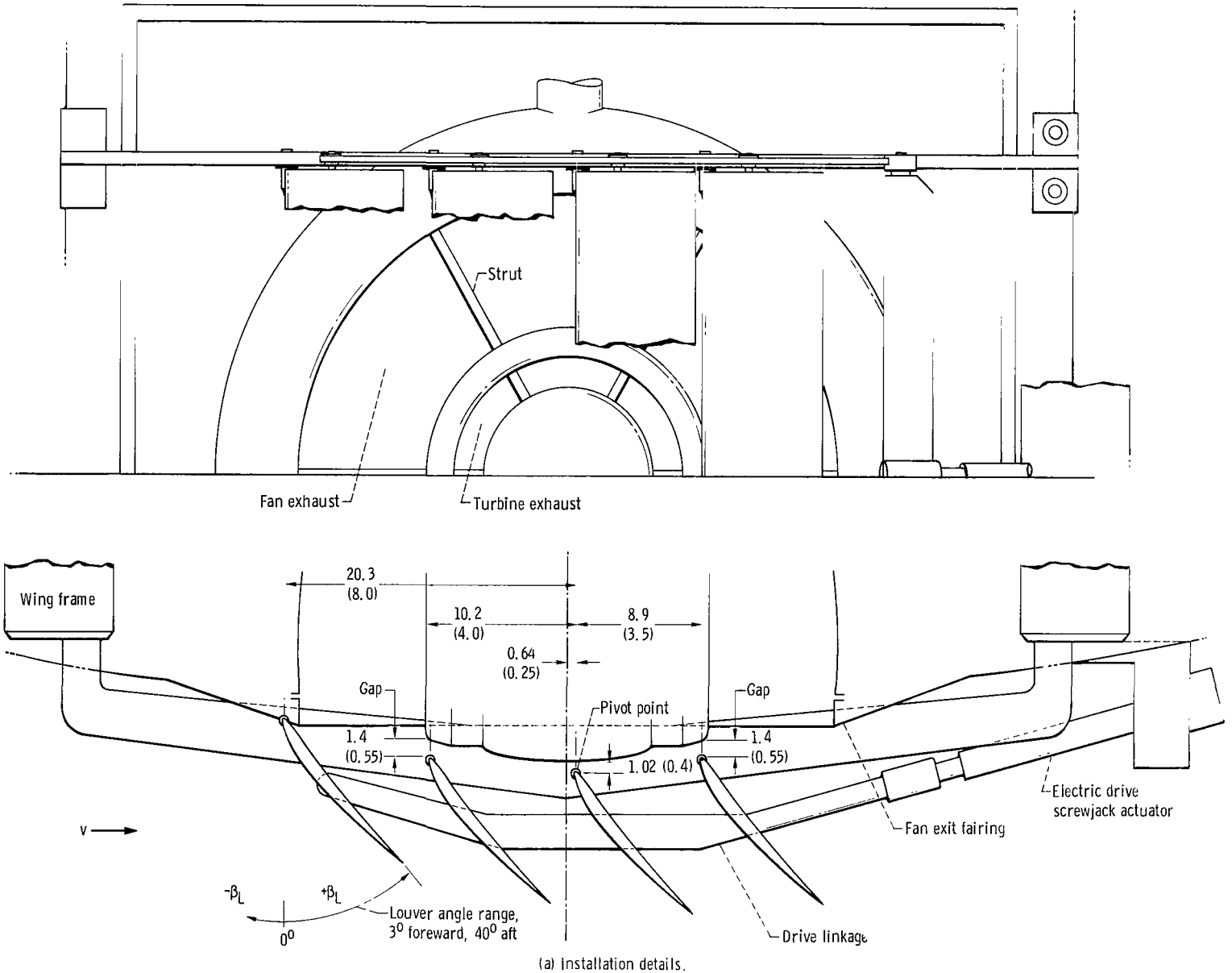

(a) Installation details.

Figure 7. - Exit louvers. (All dimensions are in cm (in.).)

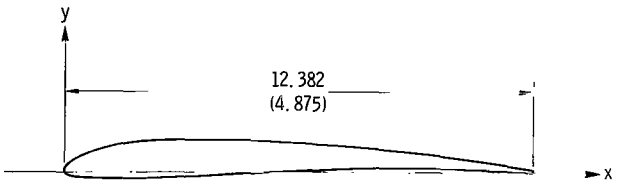

Coordinates of exit louver airfoil section
(Modified NACA 63 series; zero lift coefficient, 0.6; thickness ratio, 0.08)

(Station and ordinates given in percent of airfoil chord)

Upper surface		Lower surface	
Station, x	Ordinate, y	Station, x	Ordinate, y
0	0	0	0
.849	1.803	1.651	-.853
2.025	2.745	2.975	-1.117
4.488	4.069	5.512	-1.371
9.546	5.693	10.454	-1.455
14.650	6.567	15.350	-1.263
19.755	7.016	20.245	-.968
24.844	7.232	25.156	-.682
29.917	7.270	30.083	-.418
34.977	7.136	35.023	-.148
40.024	6.930	39.976	.054
45.059	6.592	44.941	.264
50.082	6.170	49.918	.450
55.096	5.677	54.904	.609
60.101	5.133	59.899	.737
65.099	4.548	64.901	.826
70.091	3.943	69.909	.871
75.081	3.327	74.919	.863
80.068	2.713	79.932	.793
85.056	2.115	84.944	.655
90.046	1.538	89.954	.432
95.041	.985	94.959	.109
100	0	100	0

(b) Louver airfoil section coordinates. Leading-edge radius, 0.705; slope of radius through leading edge, 0.374; trailing-edge radius, 0.400.

Figure 7. - Concluded.

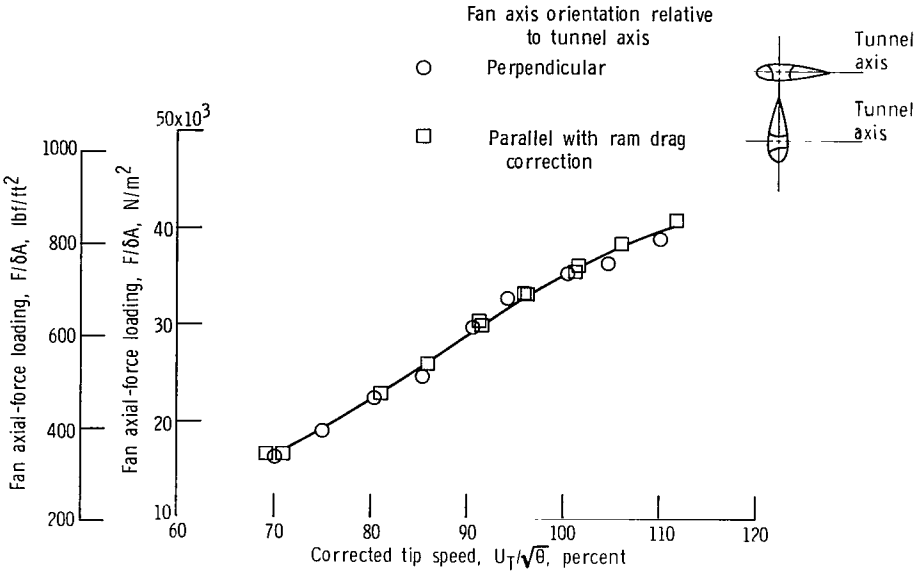

Figure 8. - Fan axial-force loading. Static conditions; louvers off.

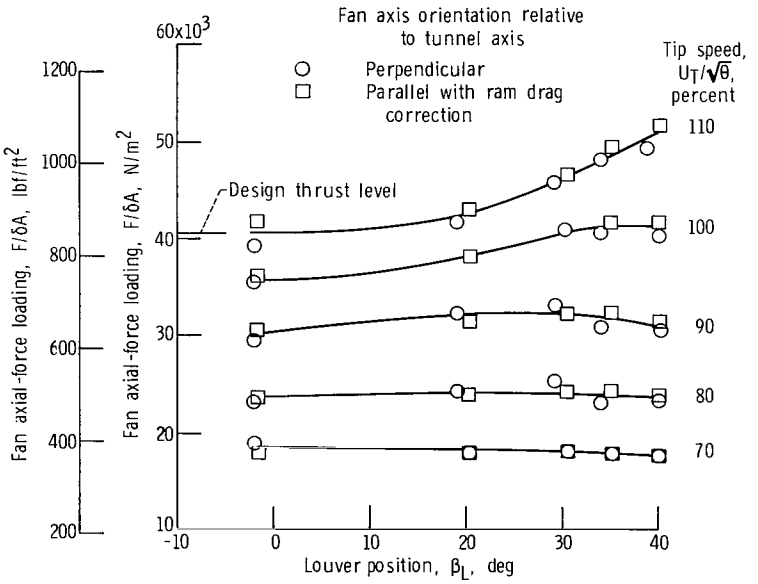

Figure 9. - Effect of exit louvers on fan axial-force loading. Static conditions.

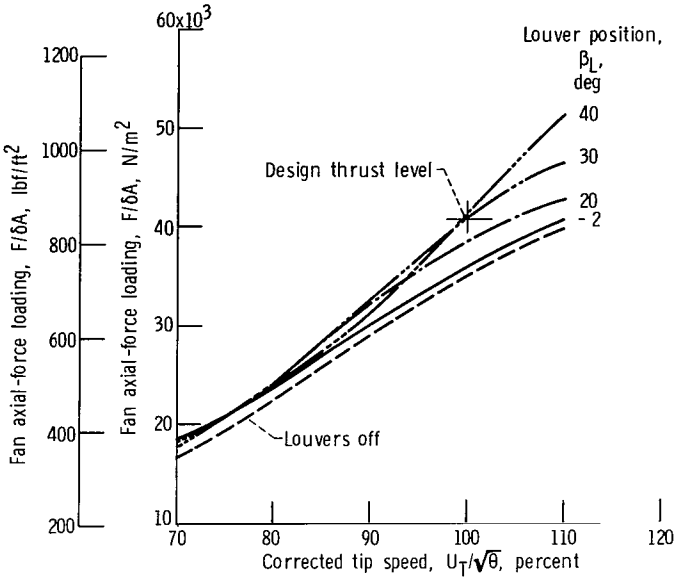

Figure 10. - Fan axial-force loading. Static conditions.

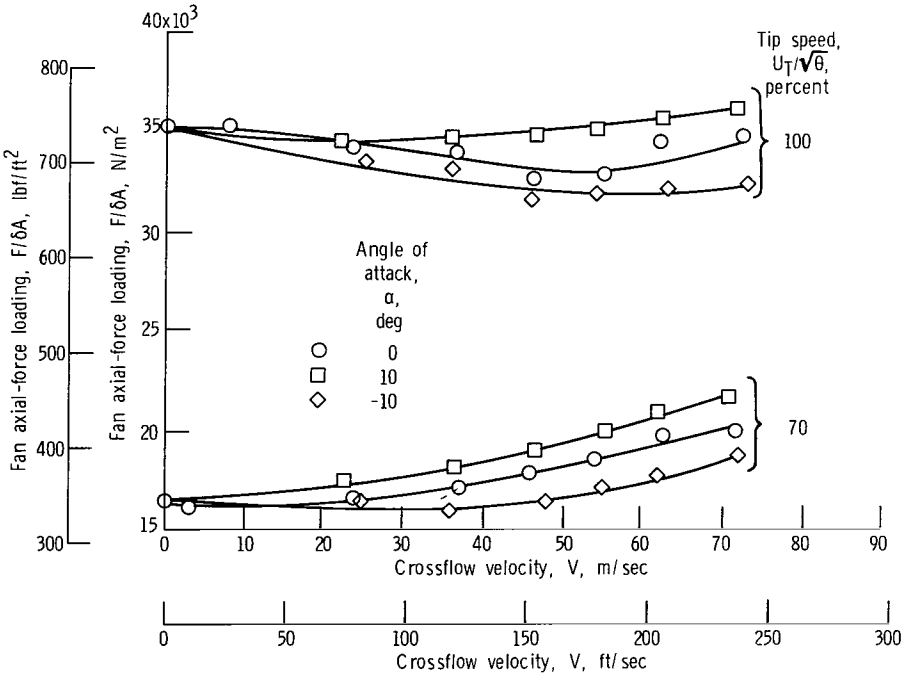

Figure 11. - Fan axial-force loading in crossflow. Louvers off.

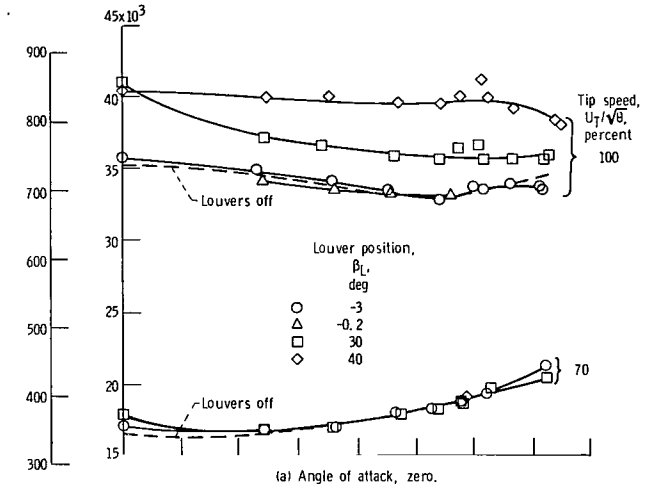

(a) Angle of attack, zero.

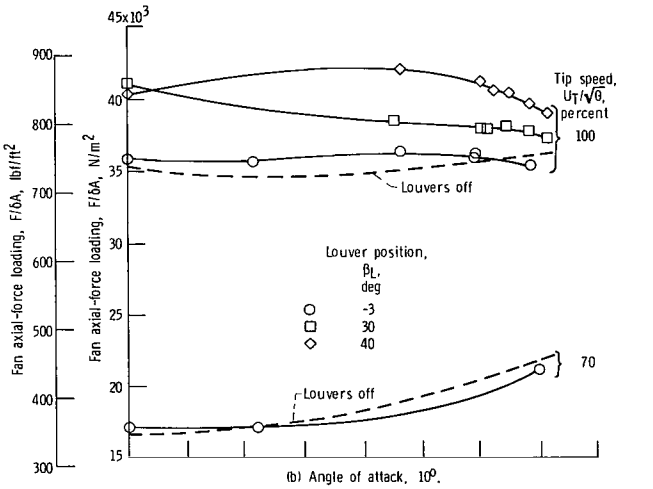

(b) Angle of attack, 10°.

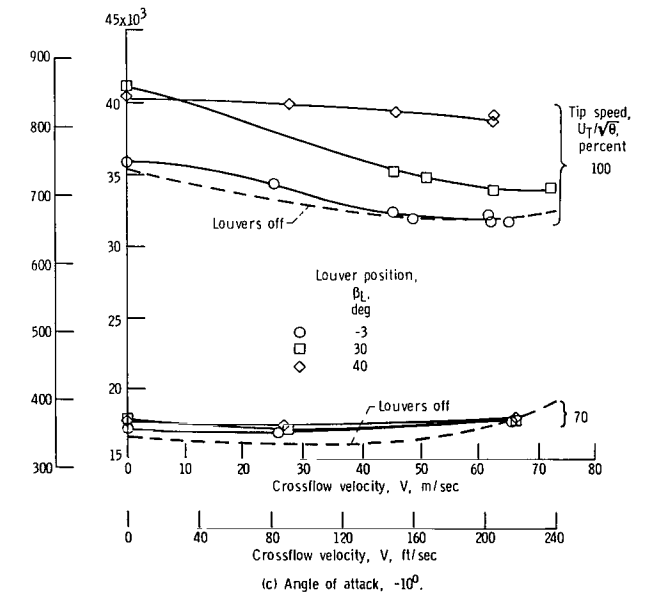

(c) Angle of attack, -10°.

Figure 12. - Fan axial-force loading in crossflow. Louvers on.

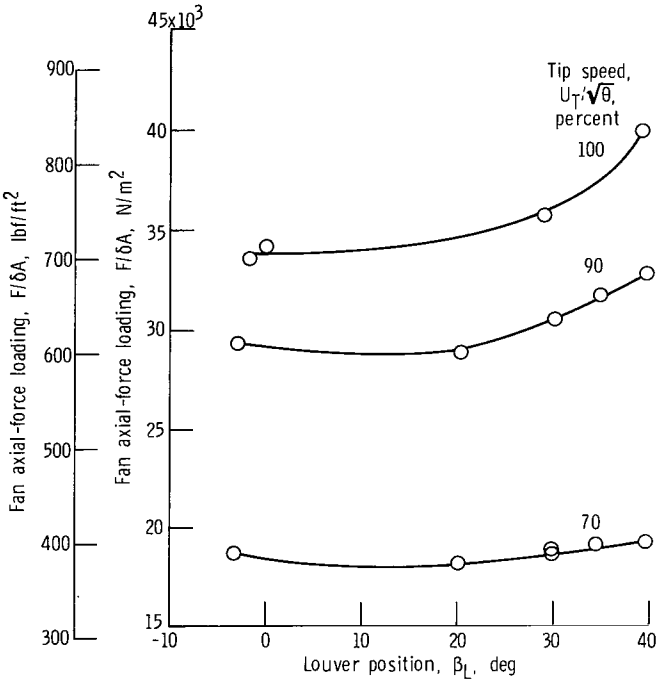

Figure 13. - Effect of louver position on fan.axail-force loading in crossflow. Angle of attack, zero; crossflow velocity, 61 meters per second (200 ft/sec).

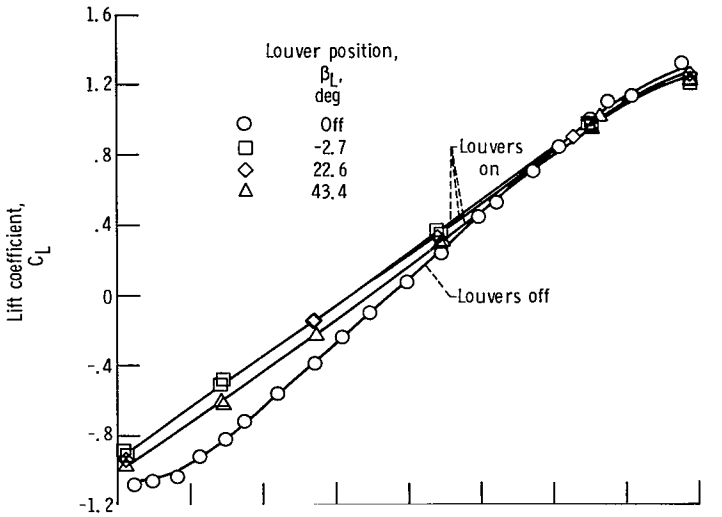

(a) Lift.

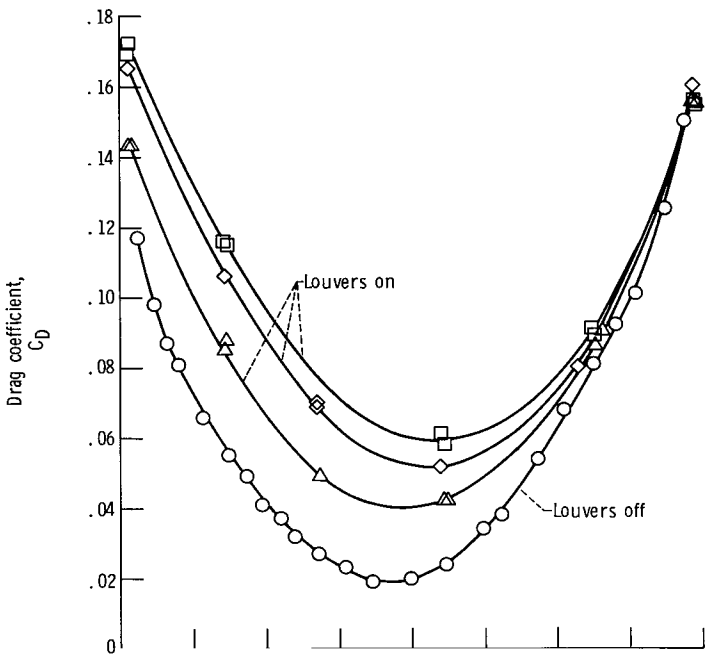

(b) Drag.

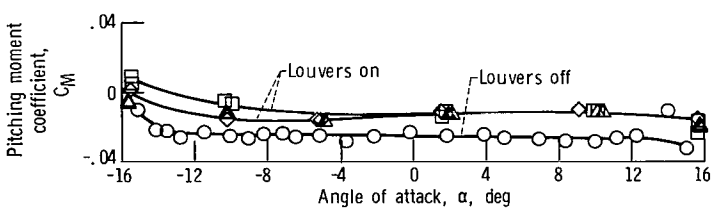

(c) Pitching moment.

Figure 14. - Aerodynamic characteristics of basic wing configuration with and without louvers.

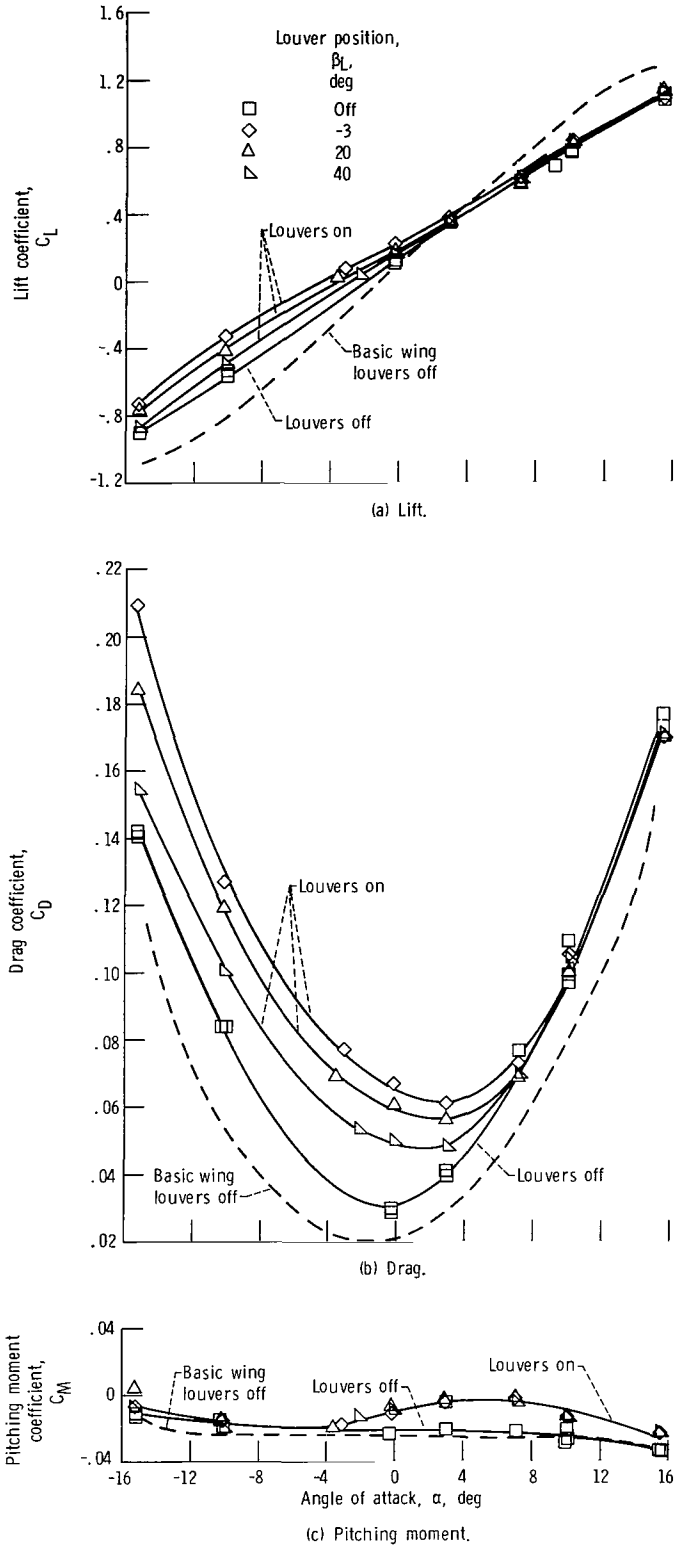

Figure 15. - Power-off aerodynamic characteristics of fan-in-wing configuration with and without exit louvers.

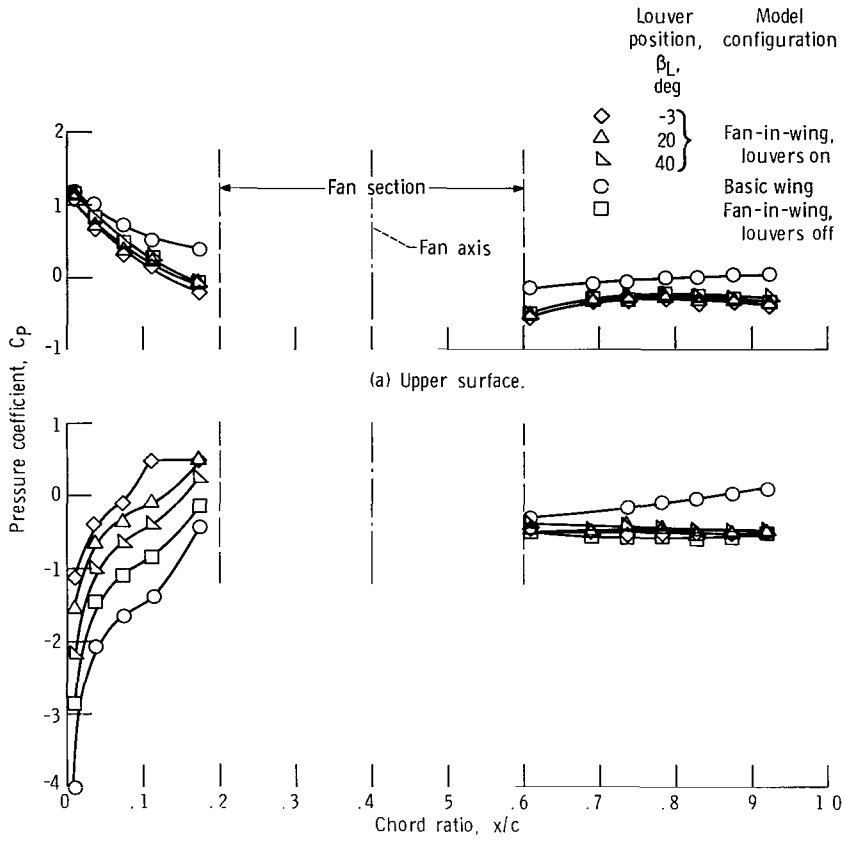

Figure 16. - Effect of louvers on power-off-wing surface pressure coefficient distribution. Angle of attack, -10°; crossflow velocity, 63 meters per second (205 ft/sec)

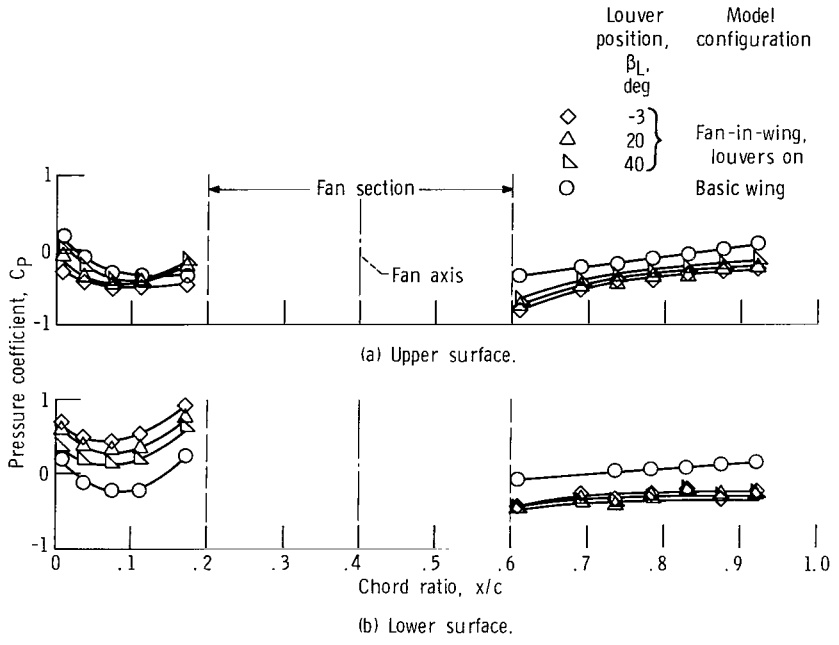

Figure 17. - Effect of louvers on power-off wing surface pressure coefficient distribution. Angle of attack, zero; crossflow velocity, 63 meters per second (205 ft/sec).

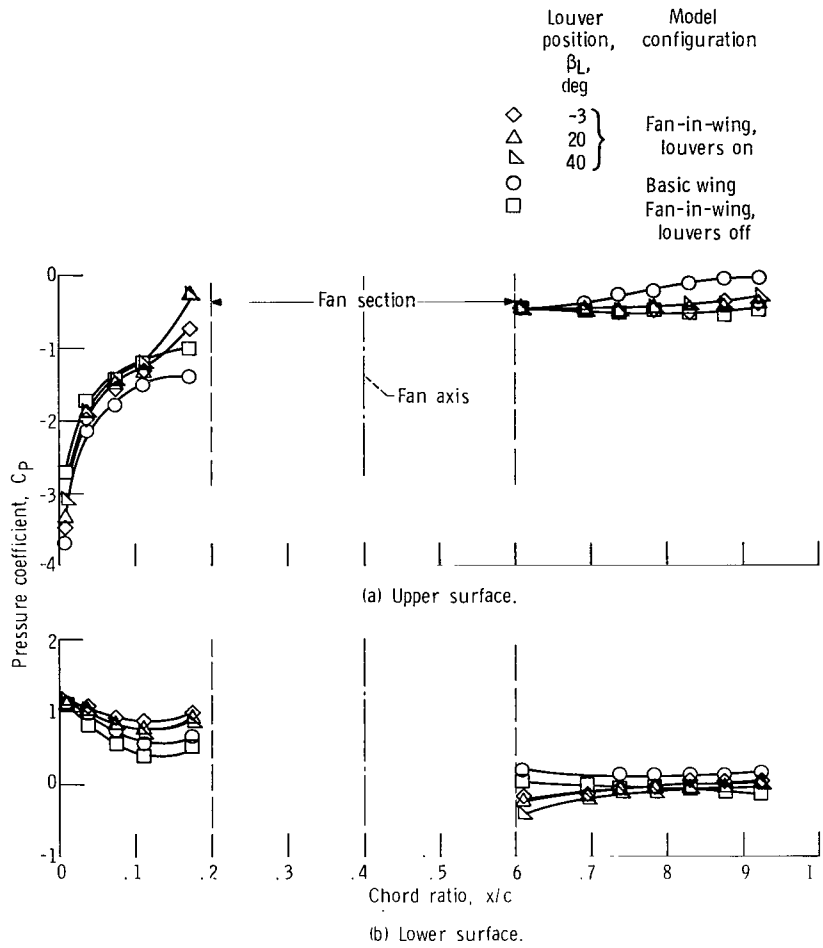

(a) Upper surface.

(b) Lower surface.

Figure 18. - Effect of louvers on power-off wing surface pressure coefficient distribution. Angle of attack, 10^0; crossflow velocity, 63 meters per second (205 ft/sec).

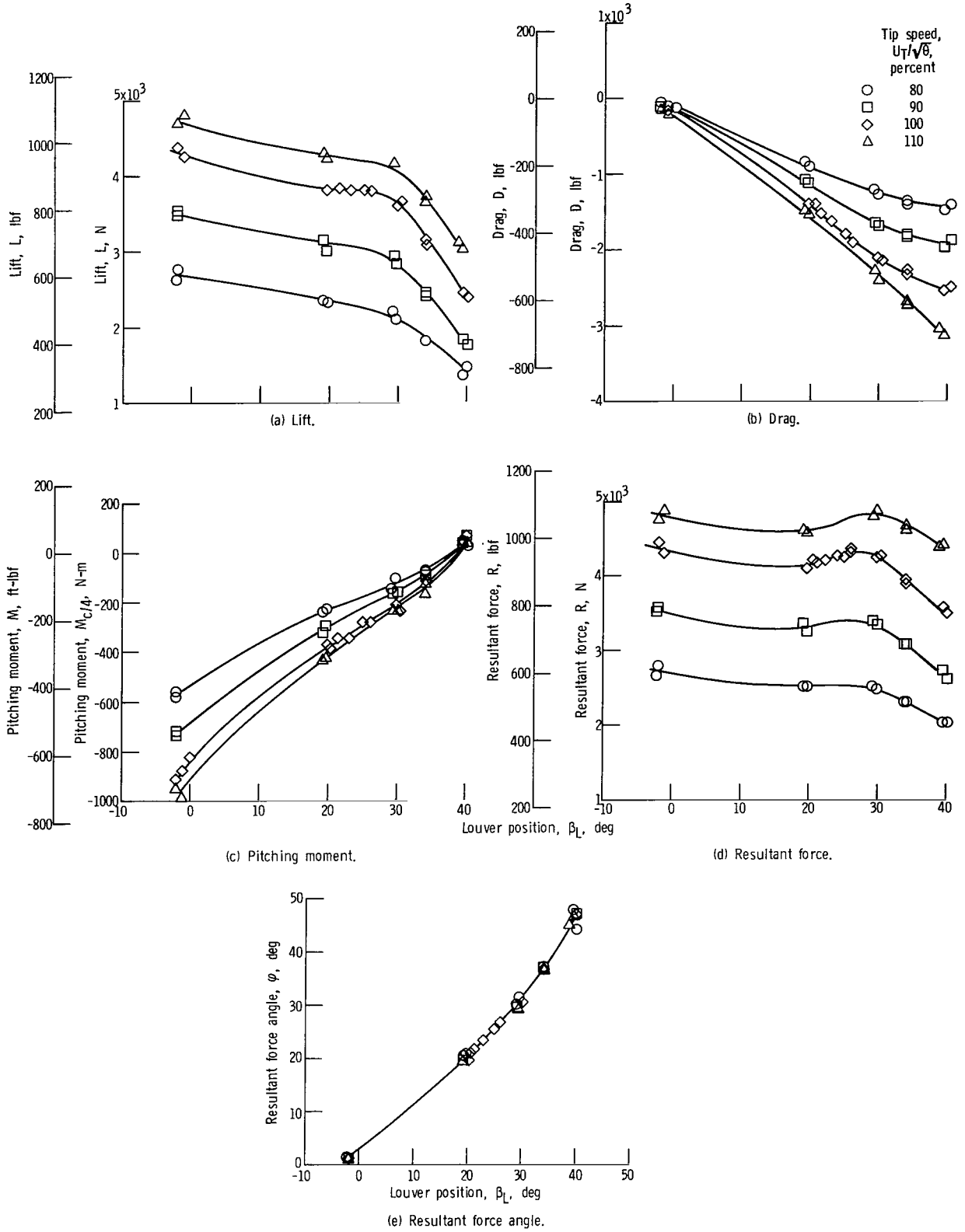

Figure 19. - Effect of exit louver position on overall fan-in-wing forces for static tests. Fan axis perpendicular to tunnel axis.

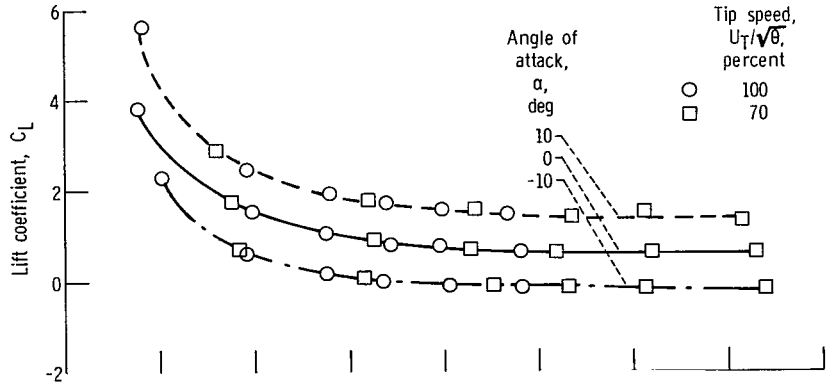

(a) Lift.

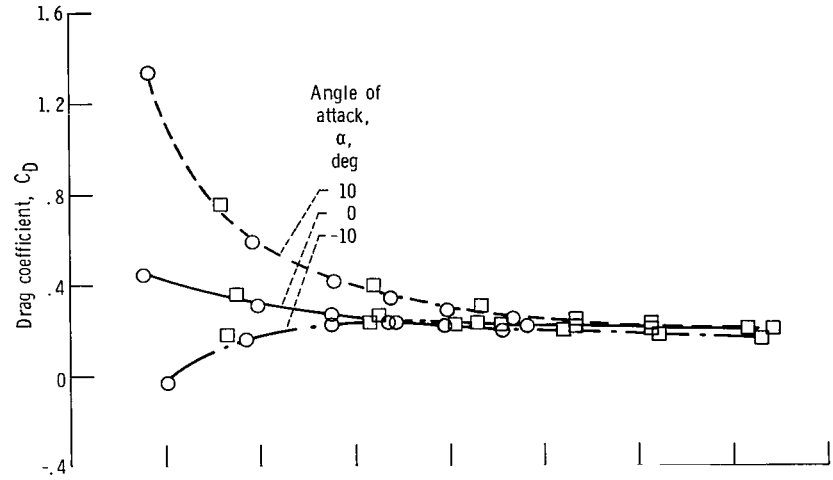

(b) Drag.

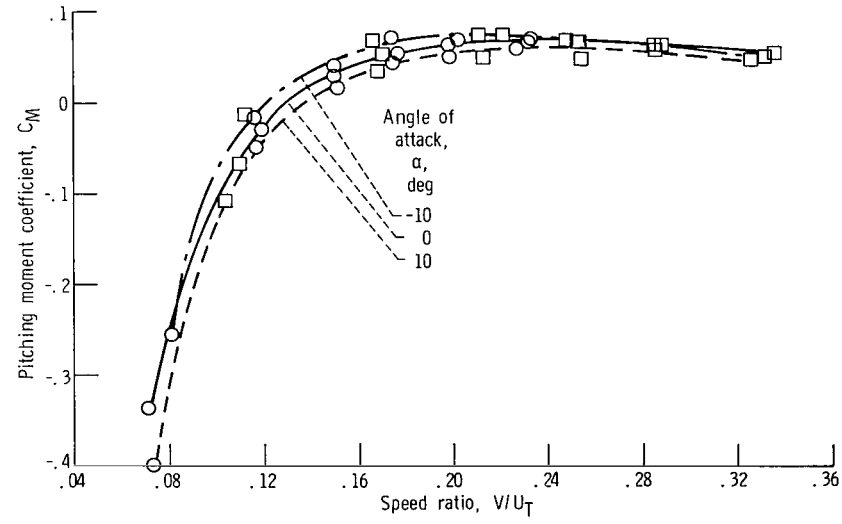

(c) Pitching moment.

Figure 20. - Overall power-on aerodynamic performance with louvers off.

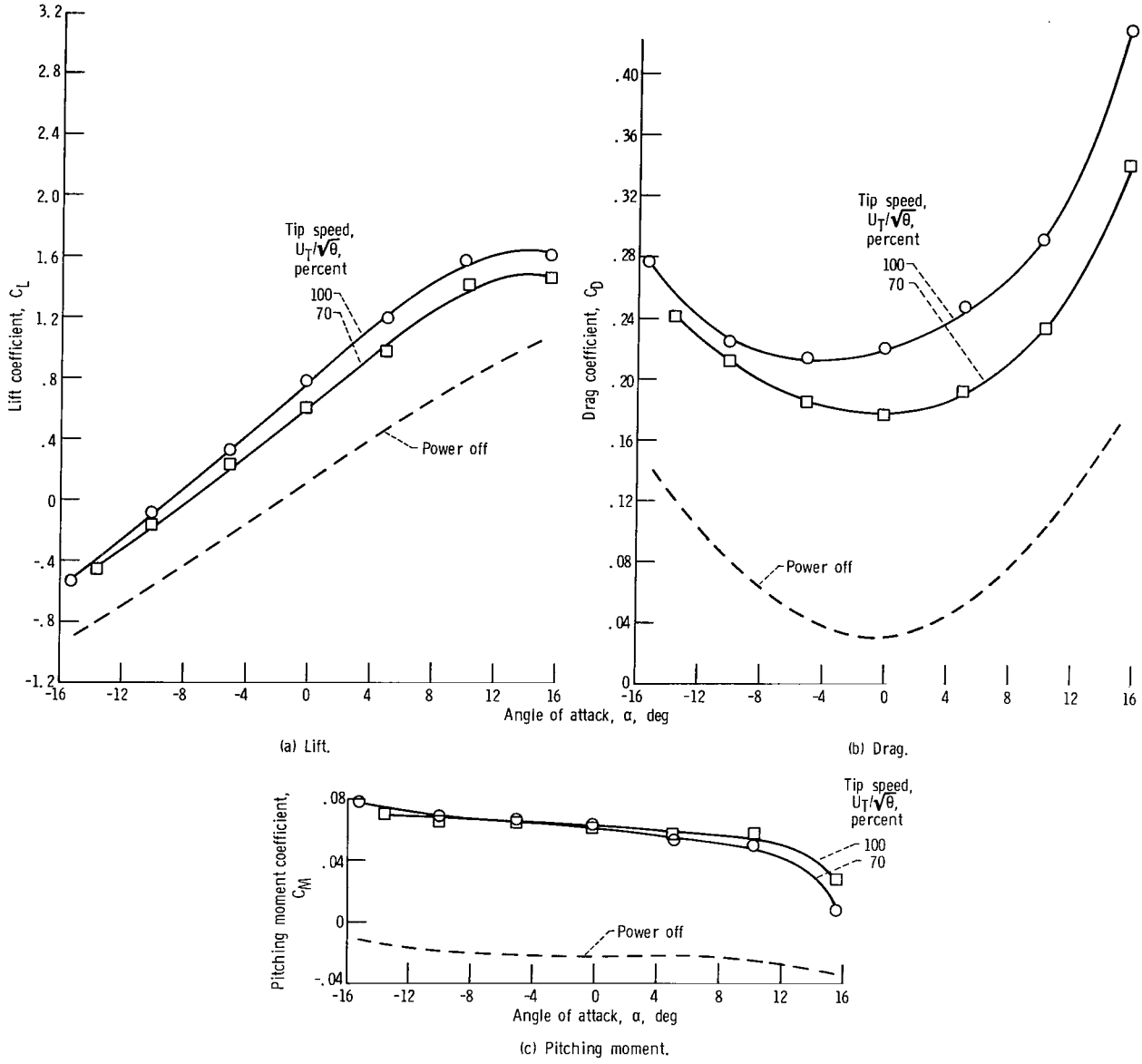

Figure 21. - Effect of angle of attack on overall aerodynamic characteristics of fan-in-wing configuration with louvers off. Crossflow velocity, 62.5 meters per second (205 ft/sec).

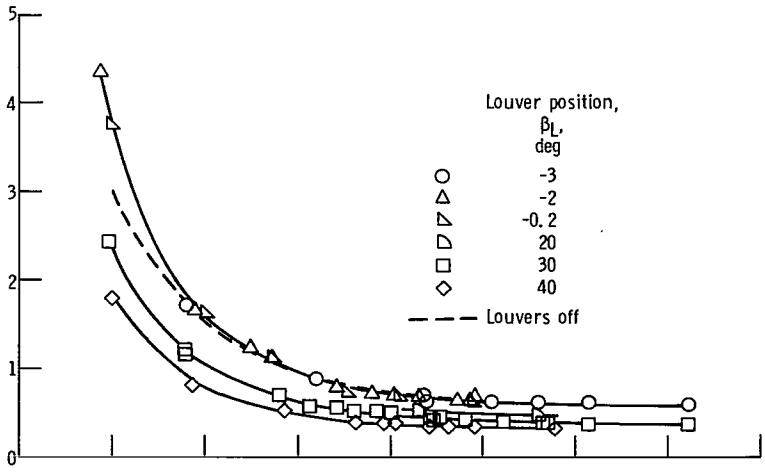

(a) Angle of attack, zero.

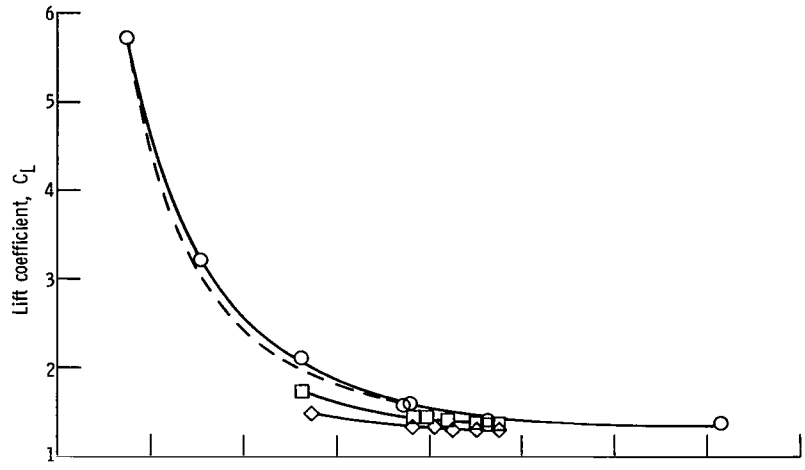

(b) Angle of attack, 10^0.

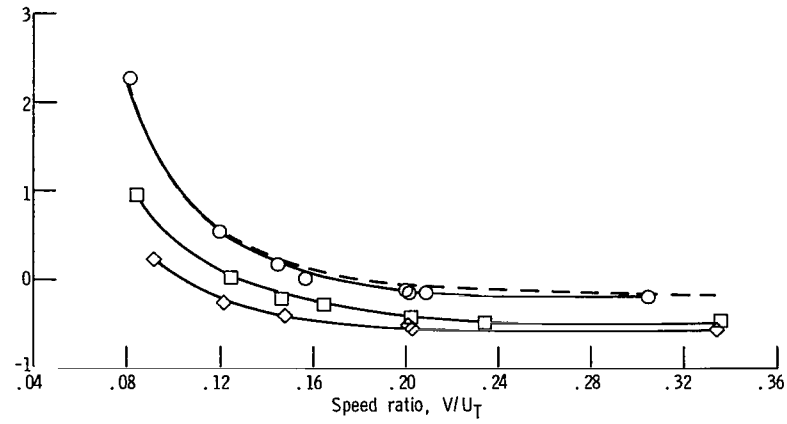

(c) Angle of attack, -10^0.

Figure 22. - Effect of exit louvers on power-on lift characteristics of fan-in-wing configuration in crossflow.

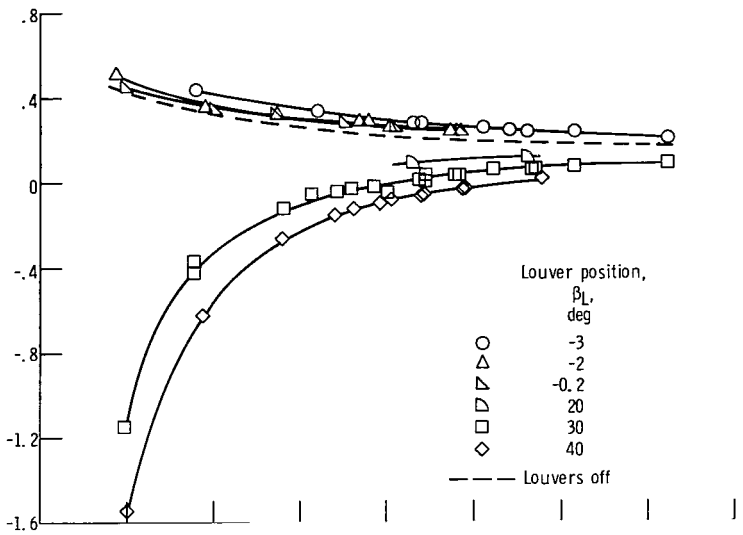

(a) Angle of attack, zero.

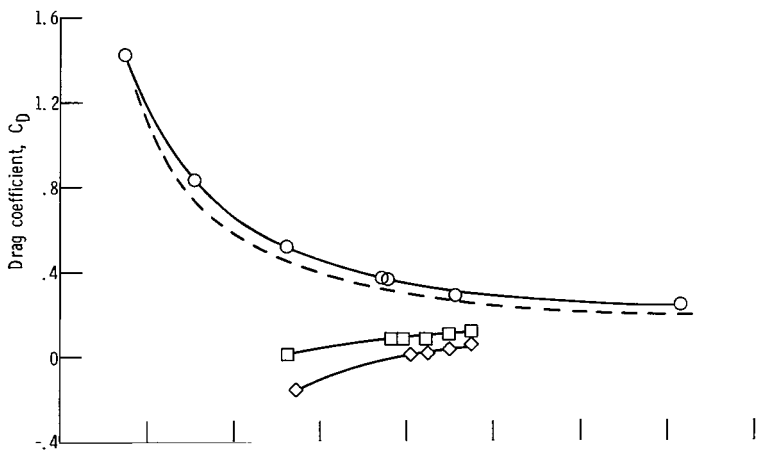

(b) Angle of attack, 10^0.

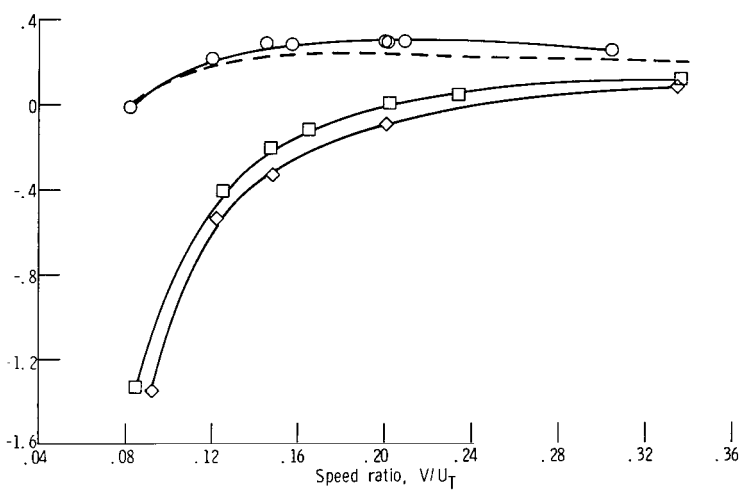

(c) Angle of attack, -10^0.

Figure 23. - Effect of exit louvers on power-on drag characteristics of fan-in-wing configuration in crossflow.

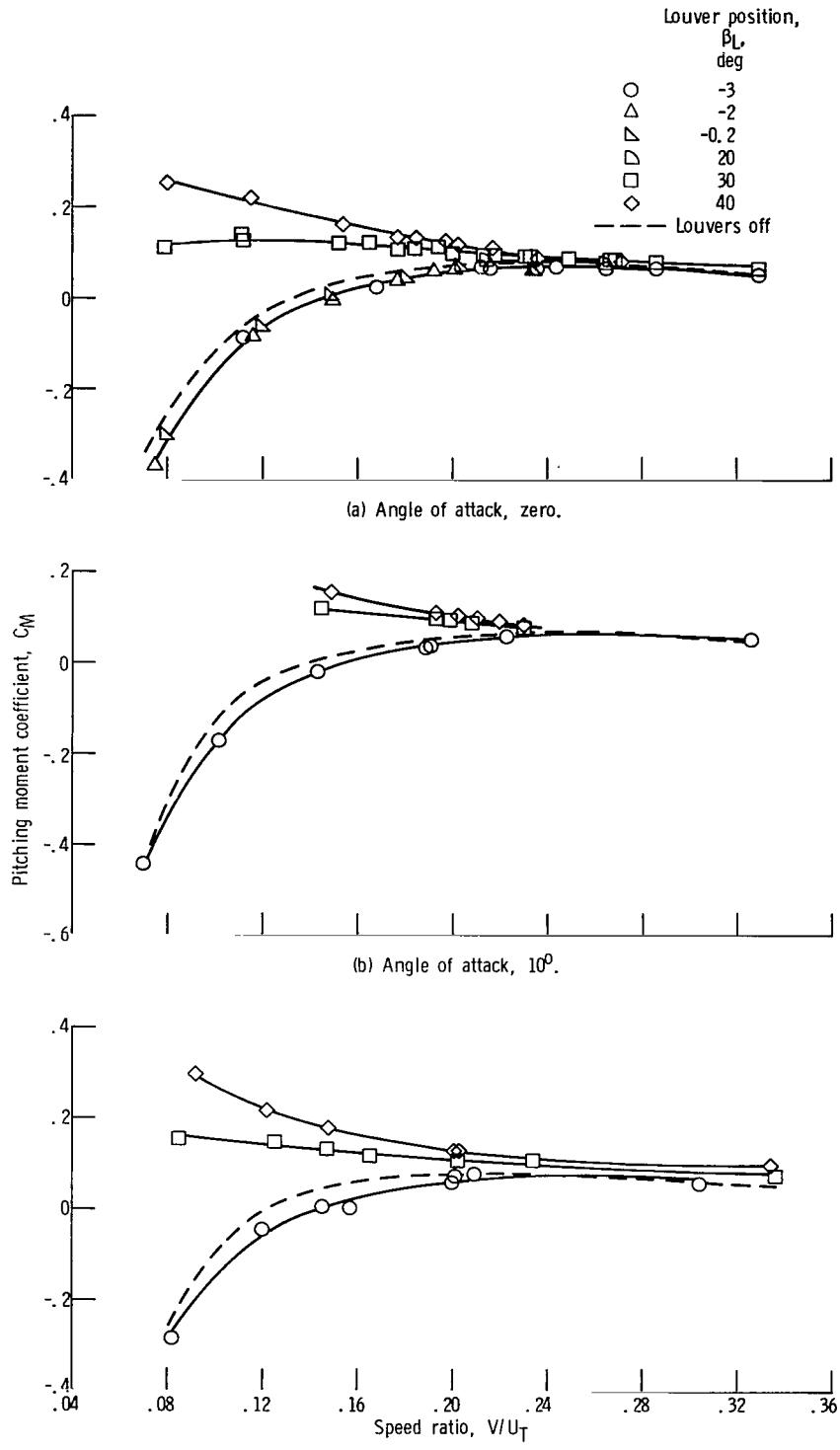

Figure 24. - Effect of exit louvers on power-on pitching moment characteristics of fan-in-wing configuration in crossflow.

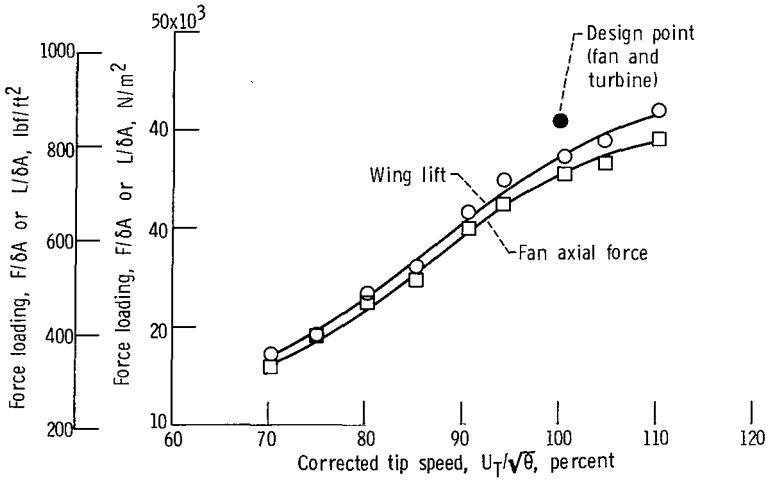

Figure 25. - Comparison of overall lift and fan axial force at zero crossflow velocity. Louvers off; zero angle of attack.

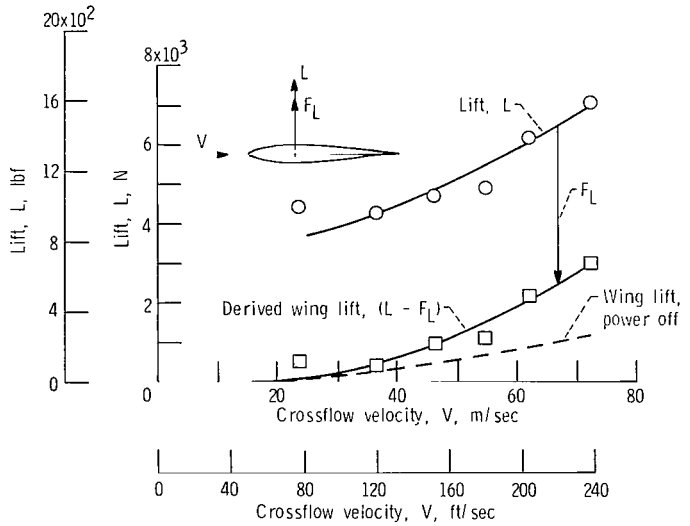

(a) Angle of attack, zero.

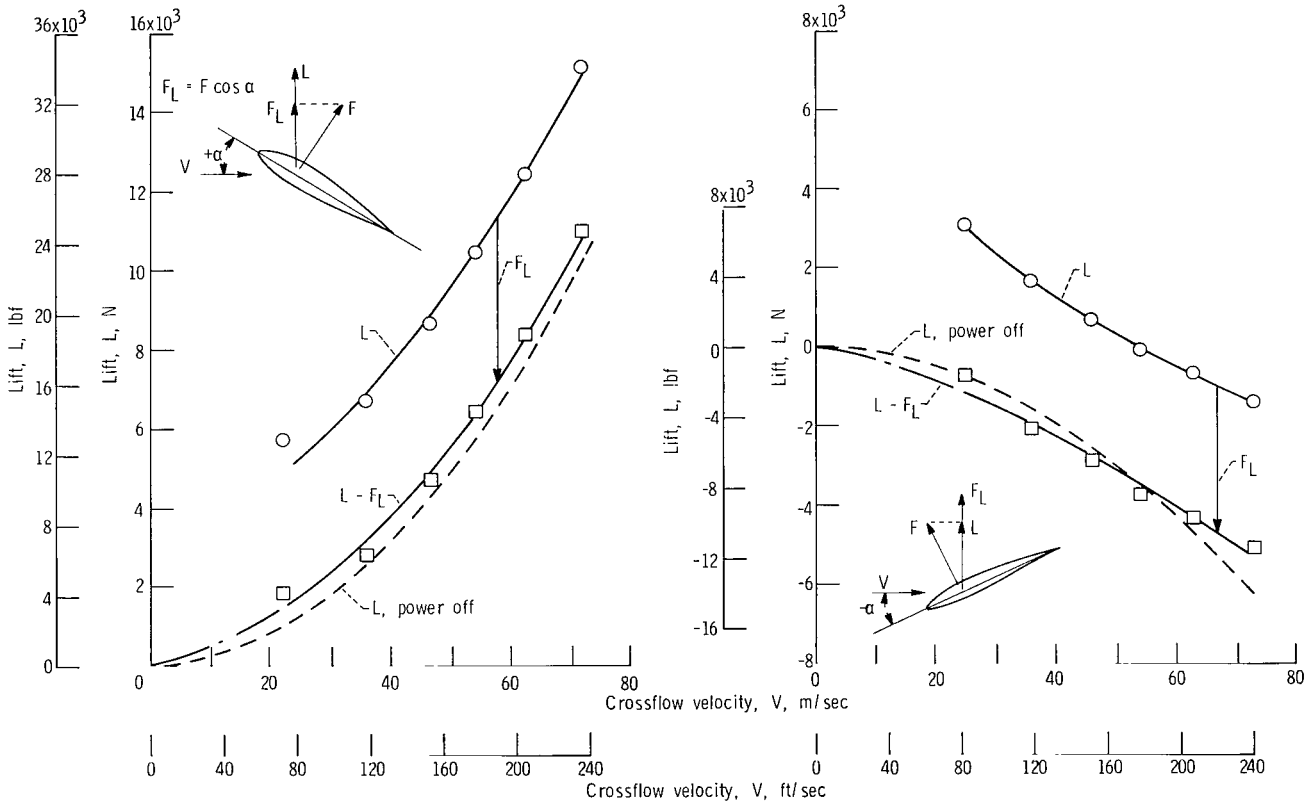

(b) Angle of attack, 10^{0}.

(c) Angle of attack, -10^{0}.

Figure 26. - Comparison of overall lift and axial force lift component. Louvers off; corrected fan speed, 100 percent of design.

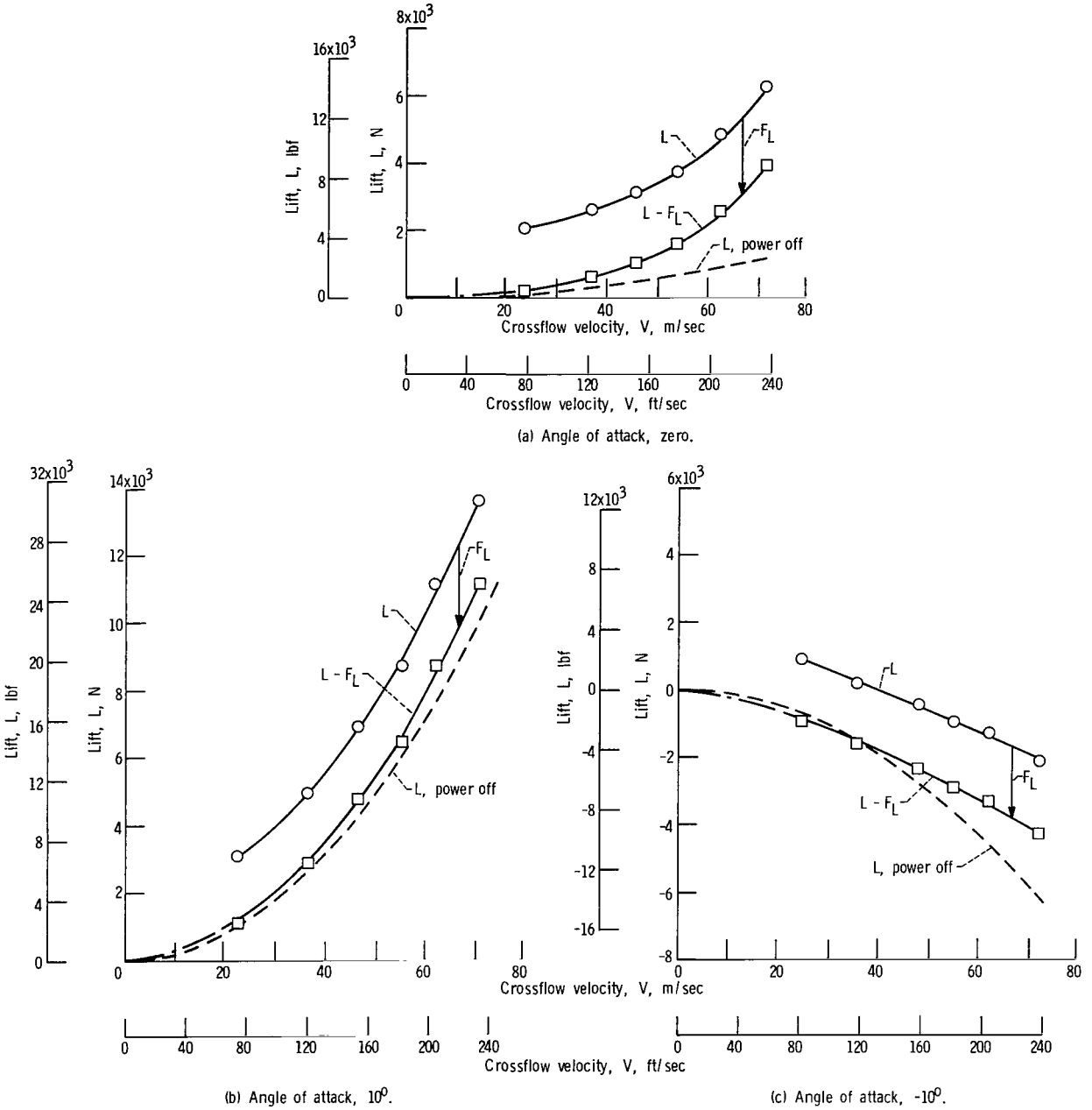

Figure 27. - Comparison of overall lift and axial-force lift component. Louvers off; corrected fan speed, 70 percent of design.

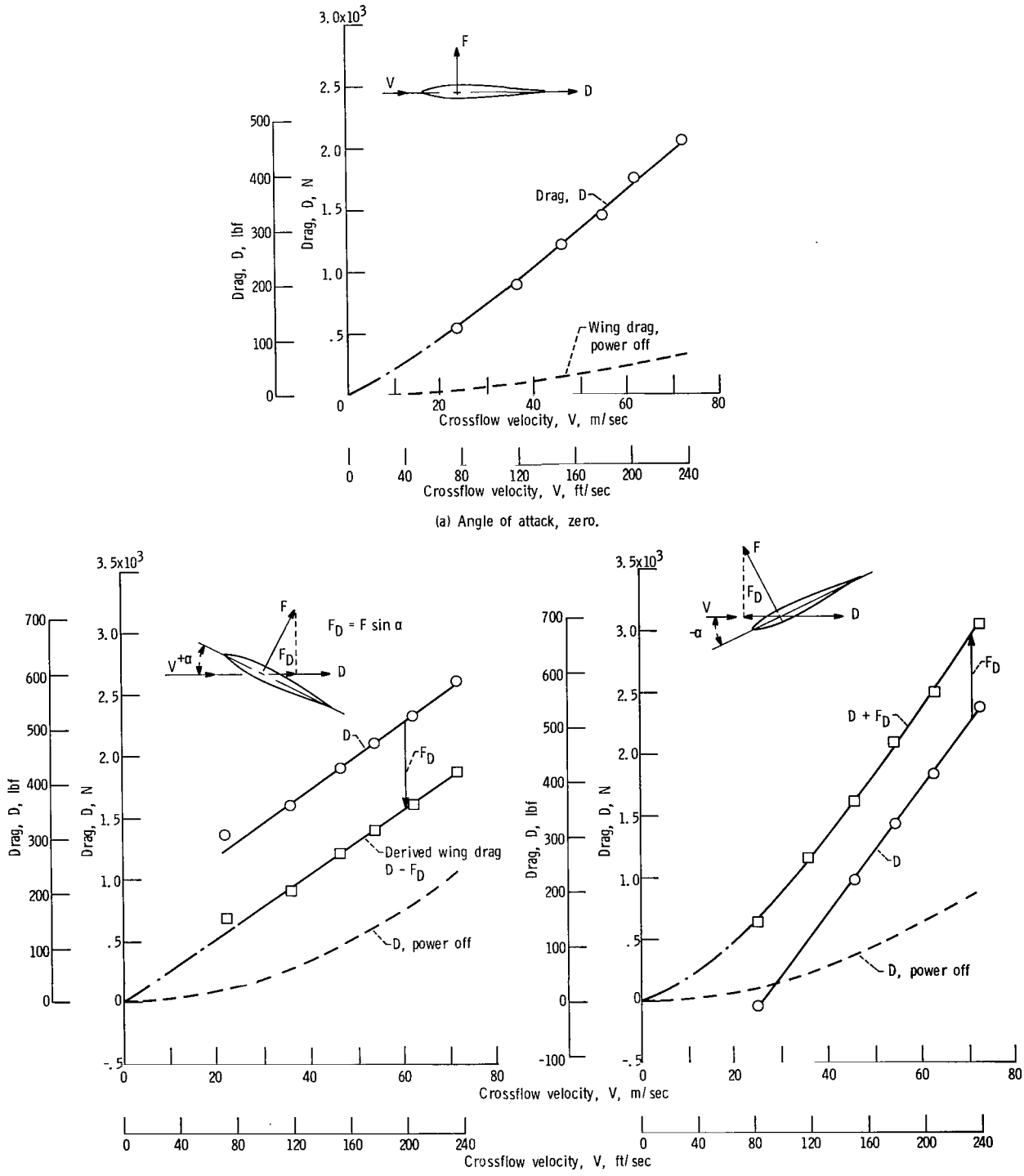

(a) Angle of attack, zero.

(b) Angle of attack, 10^0.

(c) Angle of attack, -10^0.

Figure 28. - Comparison of overall drag and axial-force drag component. Louvers off; corrected fan speed, 100 percent of design.

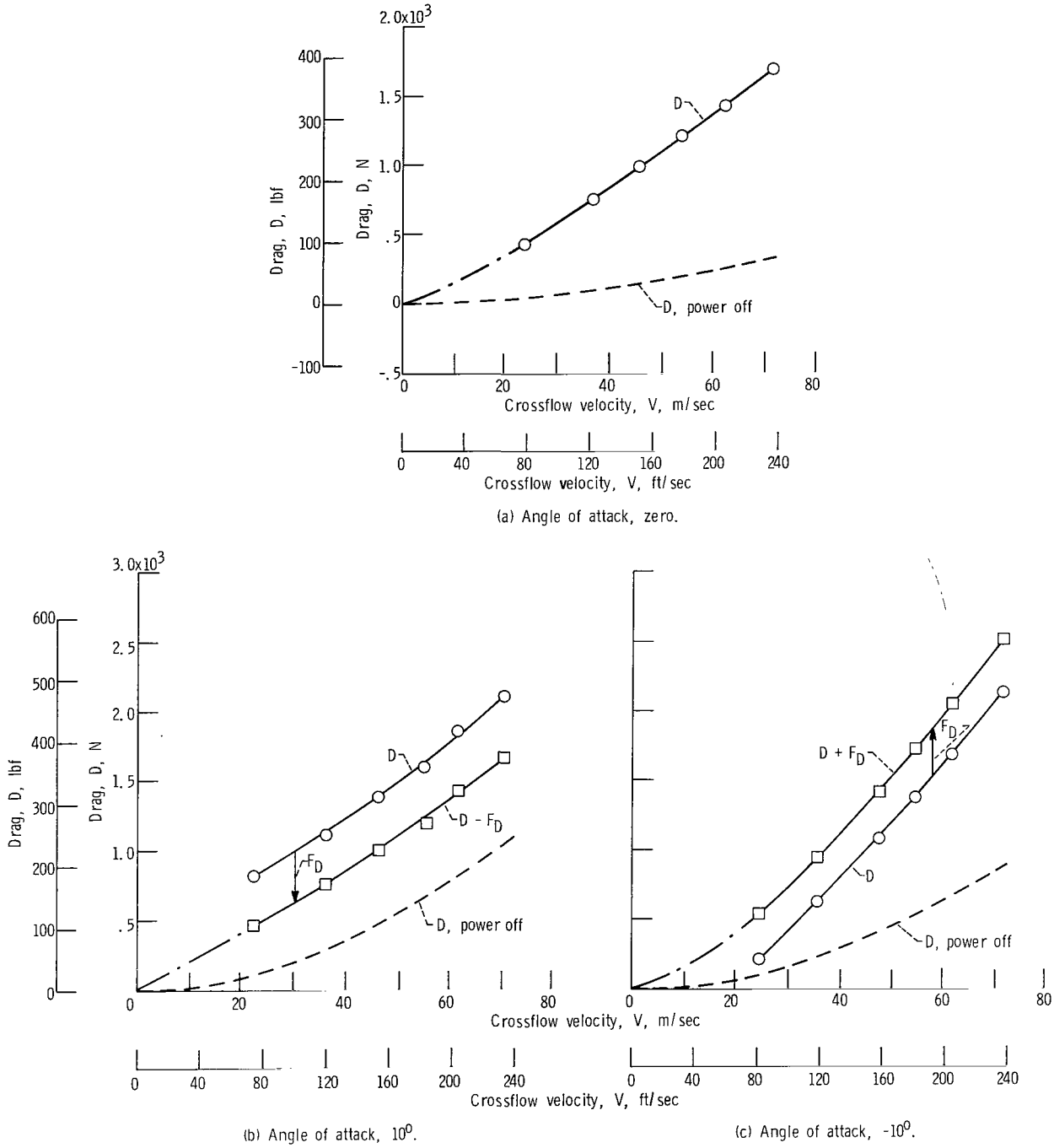

(a) Angle of attack, zero.

(b) Angle of attack, 10^{o}.

(c) Angle of attack, -10^{o}.

Figure 29. - Comparison of overall drag and axial-force drag component. Louvers off; corrected fan speed, 70 percent of design.

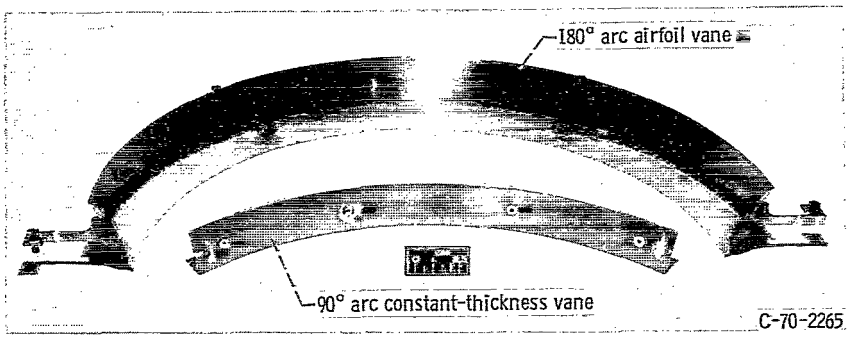

Figure 30. - Annular inlet vanes.

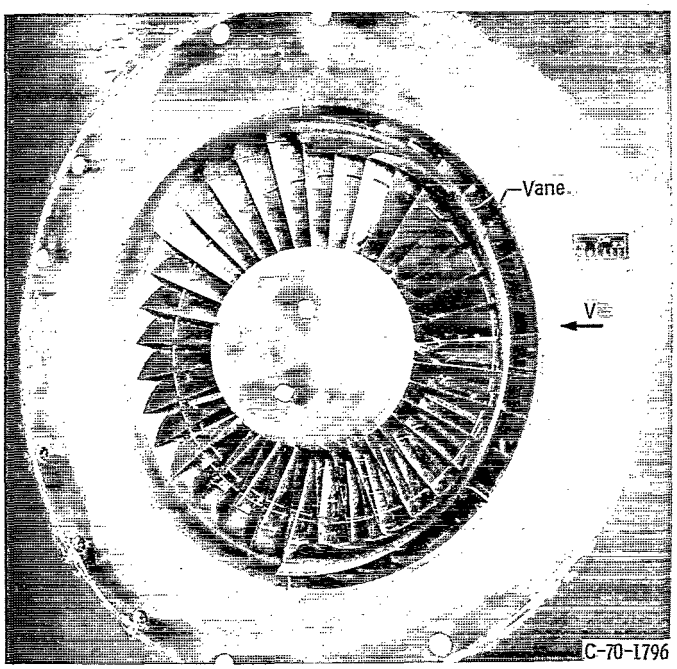

Figure 31. - 180° arc airfoil installed in fan inlet.

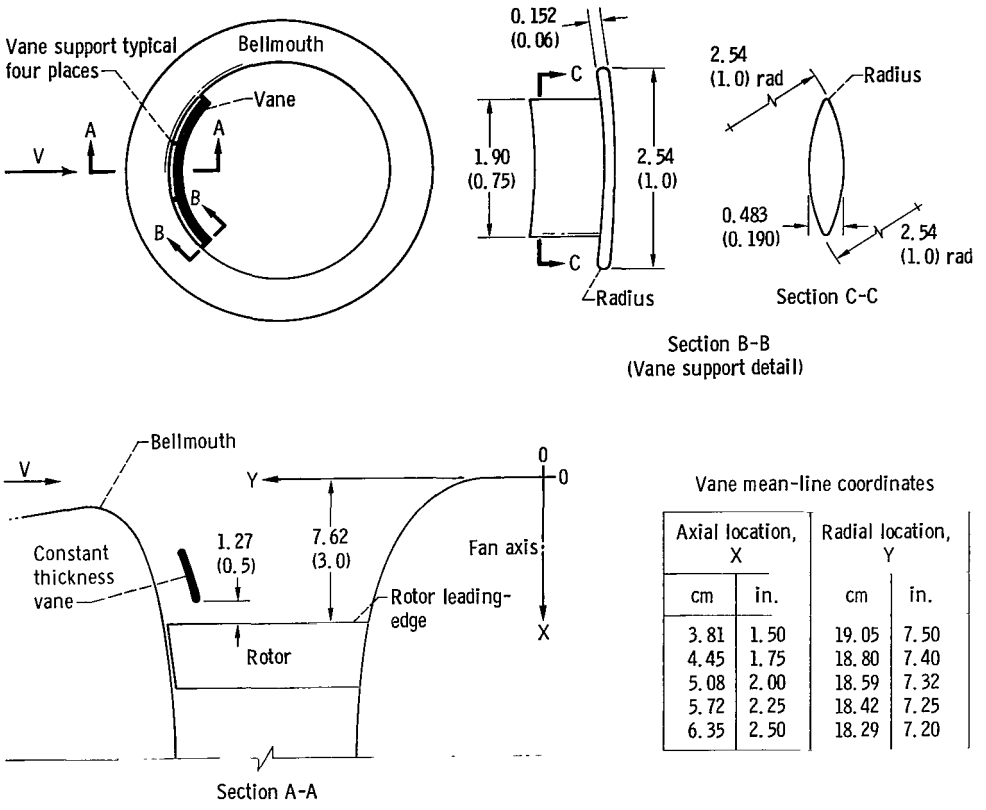

Vane mean-line coordinates

Axial location, X		Radial location, Y	
cm	in.	cm	in.
3.81	1.50	19.05	7.50
4.45	1.75	18.80	7.40
5.08	2.00	18.59	7.32
5.72	2.25	18.42	7.25
6.35	2.50	18.29	7.20

Figure 32. - 90° arc annular inlet vane. (All dimensions are in cm (in.).)

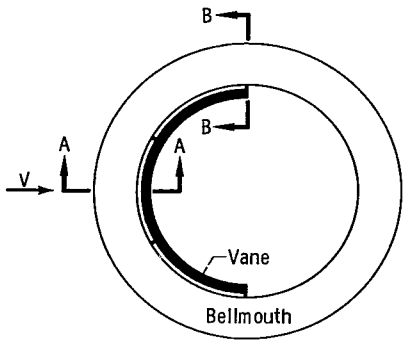

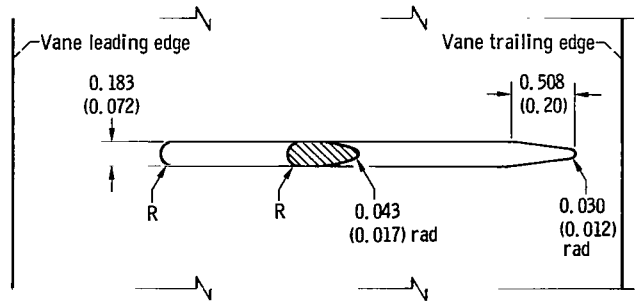

Section C-C

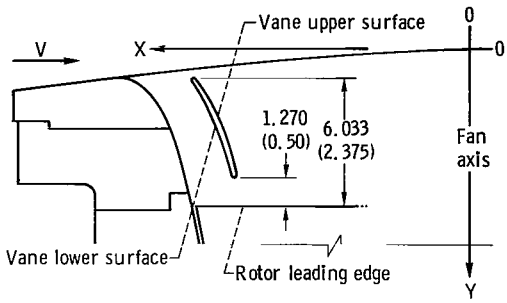

Section A-A

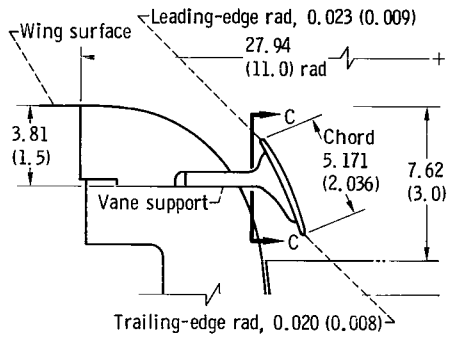

Section B-B

Vane mean line coordinates

Axial location, X		Radial location, Y	
cm	in.	cm	in.
1.57	0.62	18.819	7.409
1.78	.70	18.682	7.355
2.03	.80	18.506	7.286
2.29	.90	18.344	7.222
2.54	1.00	18.207	7.168
2.79	1.10	18.054	7.108
3.05	1.20	17.930	7.059
3.30	1.30	17.810	7.012
3.56	1.40	17.694	6.966
3.81	1.50	17.590	6.925
4.06	1.60	17.475	6.880
4.32	1.70	17.394	6.848
4.57	1.80	17.305	6.813
4.83	1.90	17.224	6.781
5.08	2.00	17.145	6.750
5.33	2.10	17.069	6.720
5.59	2.20	16.998	6.692
5.84	2.30	16.937	6.668
6.10	2.40	16.876	6.644
6.35	2.50	16.815	6.620

Figure 33. - 180° arc annular airfoil vane. NACA 65 series airfoil section; 7 percent thickness distribution.

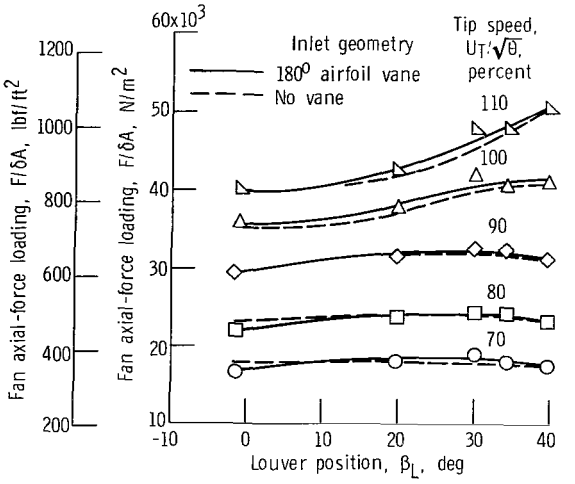

Figure 34. - Effect of 180° arc airfoil vane on fan static performance; louvers on.

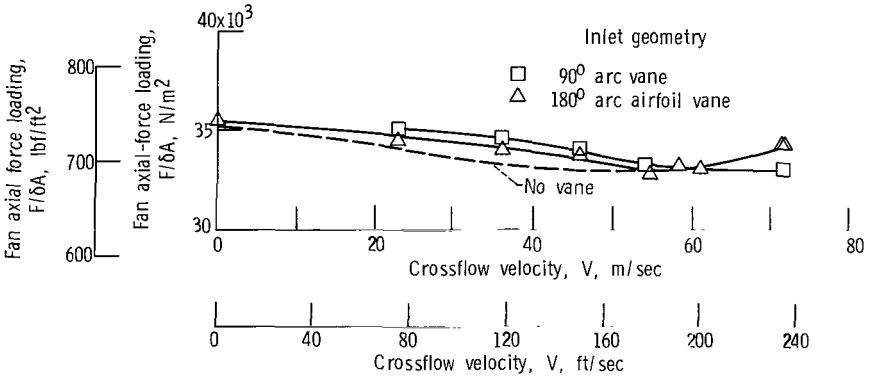

Figure 35. - Effect of inlet vanes on fan performance in crossflow. Louver position, zero; angle of attack, zero; corrected fan speed, 100 percent of design.

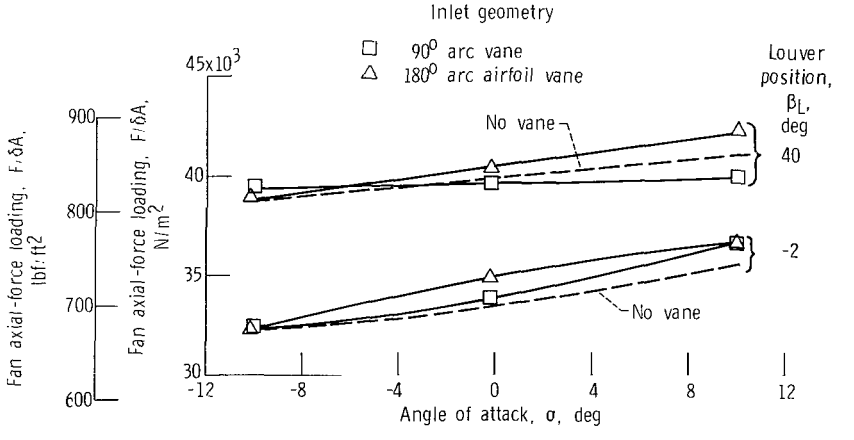

Figure 36. - Effect of inlet vanes on fan performance in crossflow performance. Corrected fan speed, 100 percent of design; crossflow velocity, 68.6 meters per second (225 ft/sec).

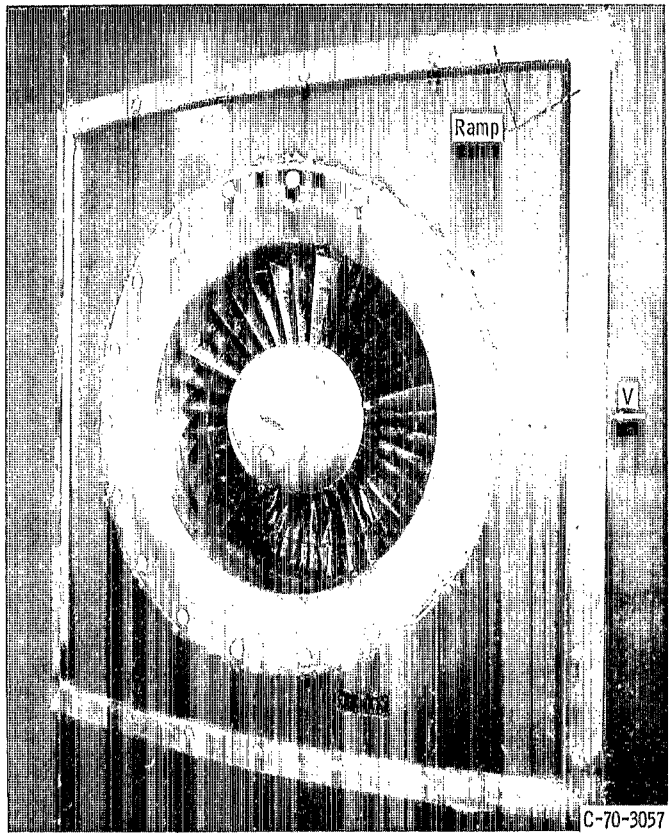

Figure 37. - Surface ramp installation.

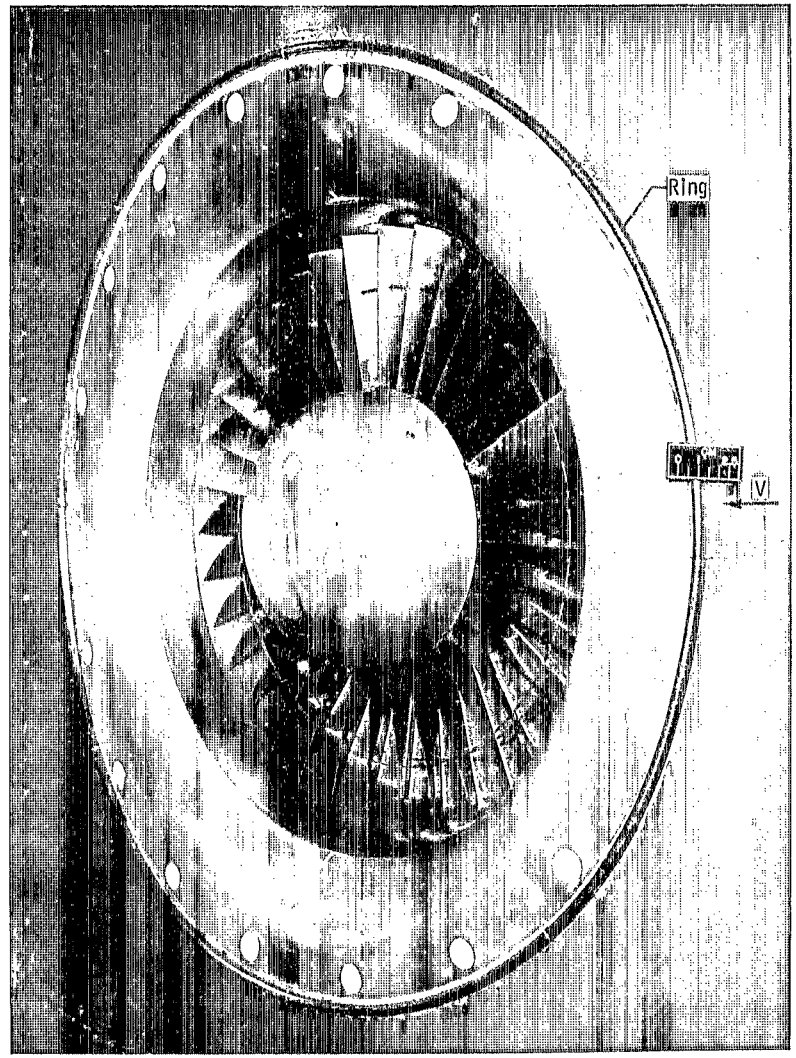

Figure 38. - Wire ring installation.

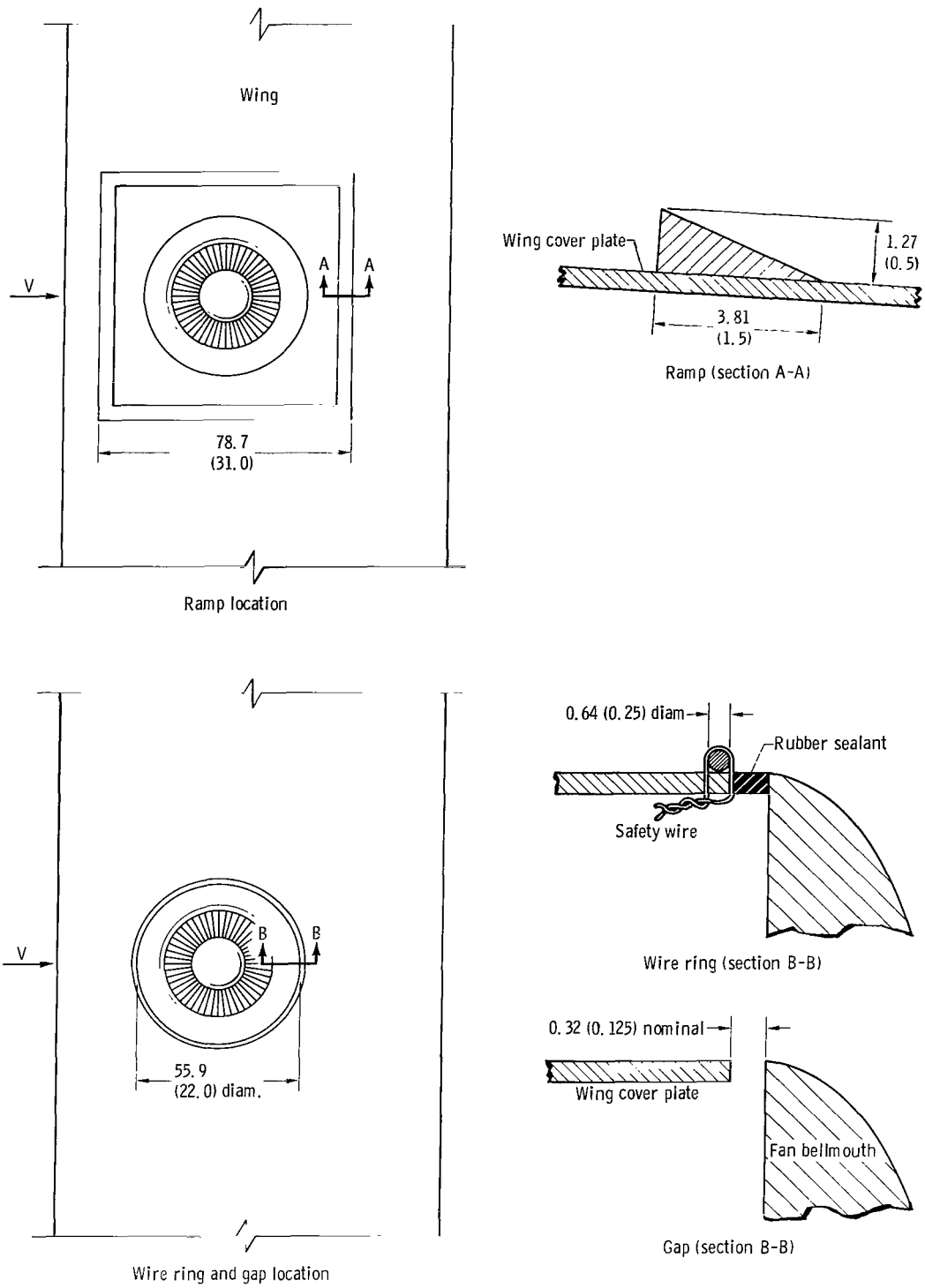

Figure 39. - Details of surface discontinuities. (All dimensions are in cm (in.).)

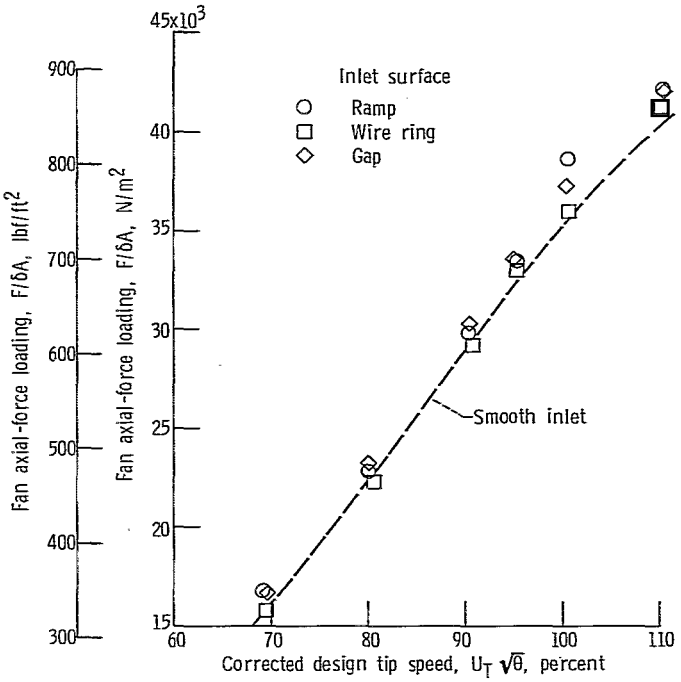

Figure 40. - Effect of inlet surface discountinuities on fan static performance; louvers off. Fan axis parallel to tunnel centerline.

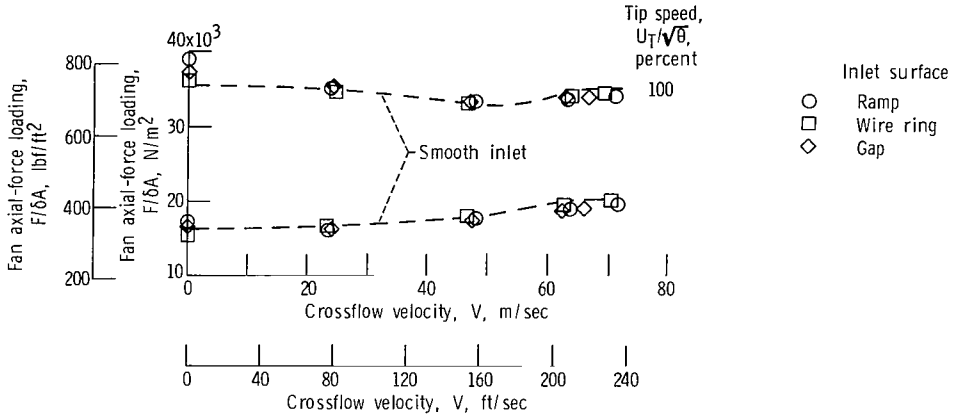

(a) Angle of attack, zero.

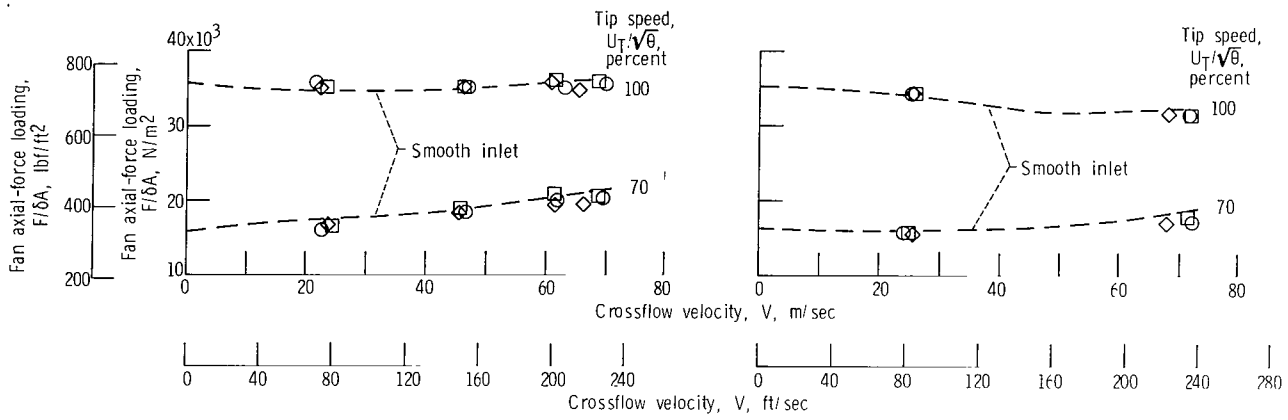

(b) Angle of attack, 10^0.

(c) Angle of attack, -10^0.

Figure 41. - Effect of inlet surface discontinuities on fan performance in crossflow; louvers off.

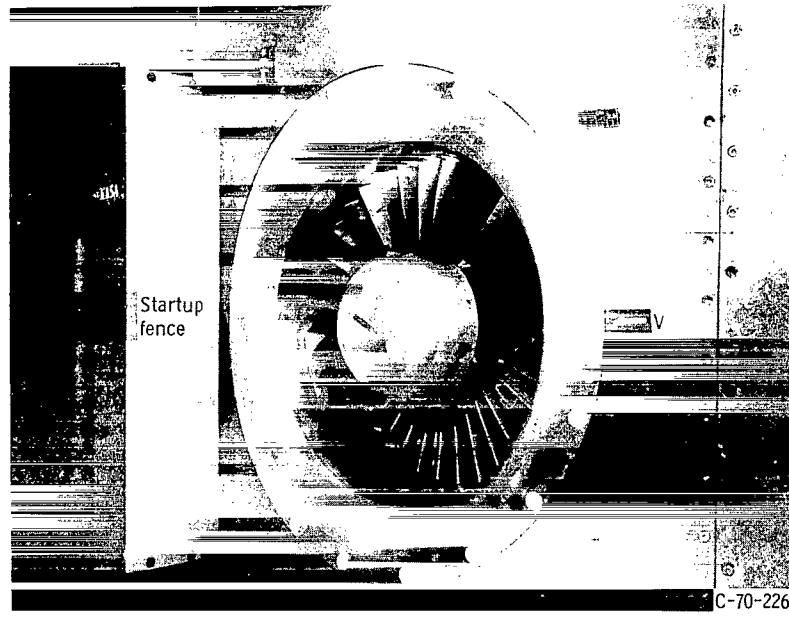

Figure 42. - Startup fence installation.

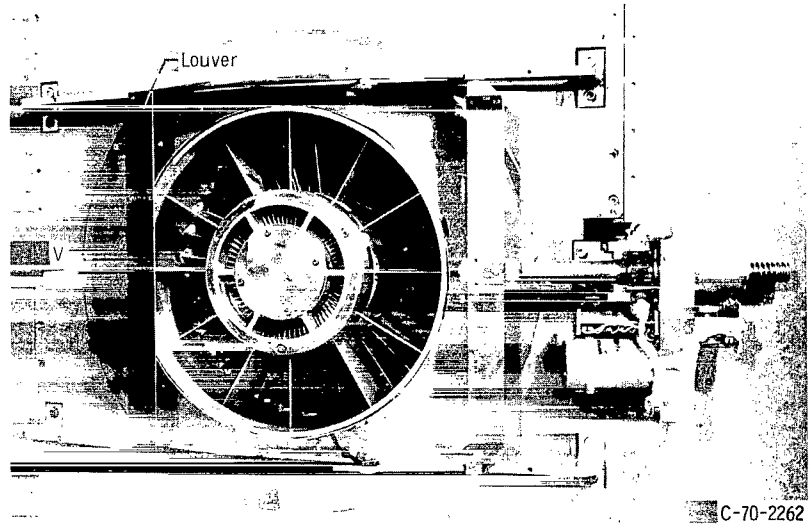

Figure 43. - Single-exit louver installation.

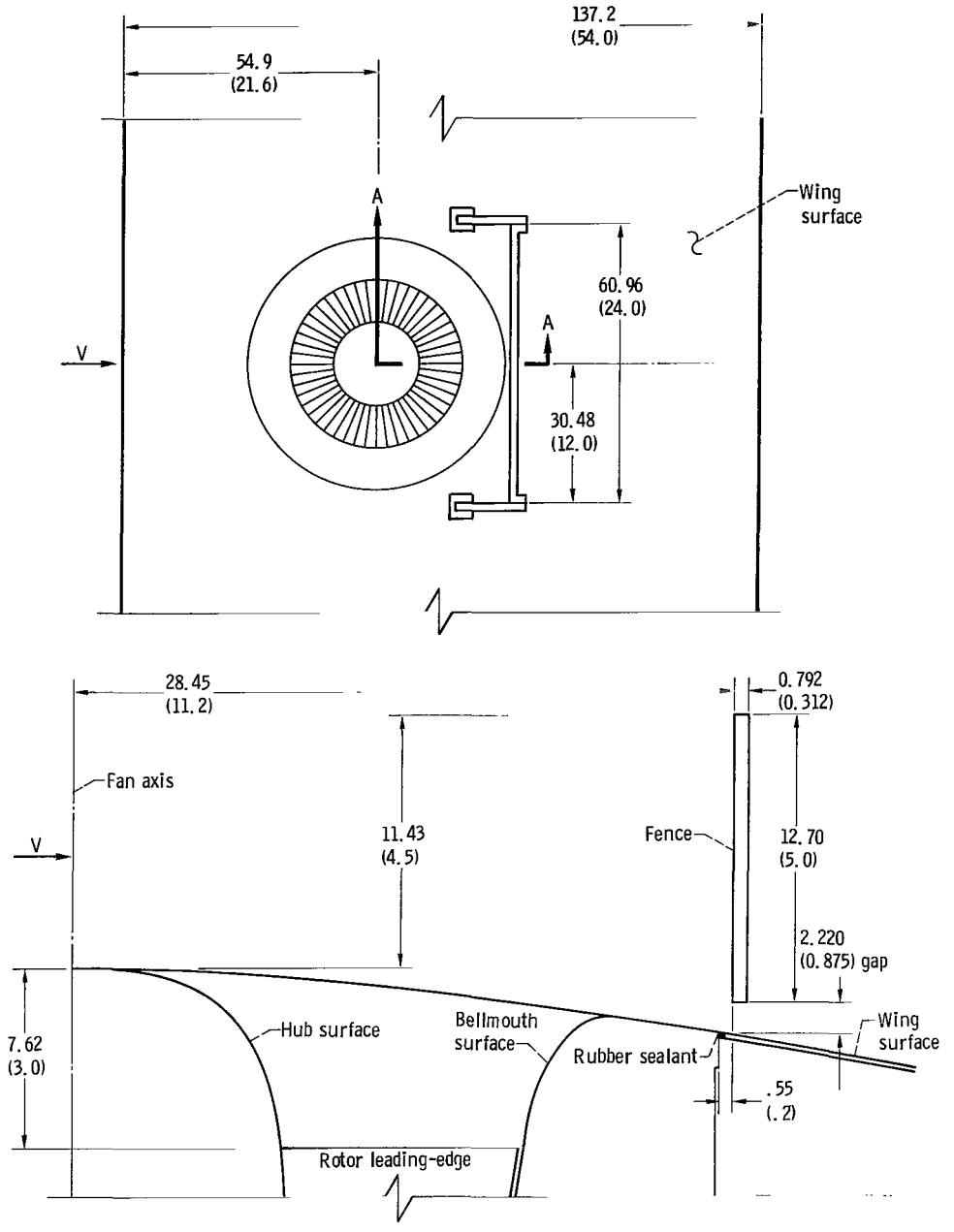

Section A-A

Figure 44. - Startup fence for fan windmill tests. (All dimensions are in cm (in.).)

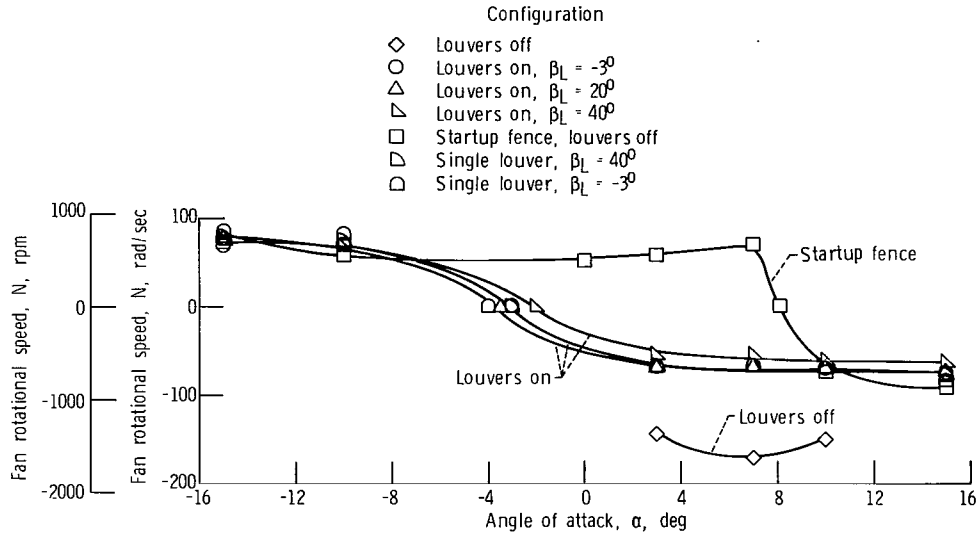

Figure 45. - Effect of various model configurations on fan windmill speed at crossflow velocity, 61 meters per second (200 ft/sec).

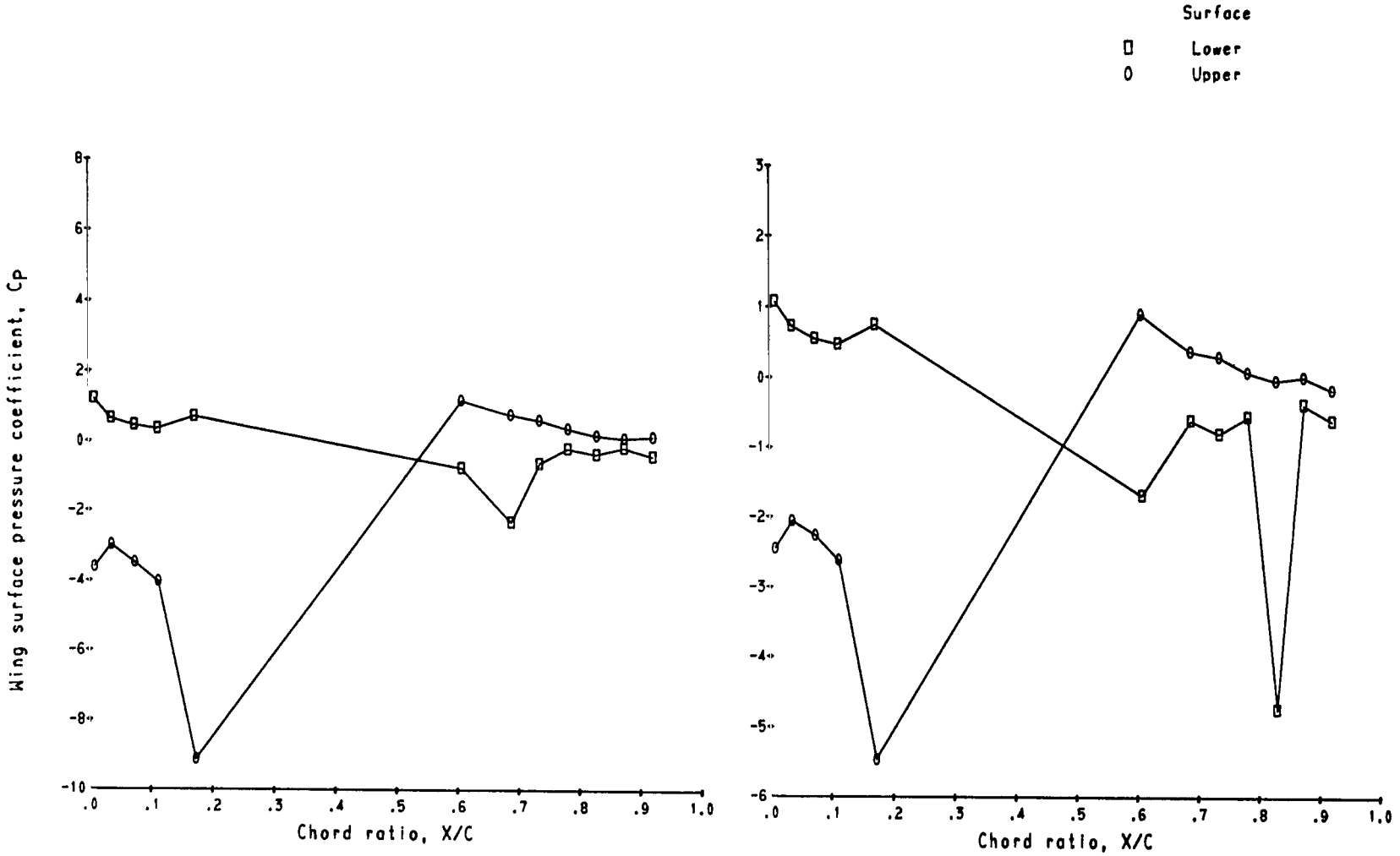

(a) Speed ratio, 0.071.

(b) Speed ratio, 0.119.

Figure 46. - Wing surface pressure coefficient distribution variation with speed ratio. Louvers off; angle of attack, zero.

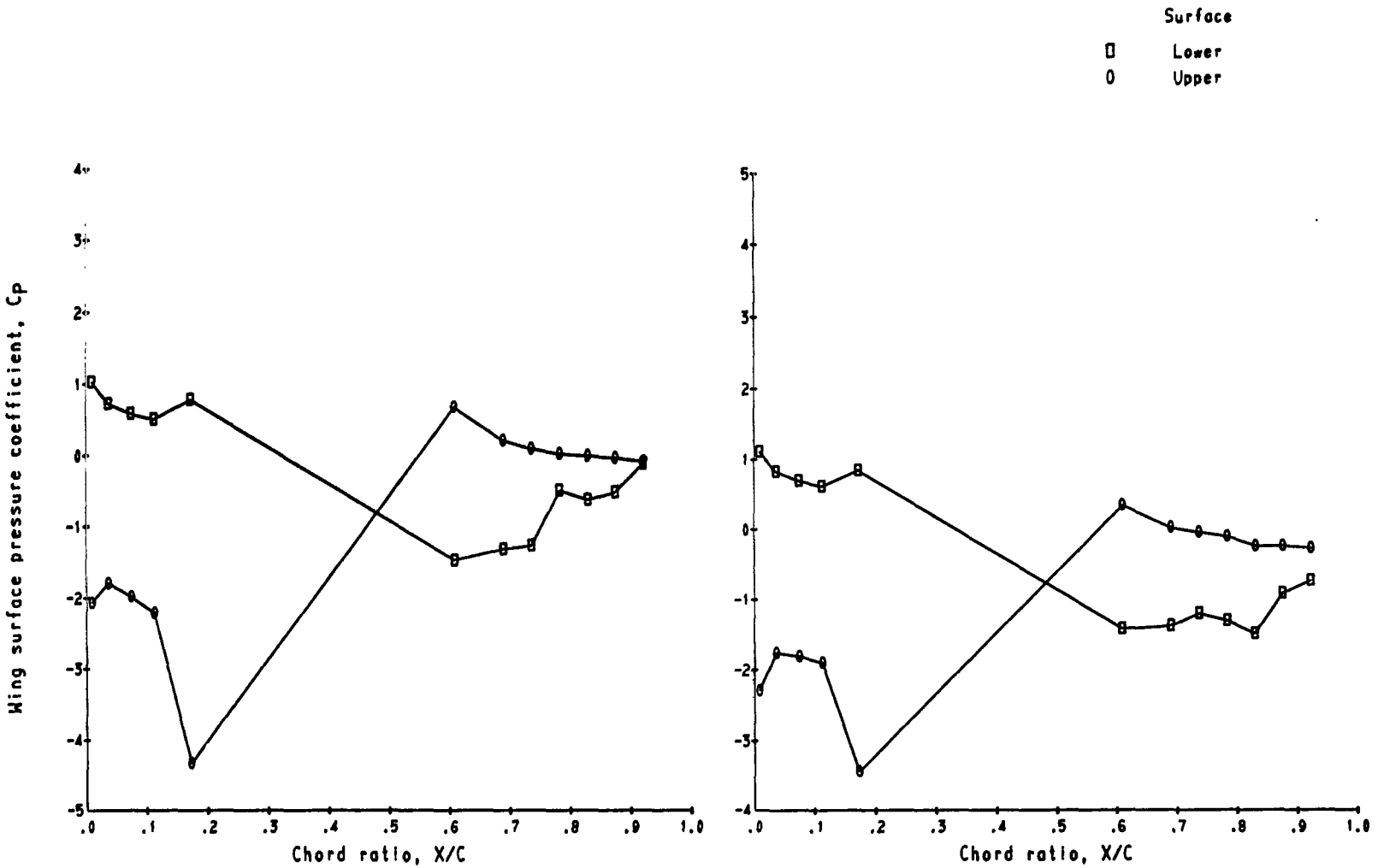

(c) Speed ratio, 0.150.

(d) Speed ratio, 0.198.

Figure 46. - Continued.

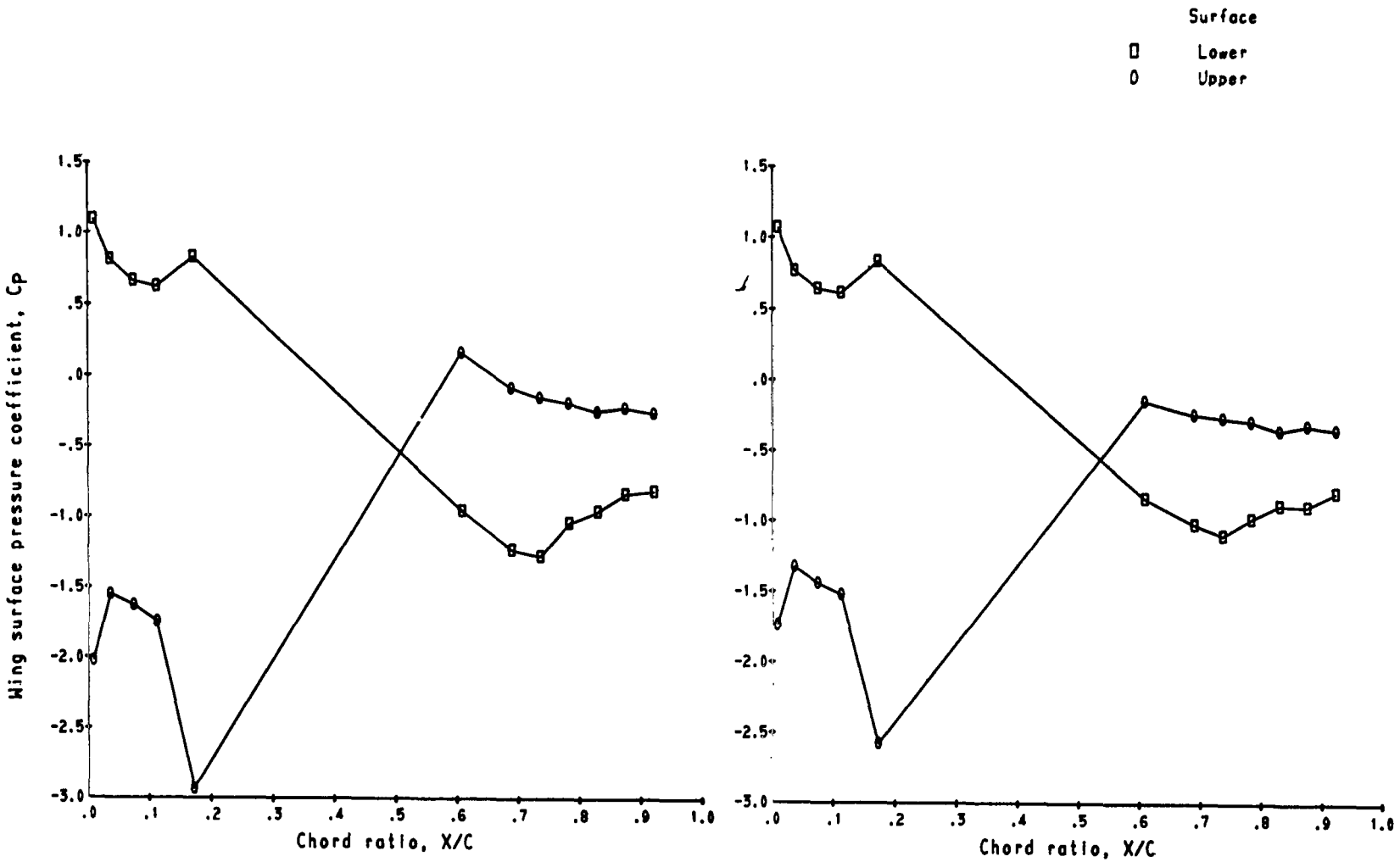

(e) Speed ratio, 0.232.

(f) Speed ratio, 0.332.

Figure 46. - Concluded.

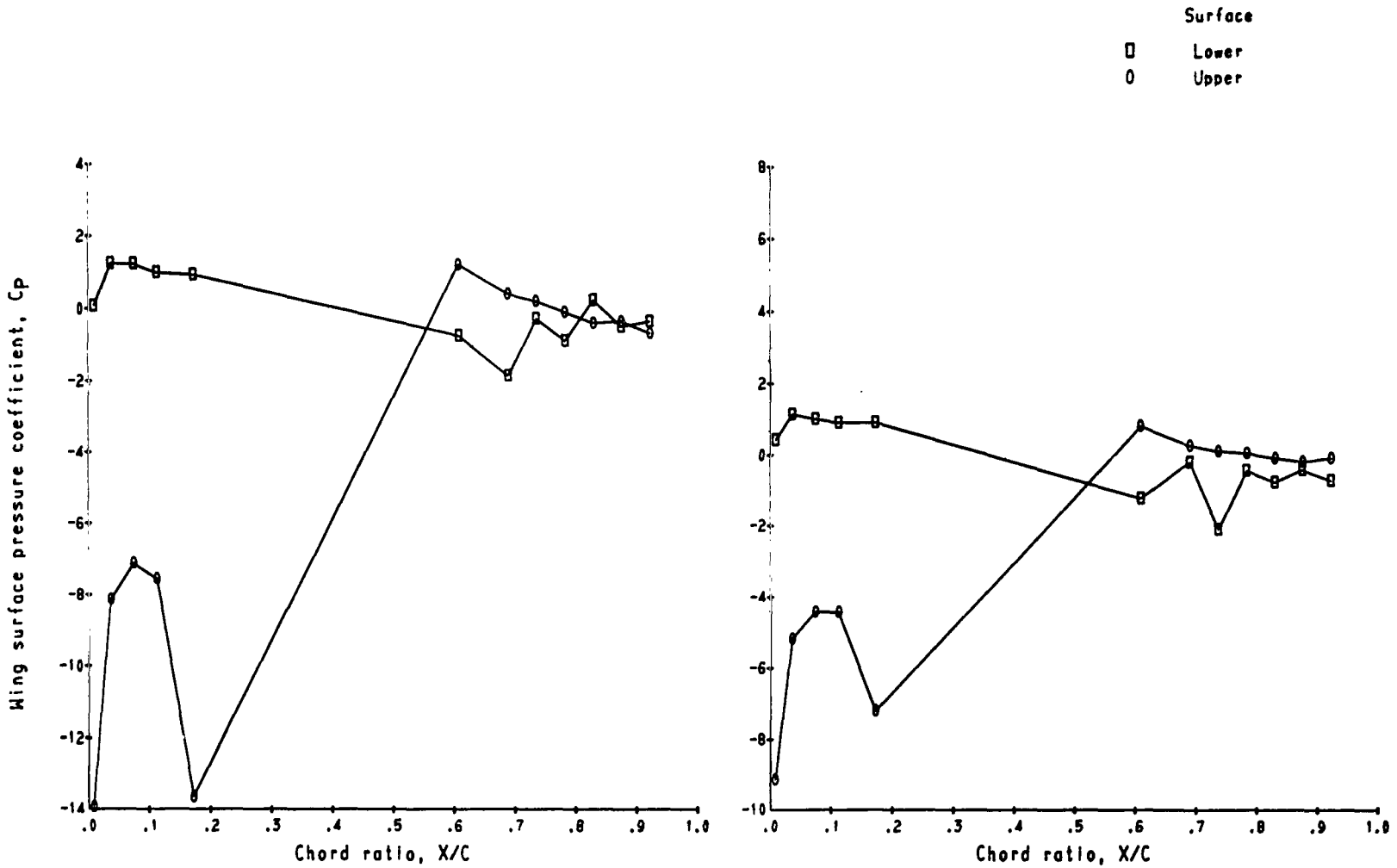

(a) Speed ratio, 0.073.

(b) Speed ratio, 0.117.

Figure 47. - Wing surface pressure coefficient distribution variations with speed ratio. Louvers off; angle of attack, 10^0.

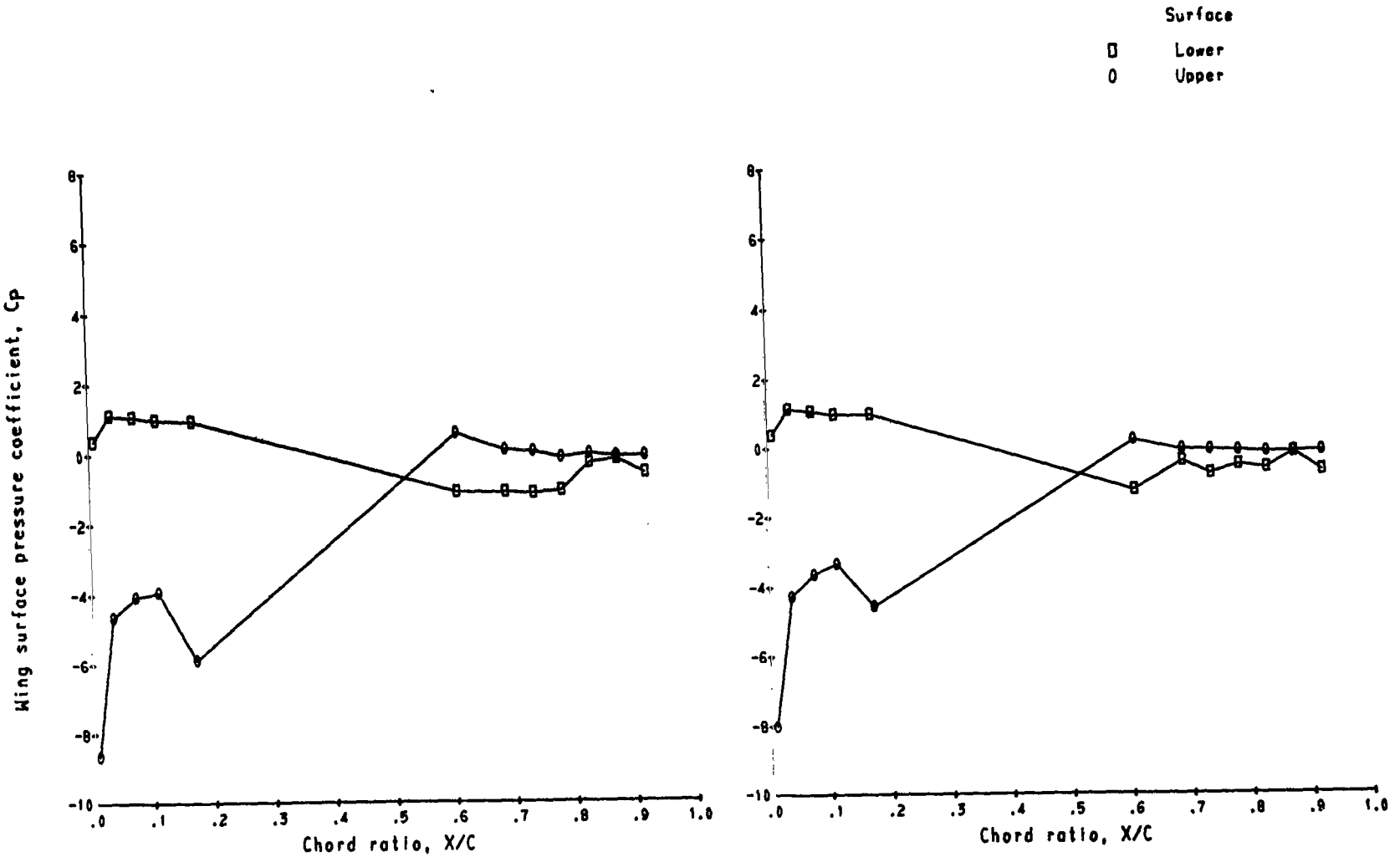

(c) Speed ratio, 0.151.

(d) Speed ratio, 0.199.

Figure 47. - Continued.

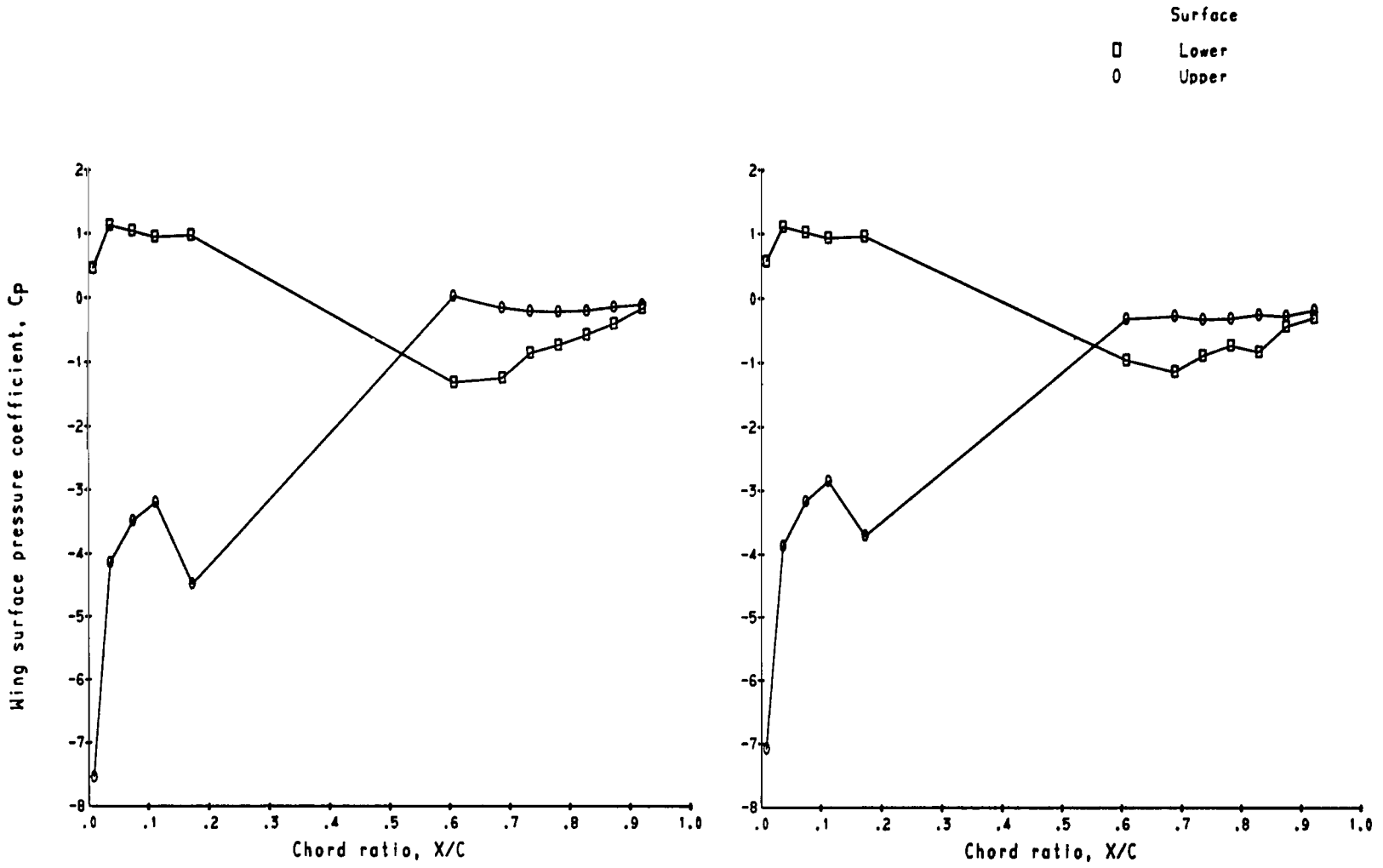

(e) Speed ratio, 0.254.

(f) Speed ratio, 0.326.

Figure 47. - Concluded.

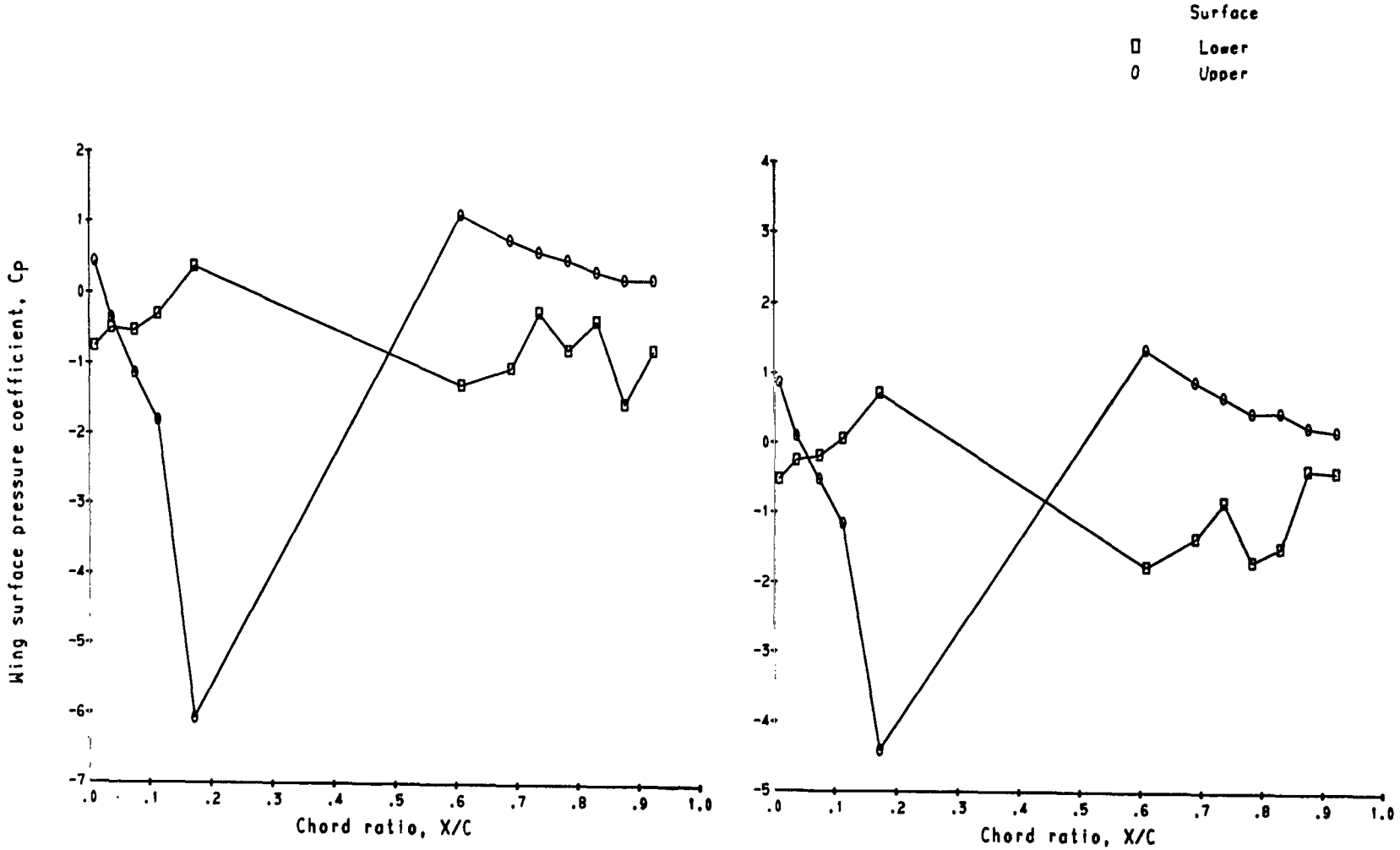

(a) Speed ratio, 0.081.

(b) Speed ratio, 0.114.

Figure 48. - Wing surface pressure coefficient distribution variations with speed ratio. Louvers off; angle of attack, -10^{0}.

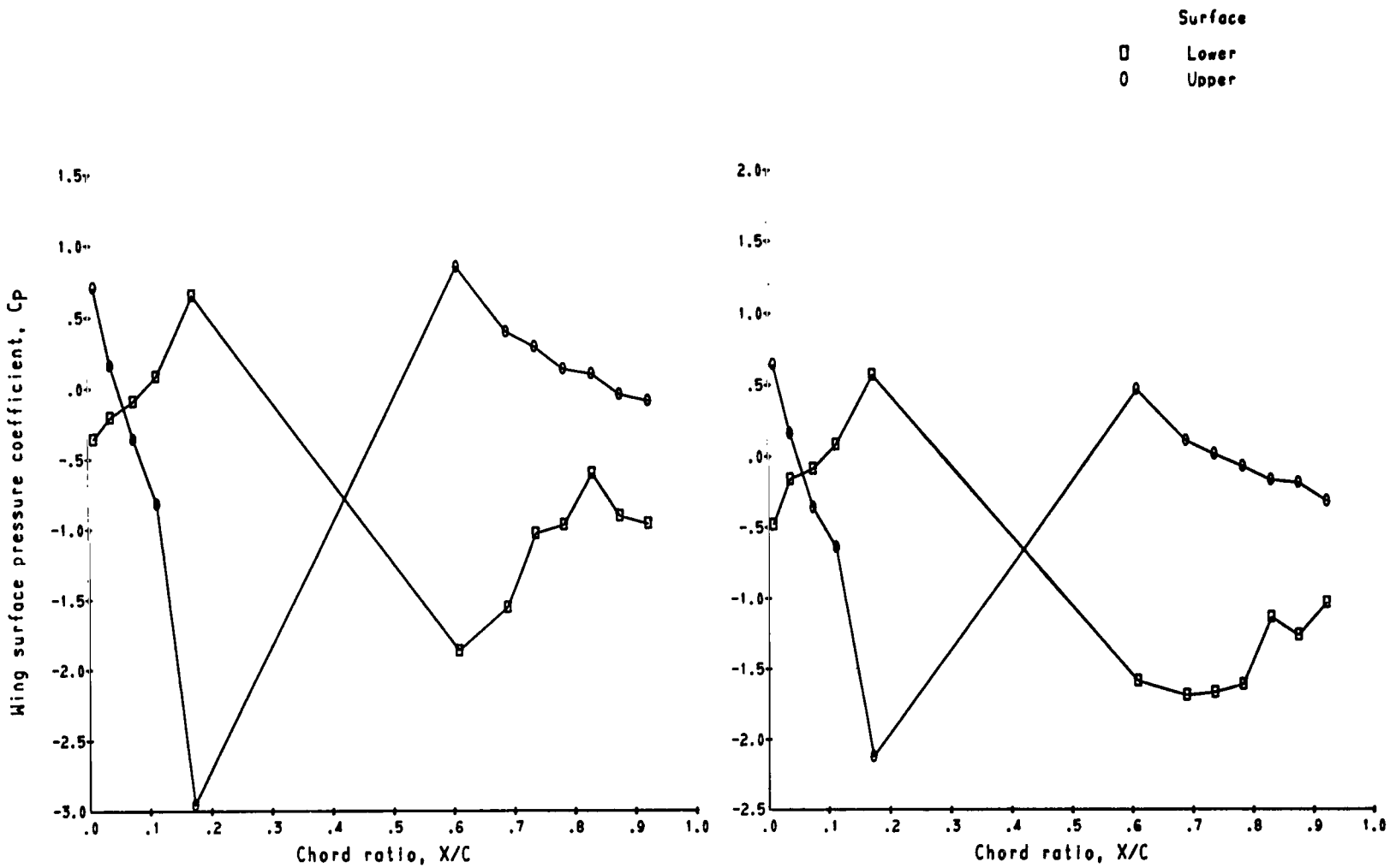

(c) Speed ratio, 0.166.

(d) Speed ratio, 0.202.

Figure 48. - Continued.

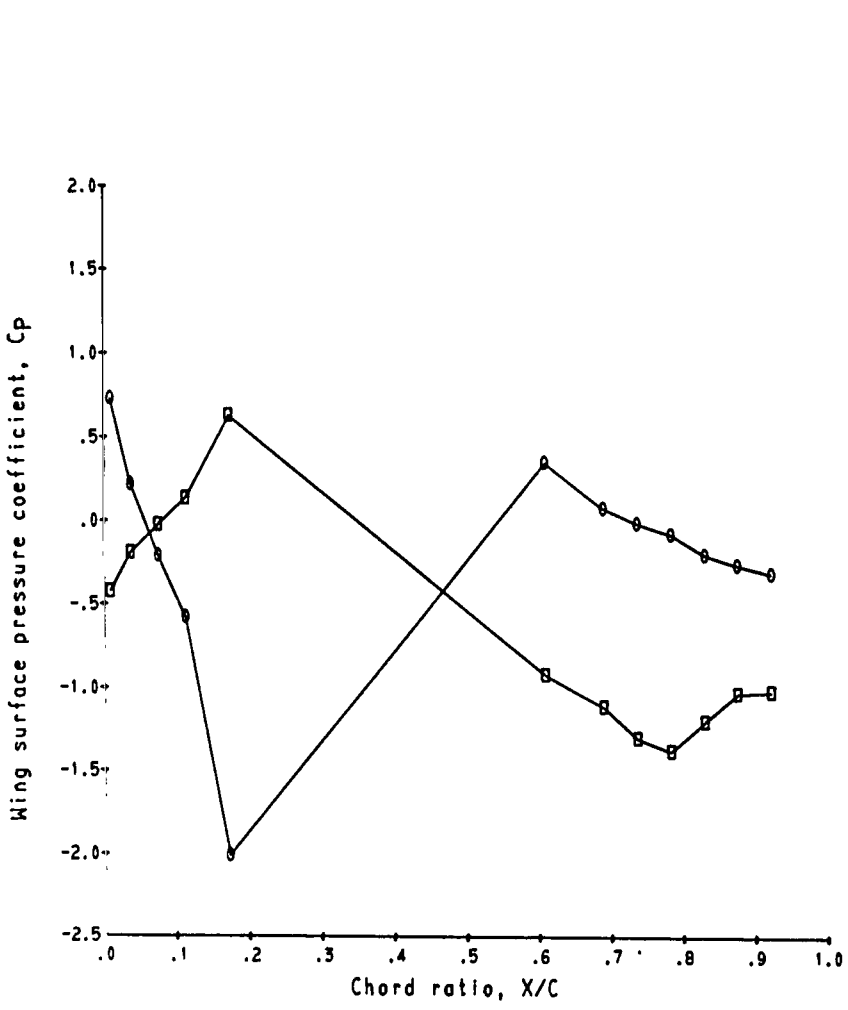

(e) Speed ratio, 0.253.

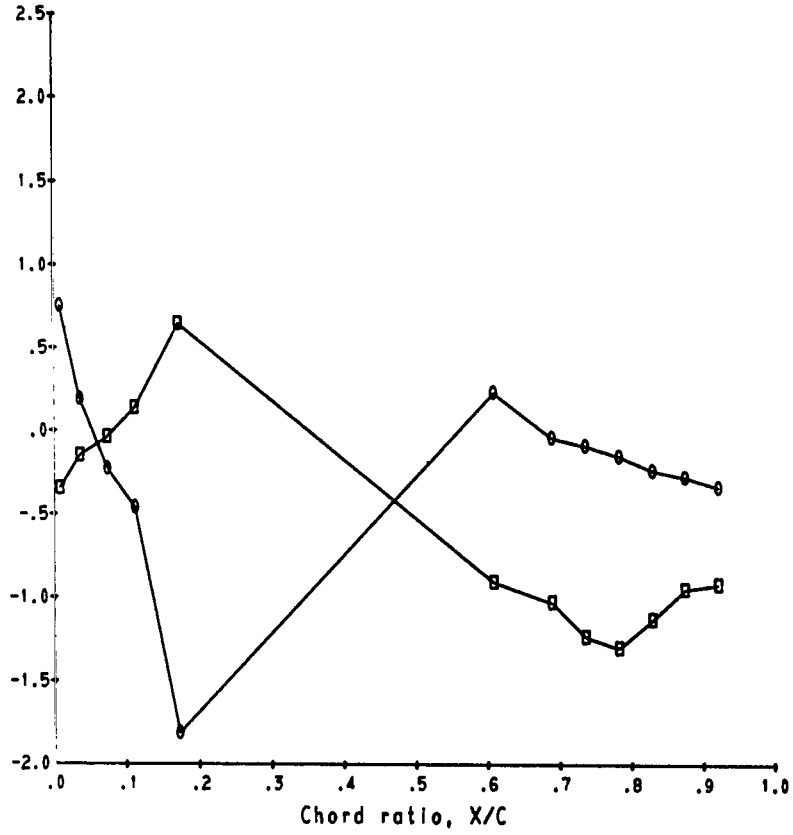

(f) Speed ratio, 0.285.

Figure 48. - Concluded.

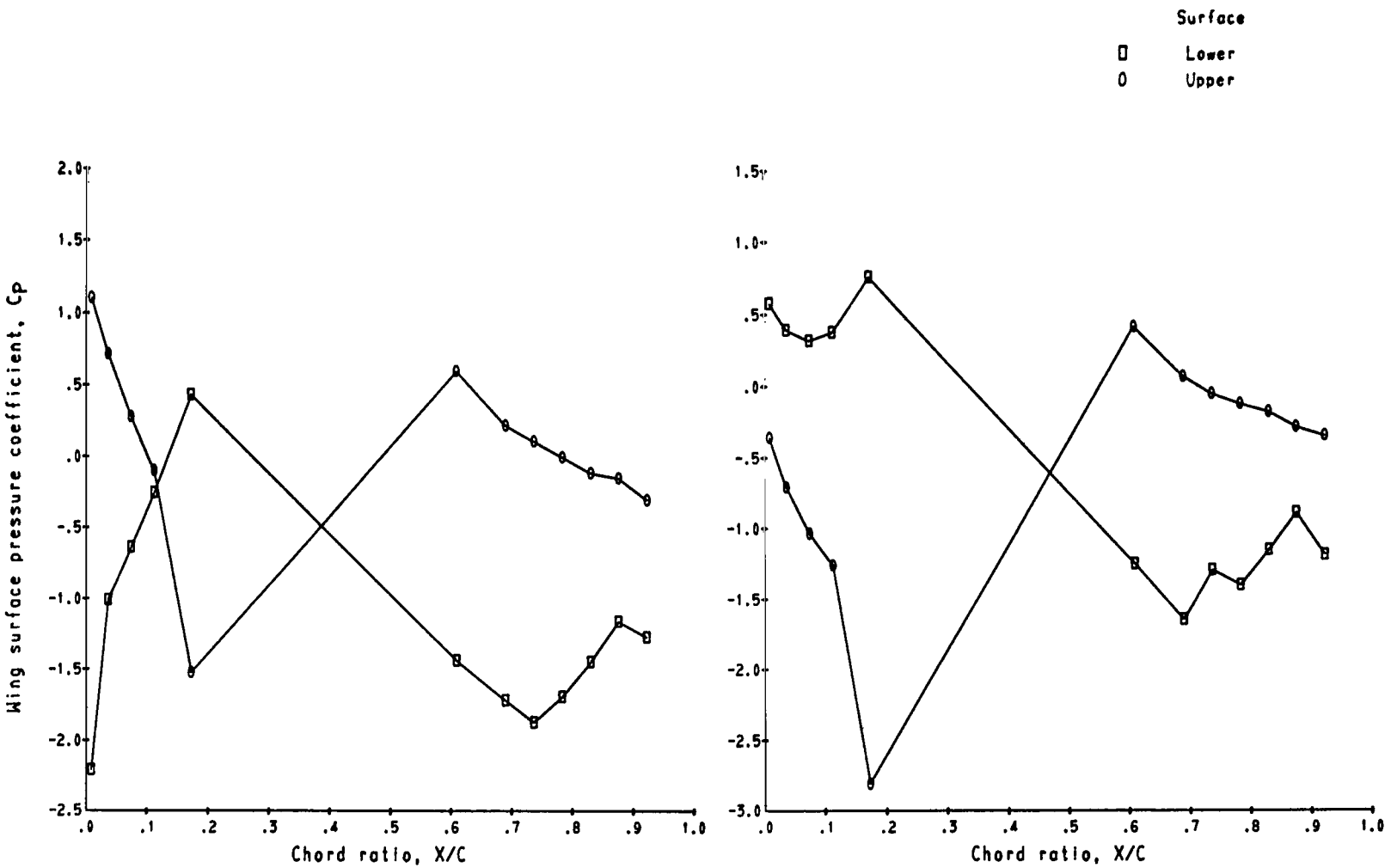

(a) Angle of attack, -15.3^{0}.

(b) Angle of attack, -5.1^{0}.

Figure 49. - Wing surface pressure coefficient distribution variations with angle of attack. Louvers off; 100 percent of fan speed; crossflow velocity, 61 meters per second (200 ft/sec).

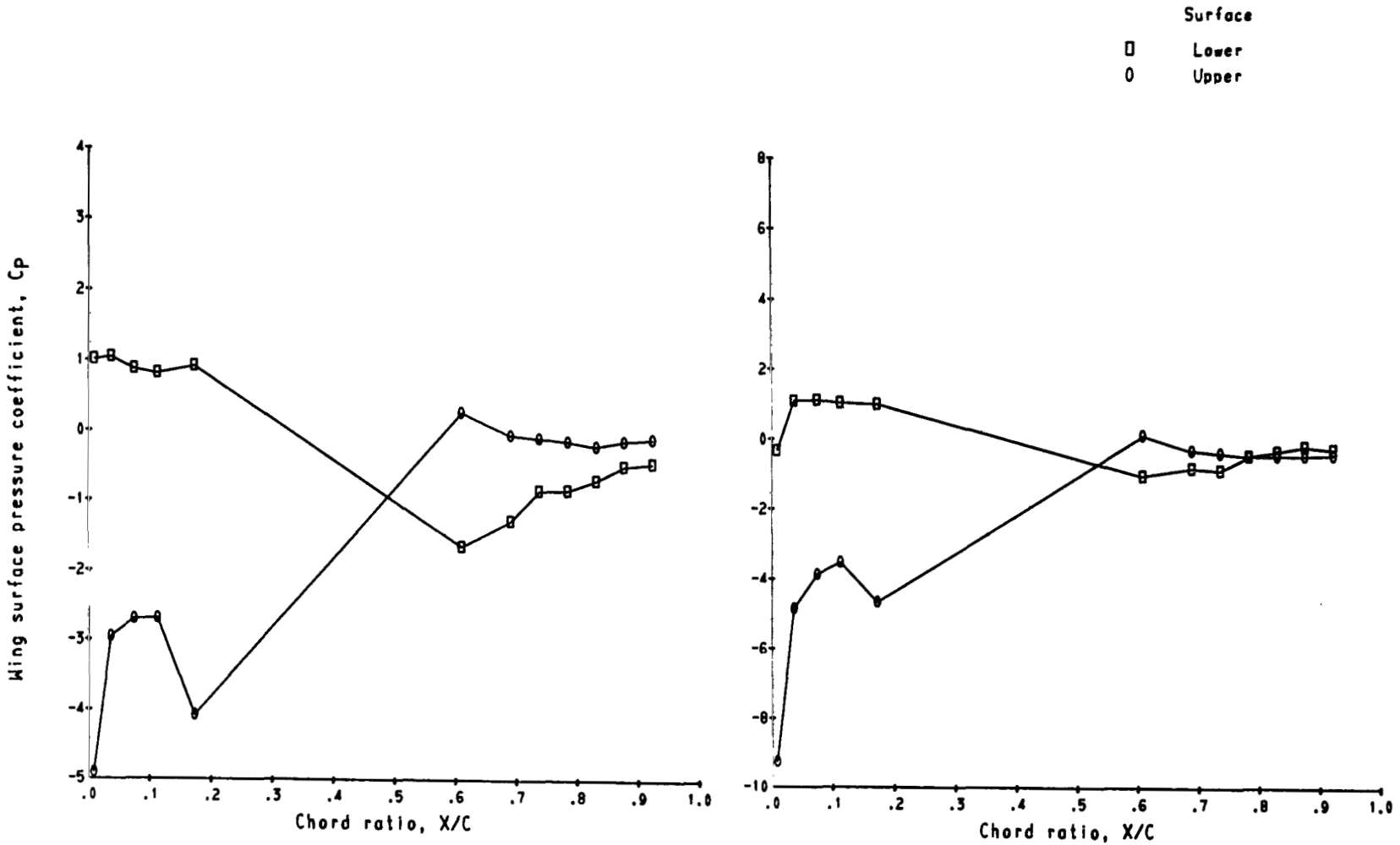

(c) Angle of attack, 5.0^{0}.

(d) Angle of attack, 15.5^{0}.

Figure 49. - Concluded.

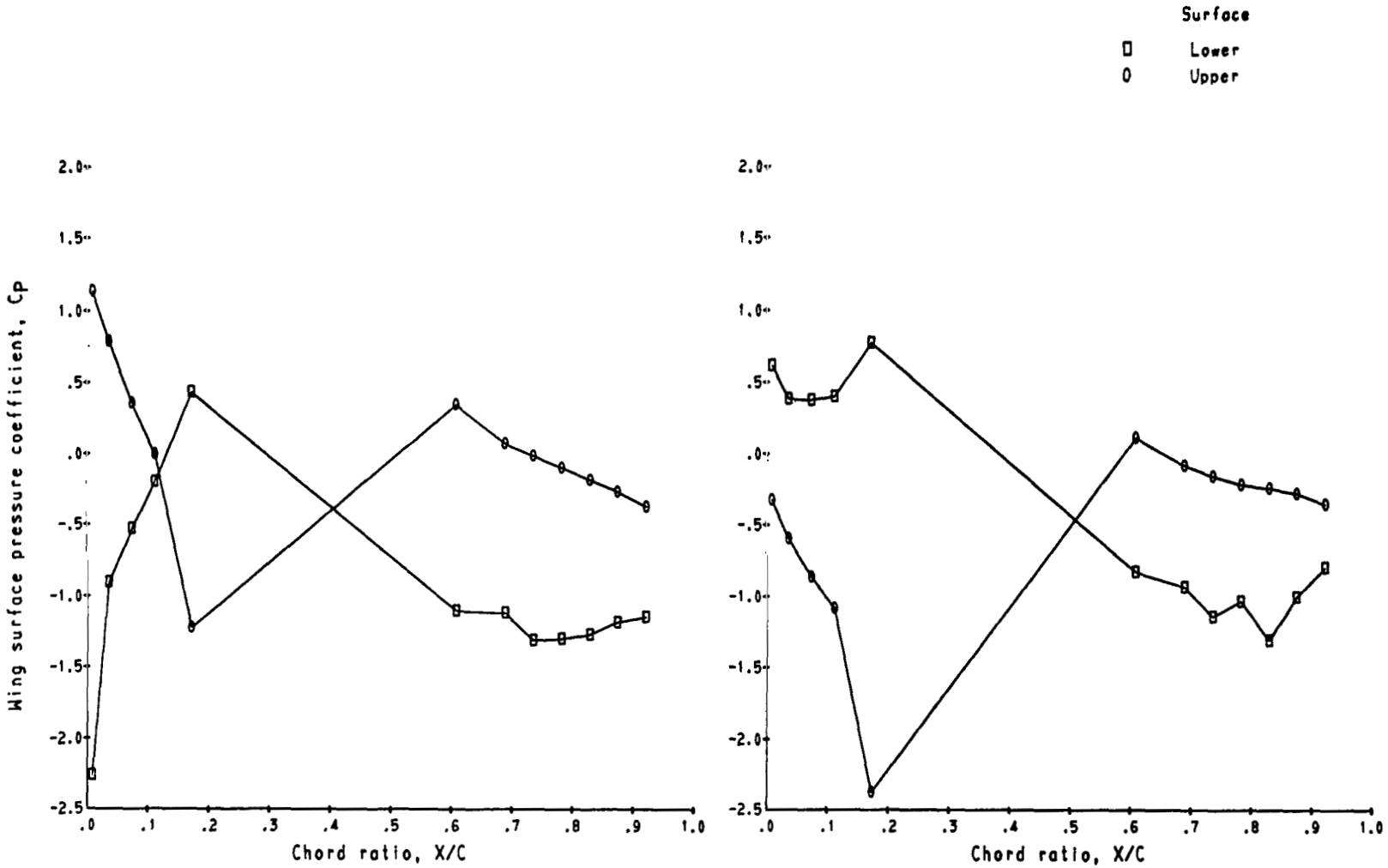

(a) Angle of attack, -13.6°.

(b) Angle of attack, -5.1°.

Figure 50. - Wing surface pressure coefficient distribution variations with angle of attack. Louvers off; 70 percent of fan speed; crossflow velocity, 61 meters per second (200 ft/sec).

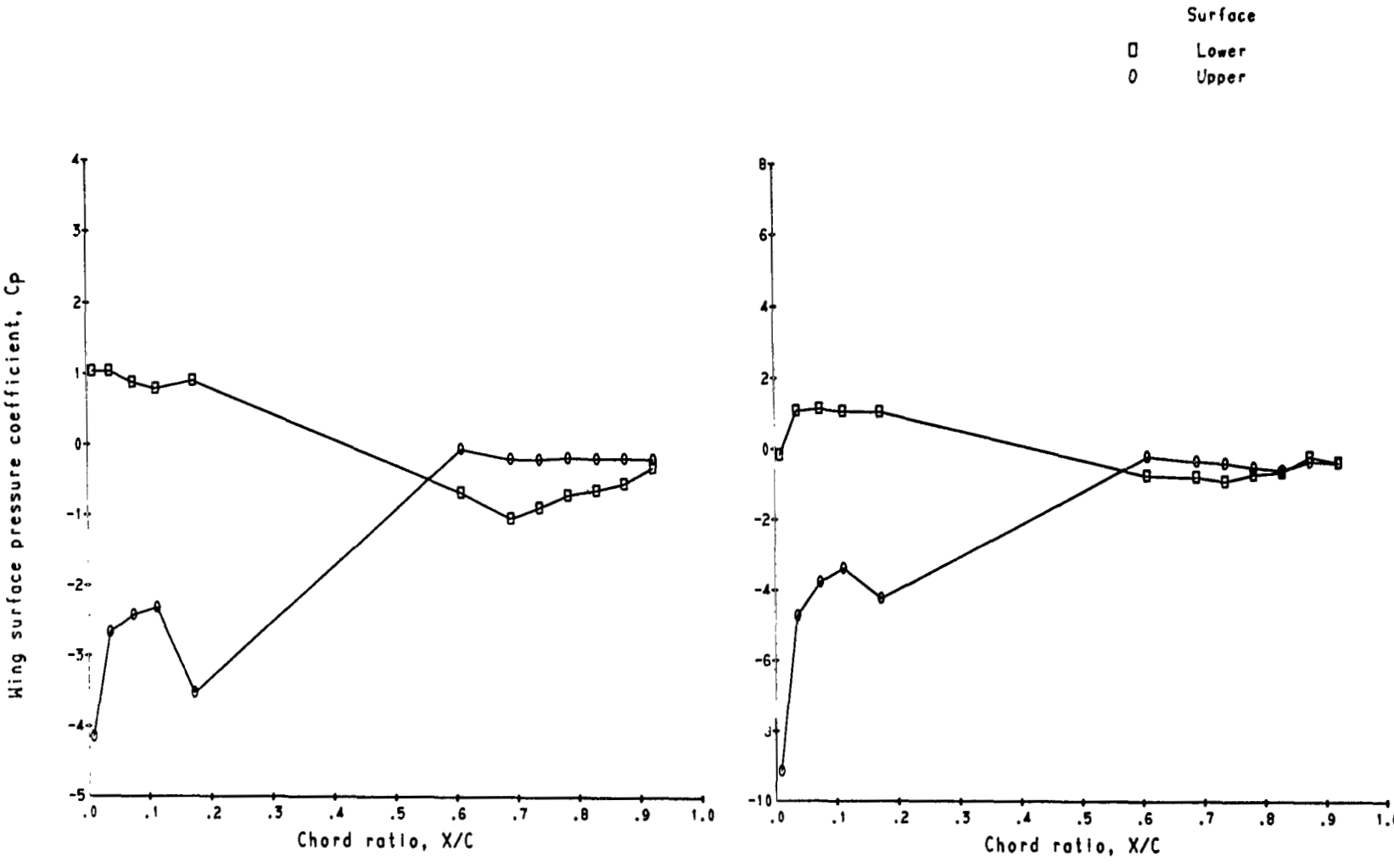

(c) Angle of attack, 4.9°.

(d) Angle of attack, 15.5°.

Figure 50. - Concluded.

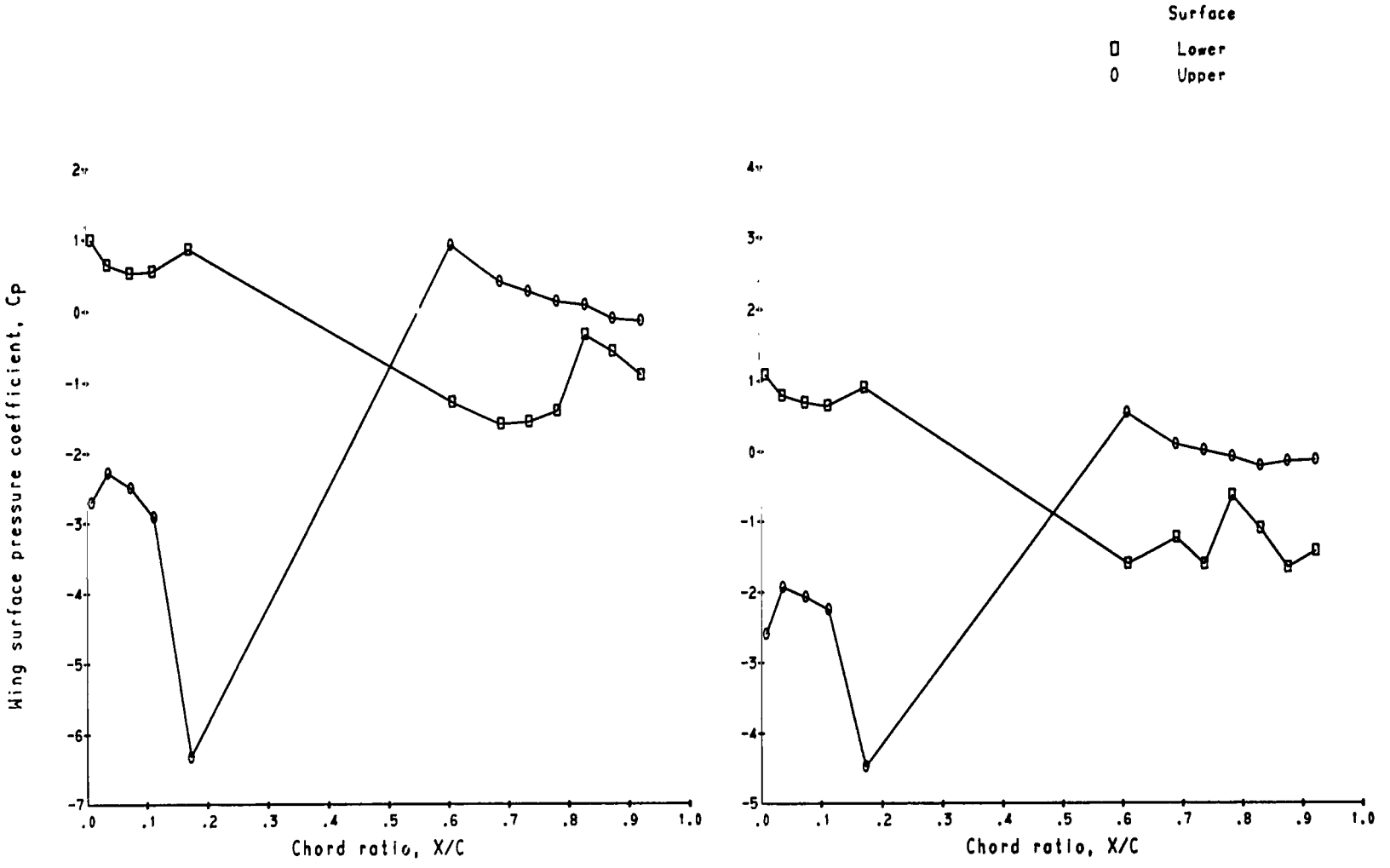

(a) Speed ratio, 0.112.

(b) Speed ratio, 0.168.

Figure 51. - Wing surface pressure coefficient distribution variations with speed ratio. Louvers on; louver angle, -3^{0}; angle of attack, zero.

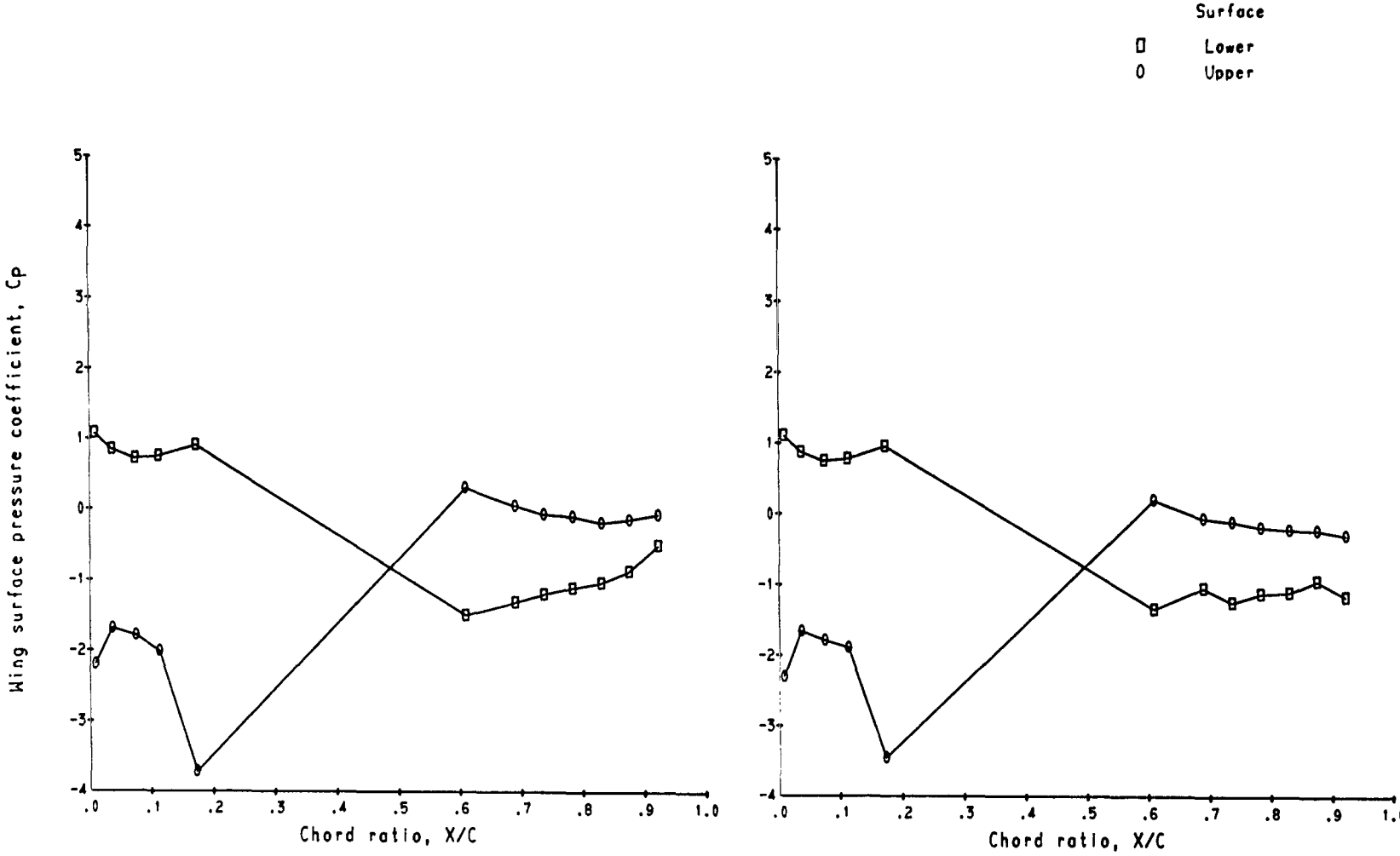

(c) Speed ratio, 0.216.

(d) Speed ratio, 0.244.

Figure 51. - Continued.

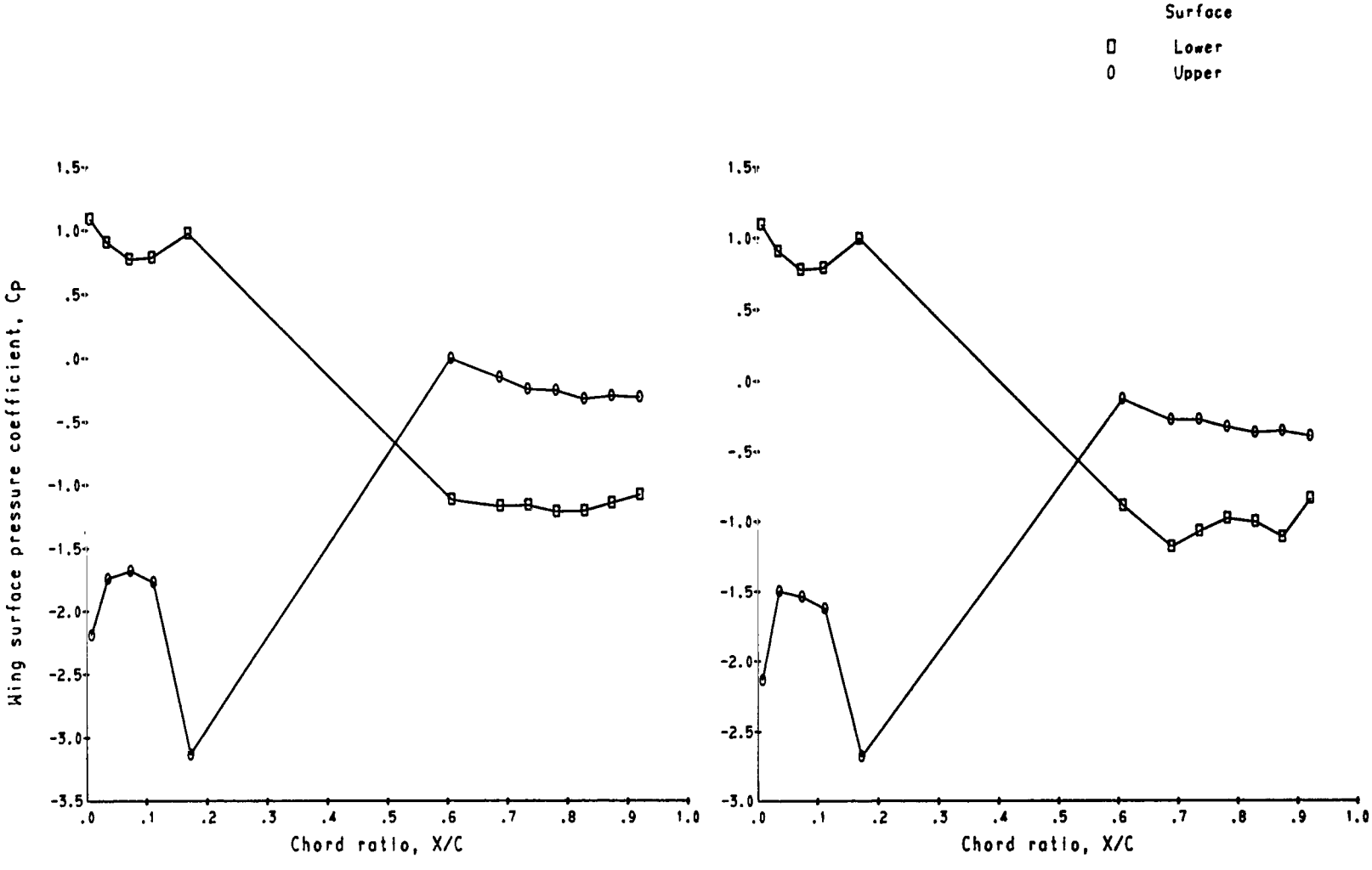

(e) Speed ratio, 0.286.

(f) Speed ratio, 0.329.

Figure 51. - Concluded.

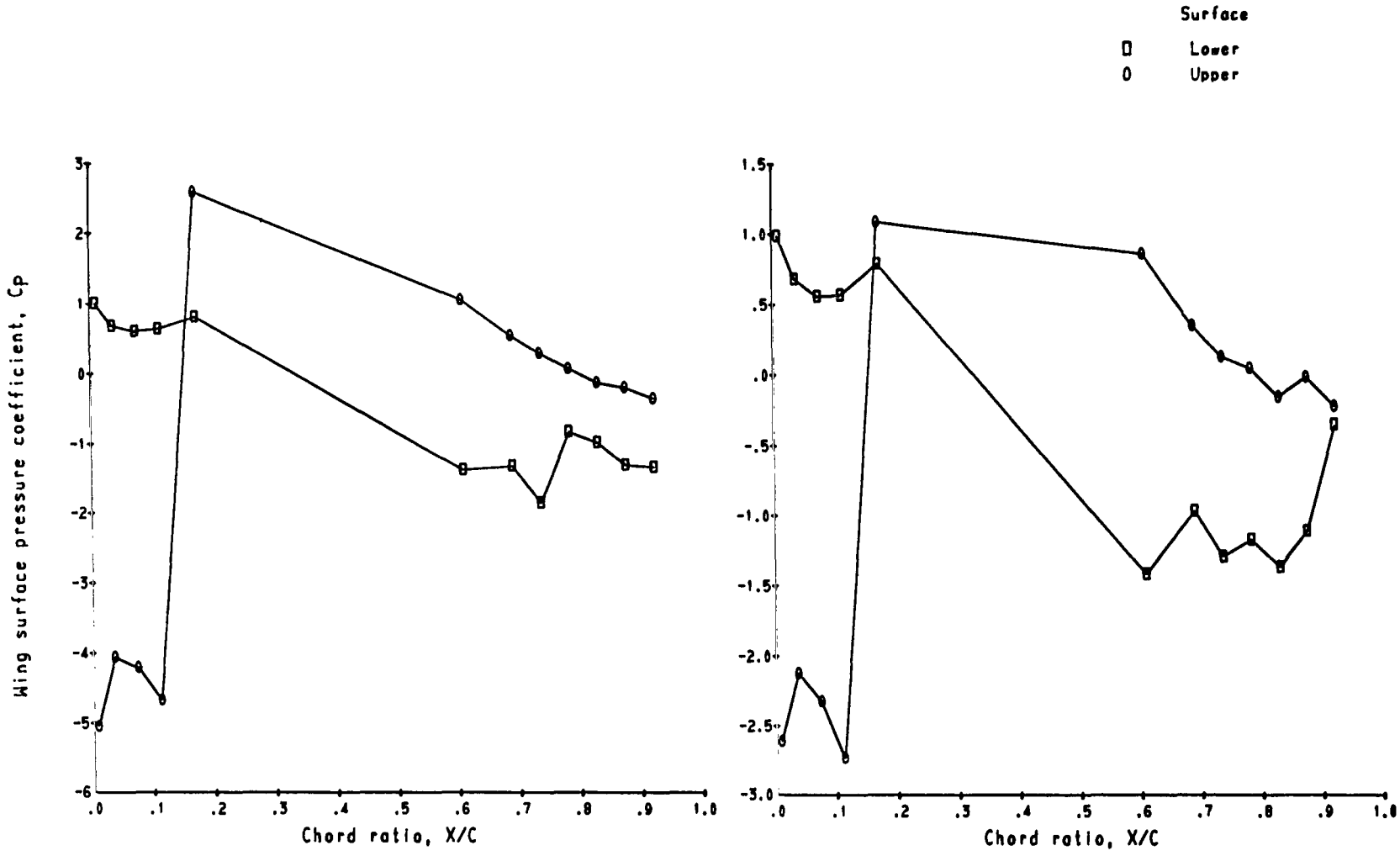

(a) Speed ratio, 0.075.

(b) Speed ratio, 0.116.

Figure 52. - Wing surface pressure coefficient distribution variations with speed ratio. Louvers on; louver angle, -2^{0}; angle of attack, zero.

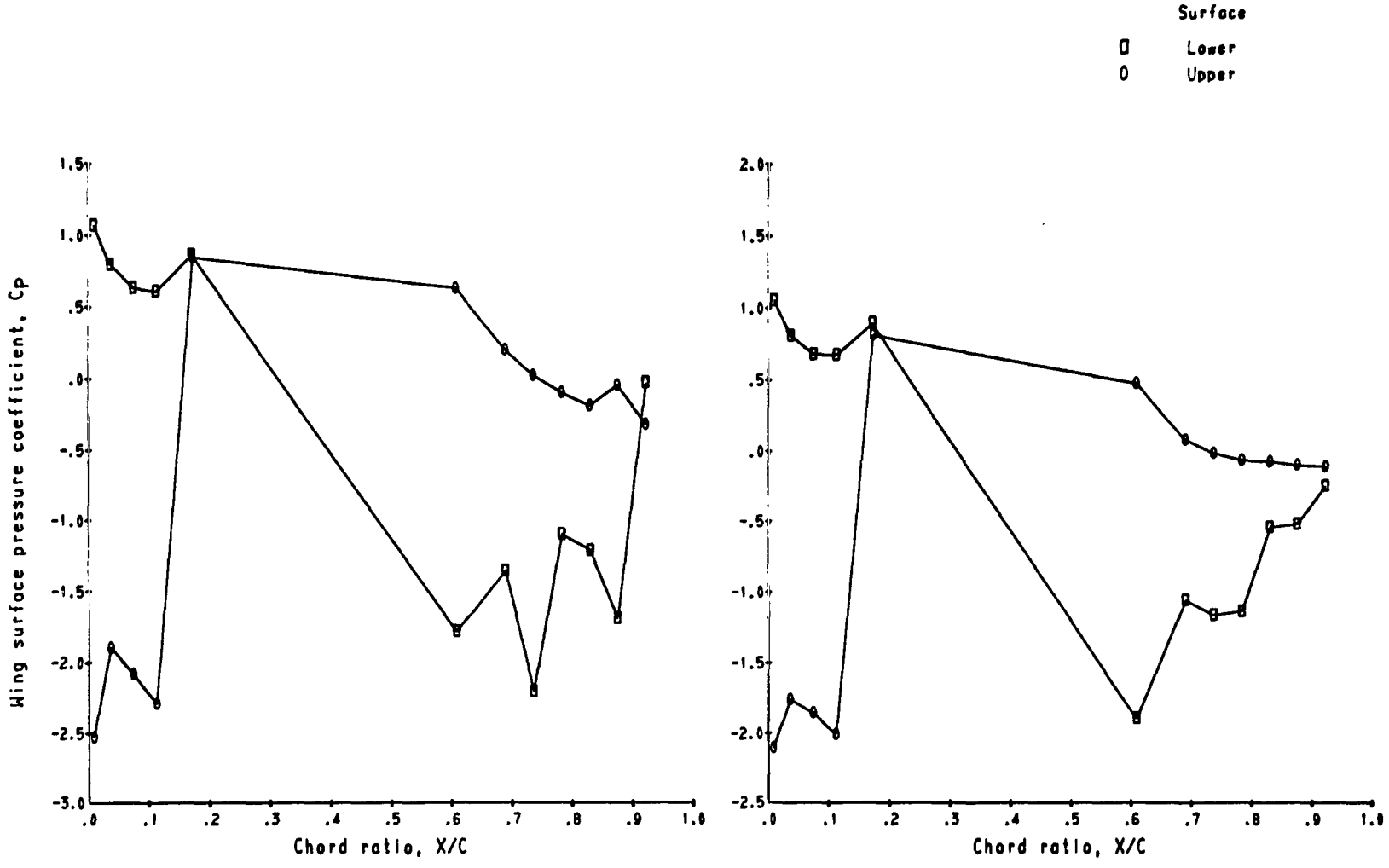

(c) Speed ratio, 0.149.

(d) Speed ratio, 0.177.

Figure 52. - Continued.

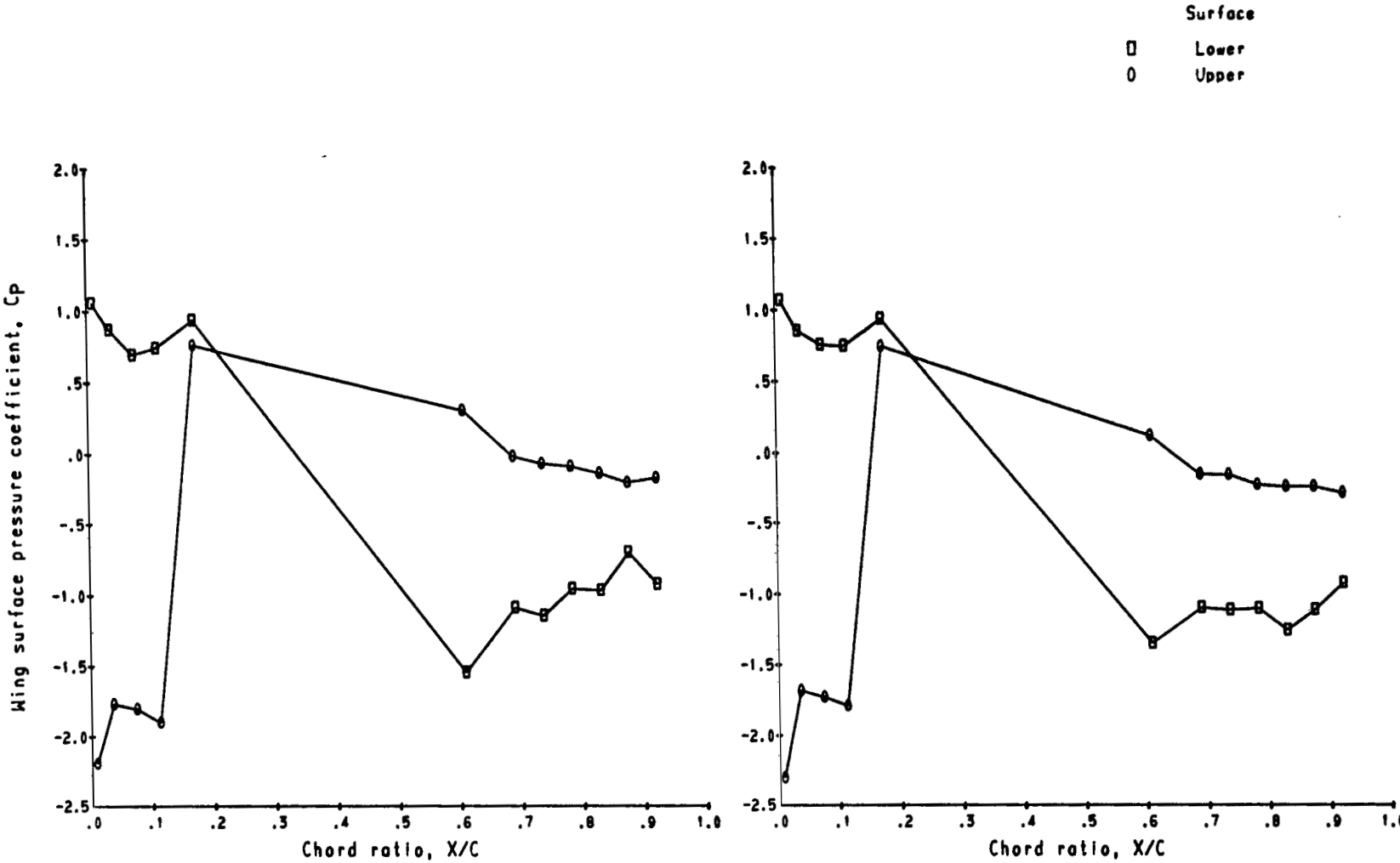

(e) Speed ratio, 0.201.

(f) Speed ratio, 0.234.

Figure 52. - Concluded.

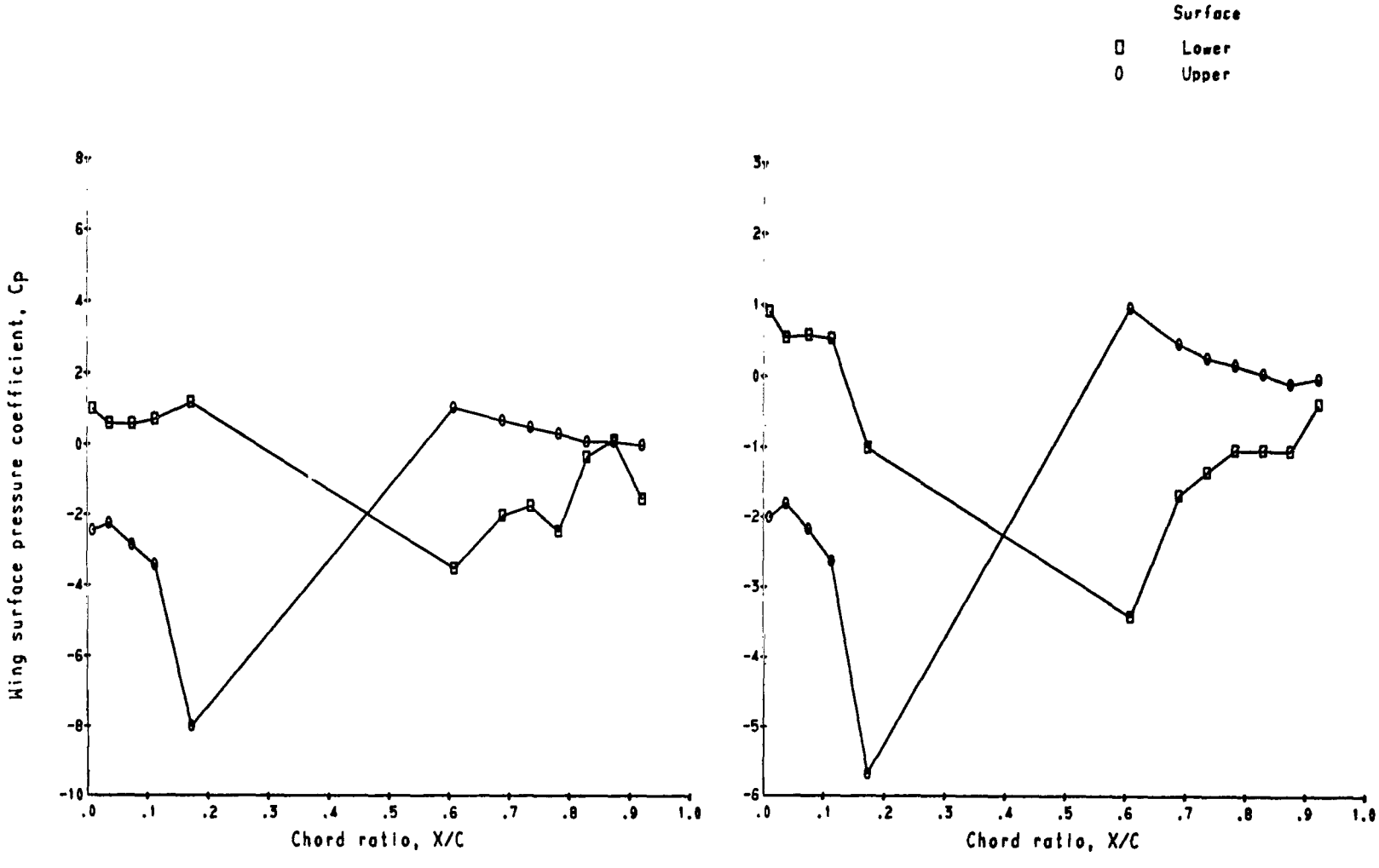

(a) Speed ratio, 0.079.

(b) Speed ratio, 0.111.

Figure 53. - Wing surface pressure coefficient distribution variations with speed ratio. Louvers on; louver angle, 30°; angle of attack, zero.

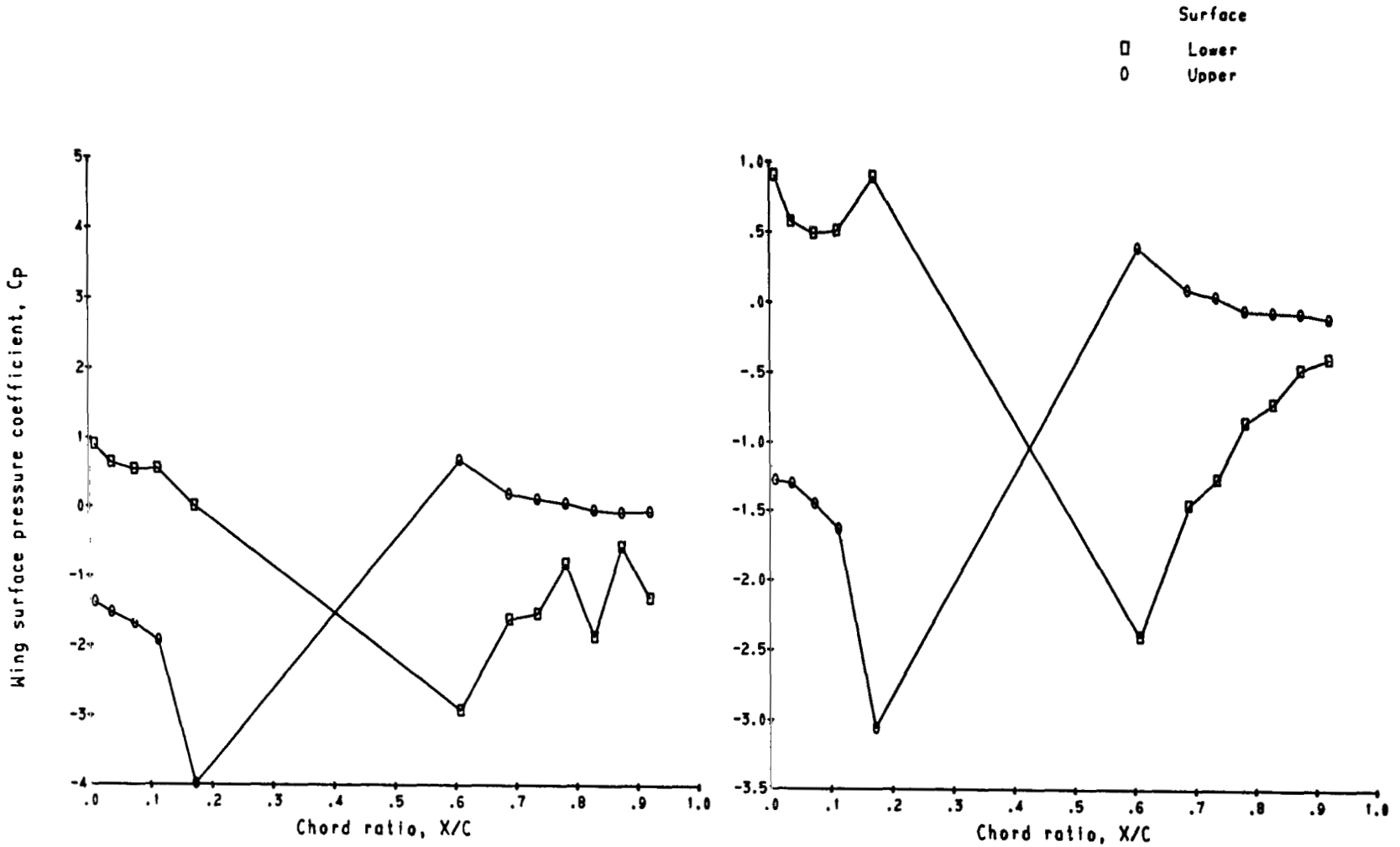

(c) Speed ratio, 0.152.

(d) Speed ratio, 0.200.

Figure 53. - Continued.

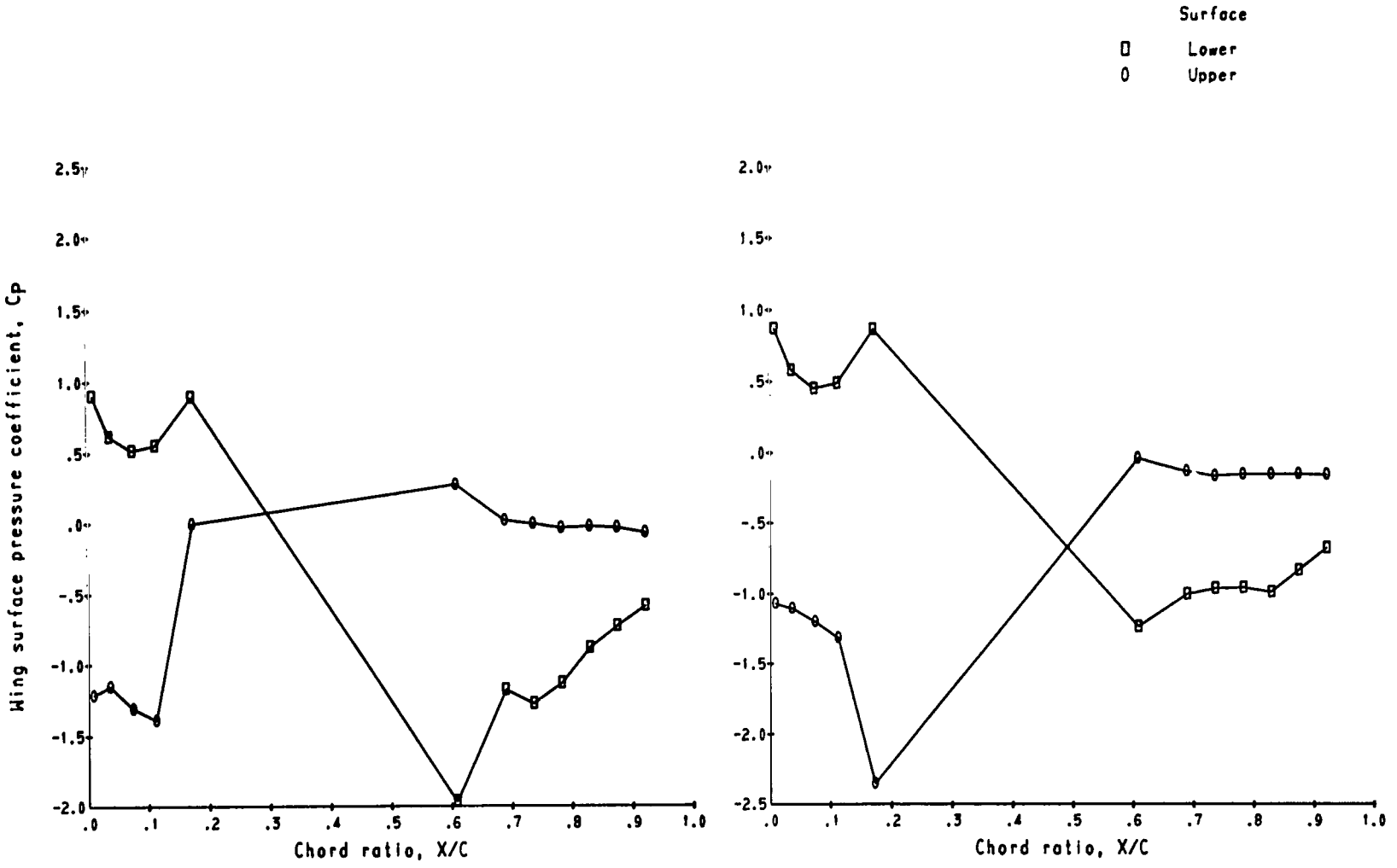

(e) Speed ratio, 0.233.

(f) Speed ratio, 0.329.

Figure 53. - Concluded.

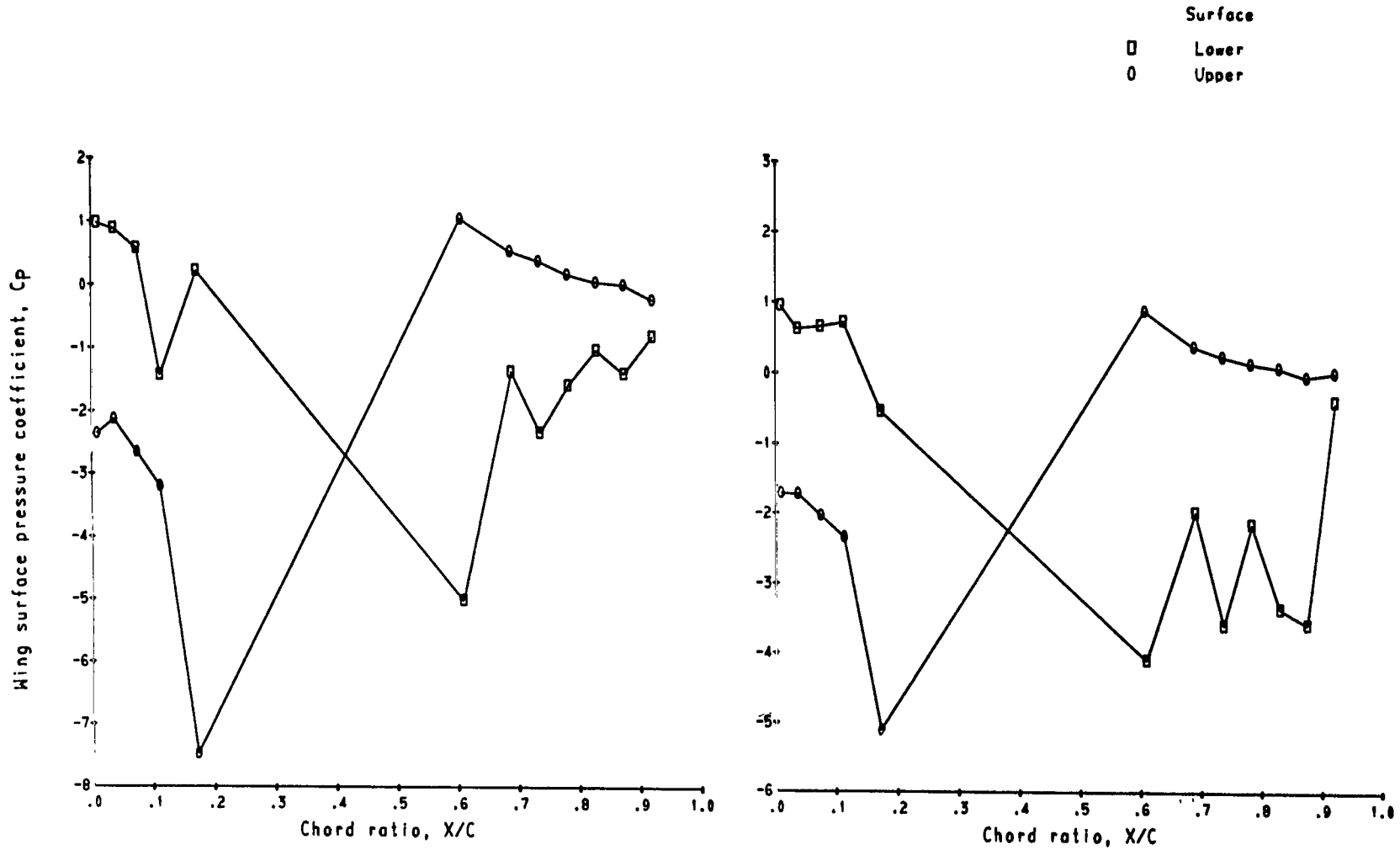

(a) Speed ratio, 0.080.

(b) Speed ratio, 0.115.

Figure 54. - Wing surface pressure coefficient distribution variations with speed ratio. Louvers on; louver angle, 40^{0}; angle of attack, zero.

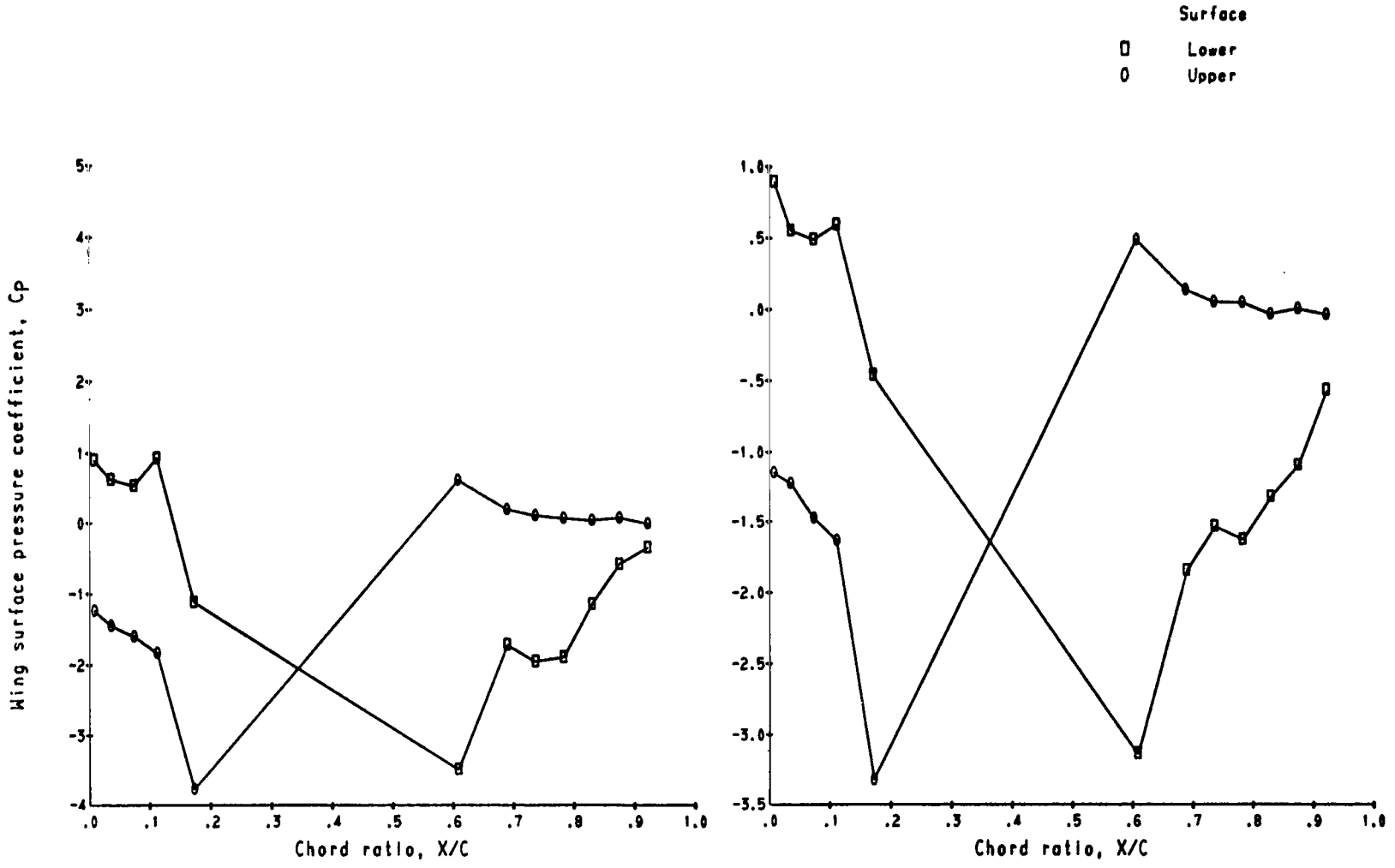

(c) Speed ratio, 0.154.

(d) Speed ratio, 0.177.

Figure 54. - Continued.

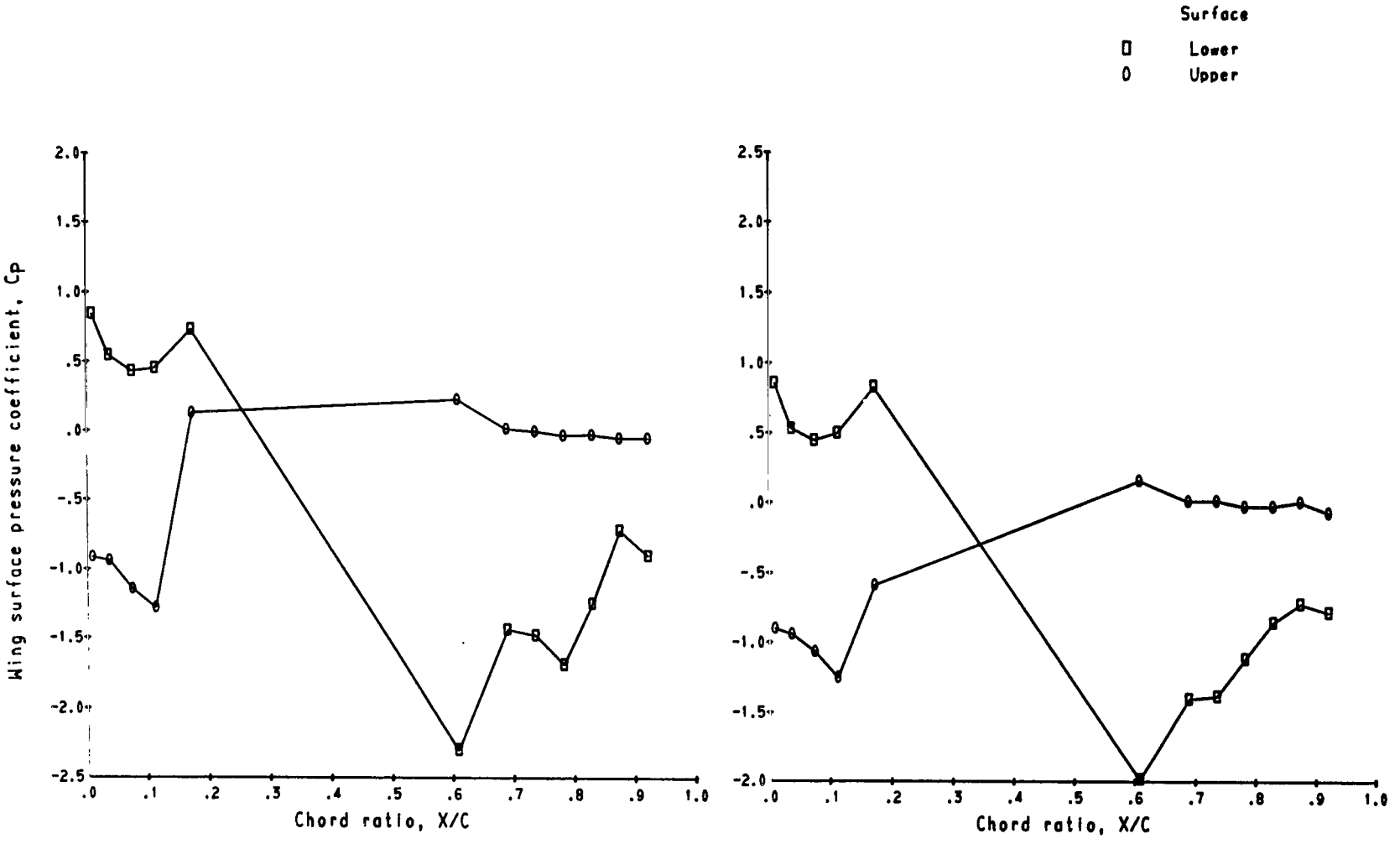

(e) Speed ratio, 0.236.

(f) Speed ratio, 0.271.

Figure 54. - Concluded.

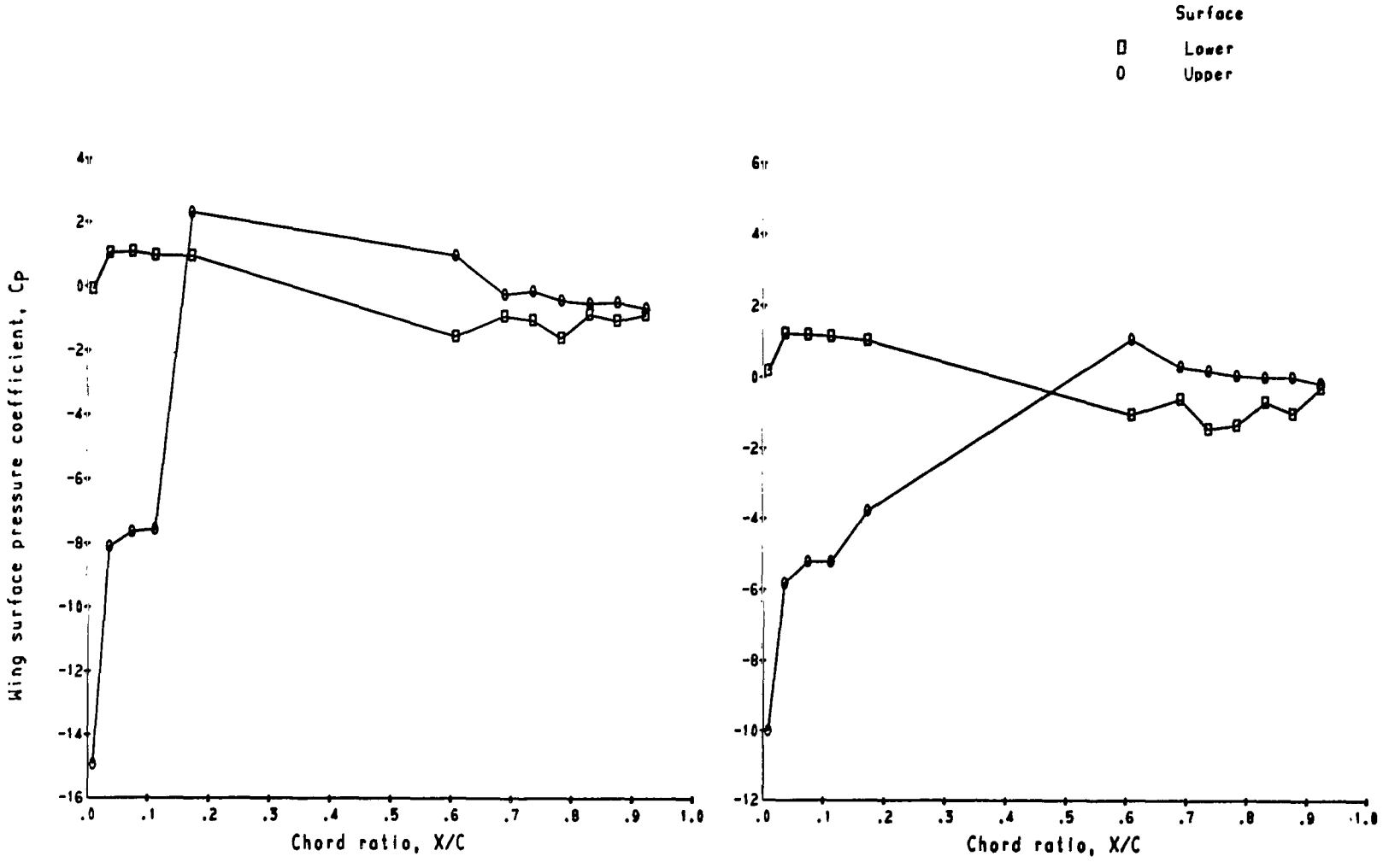

(a) Speed ratio, 0.070.

(b) Speed ratio, 0.102.

Figure 55. - Wing surface pressure coefficient distribution variations with speed ratio. Louvers on; louver angle, -2^{0}; angle of attack, 10^{0}.

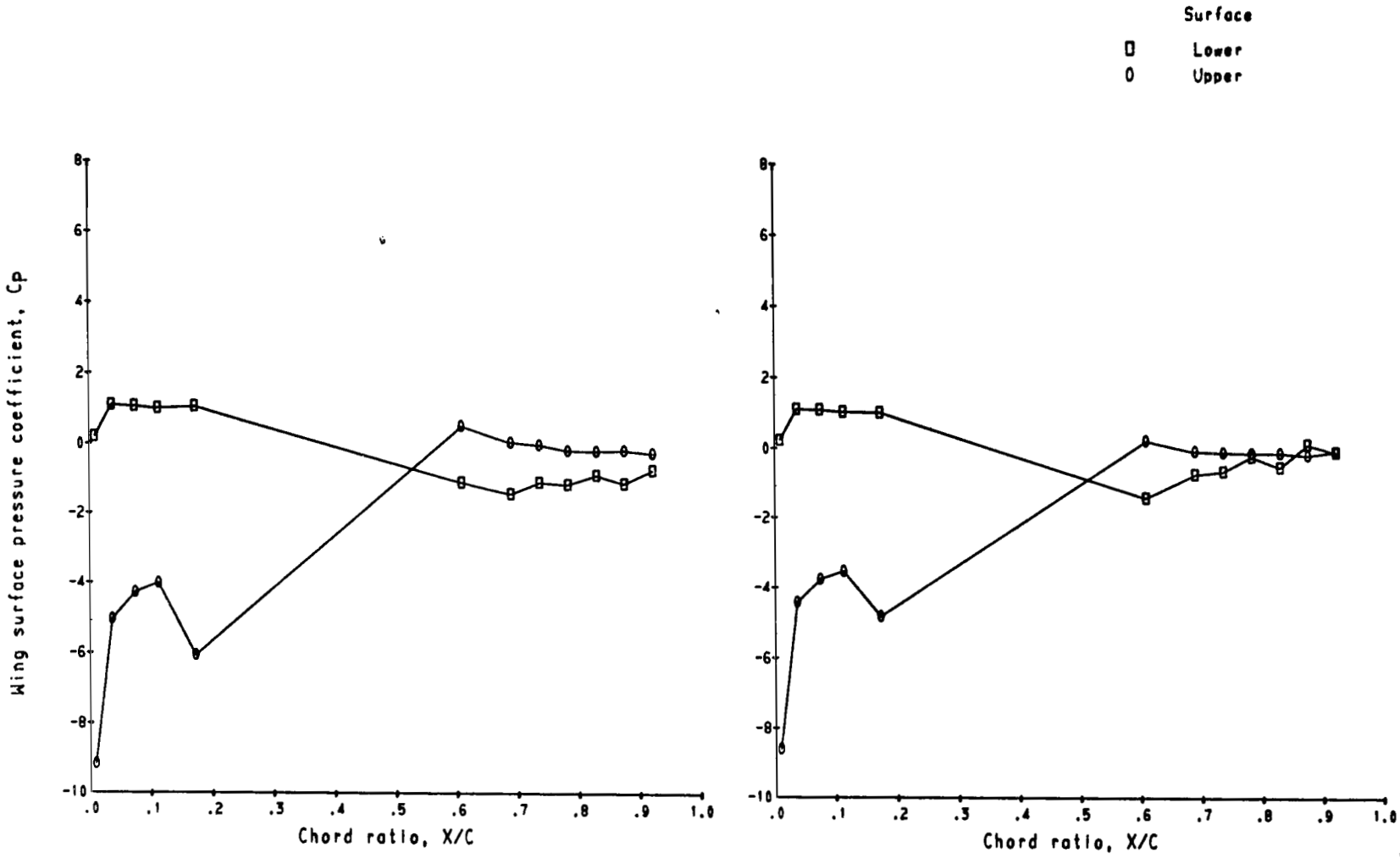

(c) Speed ratio, 0.145.

(d) Speed ratio, 0.191.

Figure 55. - Continued.

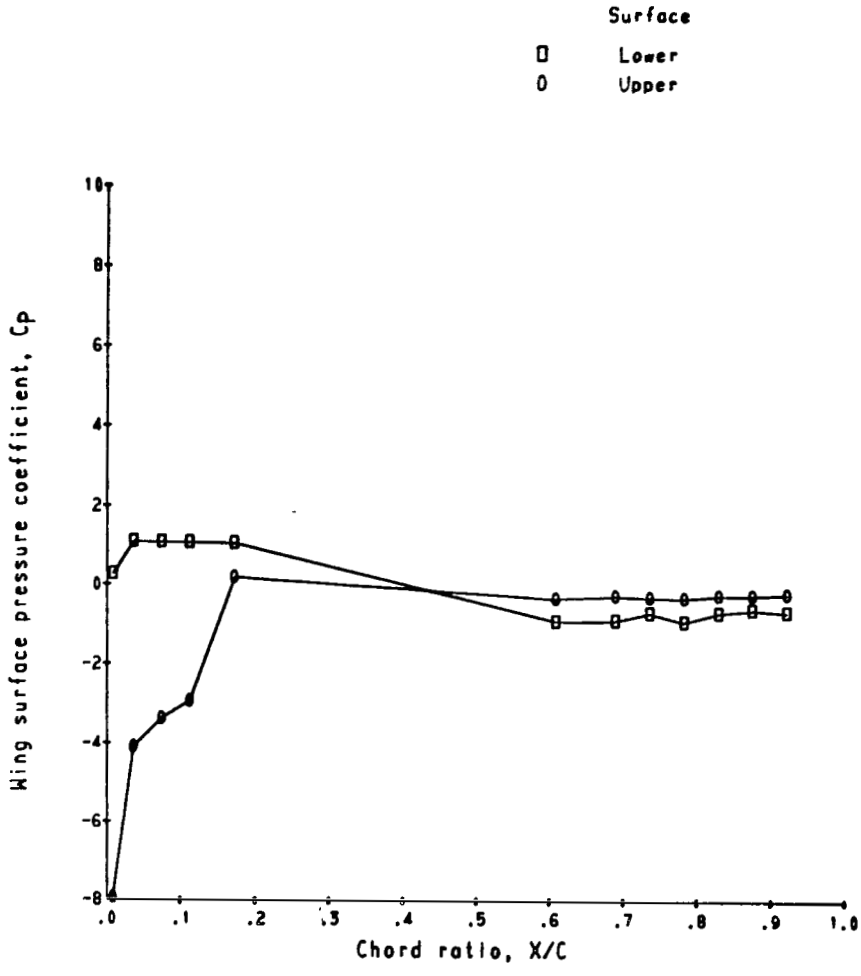

(e) Speed ratio, 0.326.

Figure 55. - Concluded.

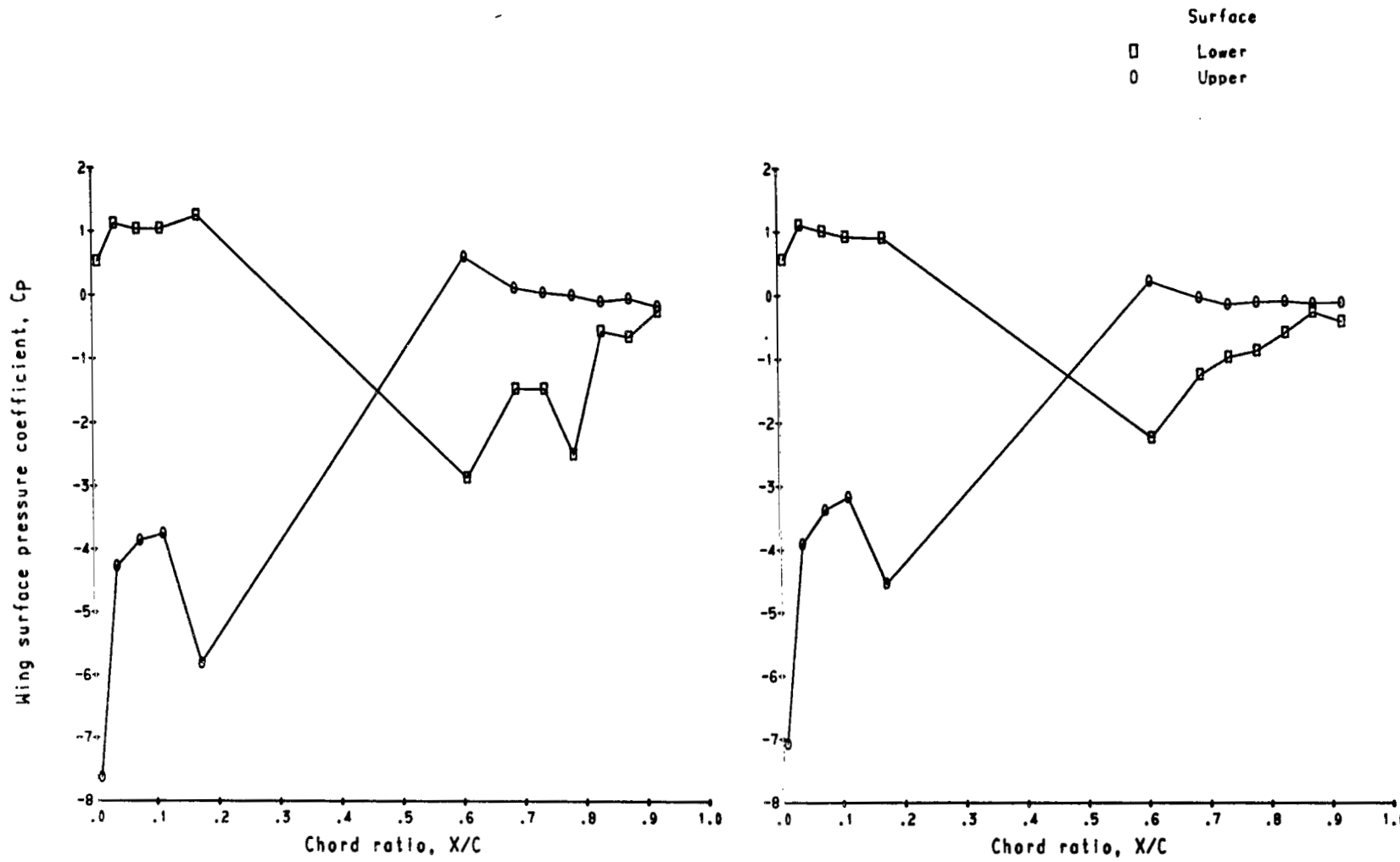

(a) Speed ratio, 0.145.

(b) Speed ratio, 0.193.

Figure 56. - Wing surface pressure coefficient distribution variations with speed ratio. Louvers on; louver angle, 30^{o}; angle of attack, 10^{o}.

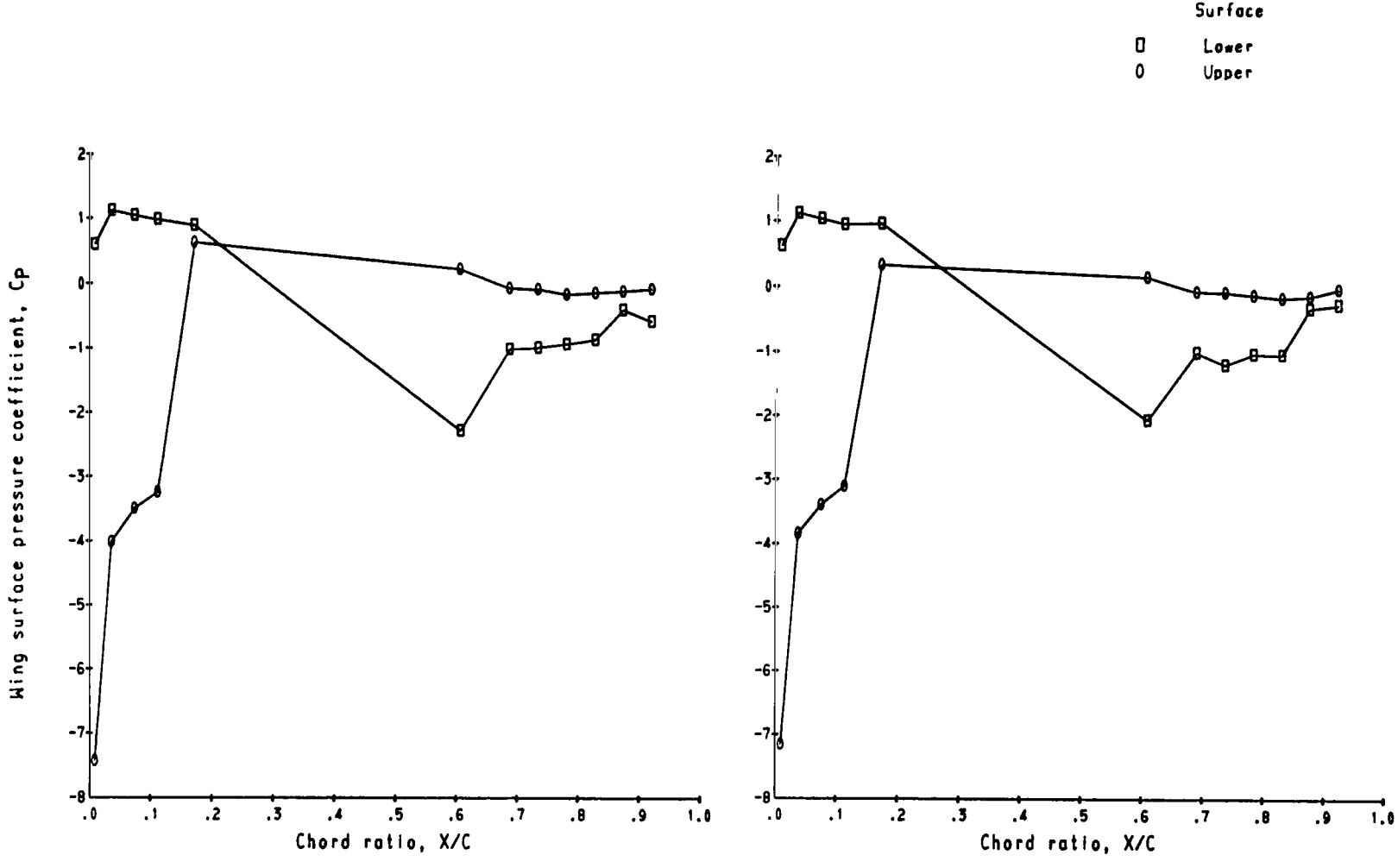

(c) Speed ratio, 0.199.

(d) Speed ratio, 0.208.

Figure 56. - Continued.

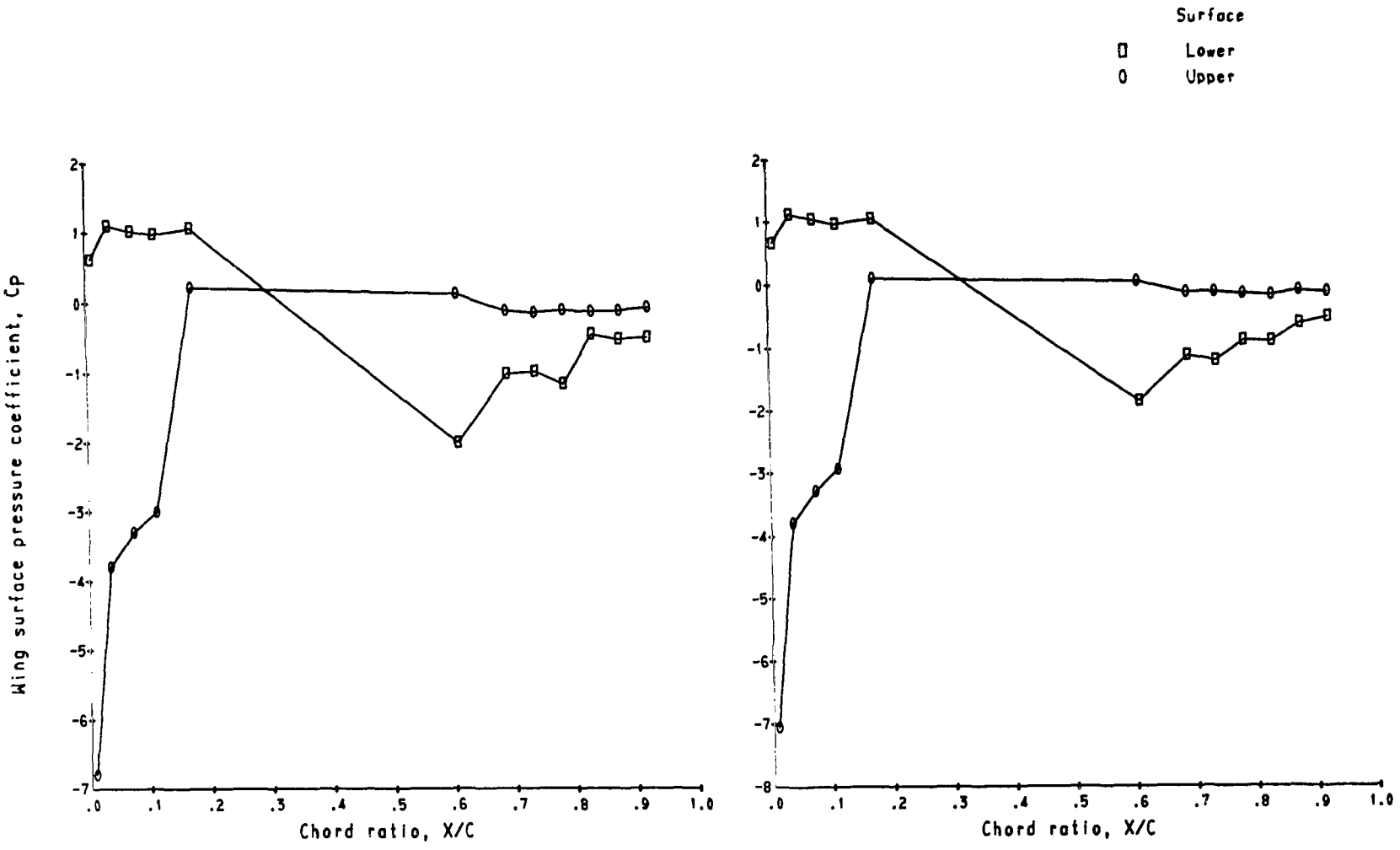

(e) Speed ratio, 0.220.

(f) Speed ratio, 0.230.

Figure 56. - Concluded.

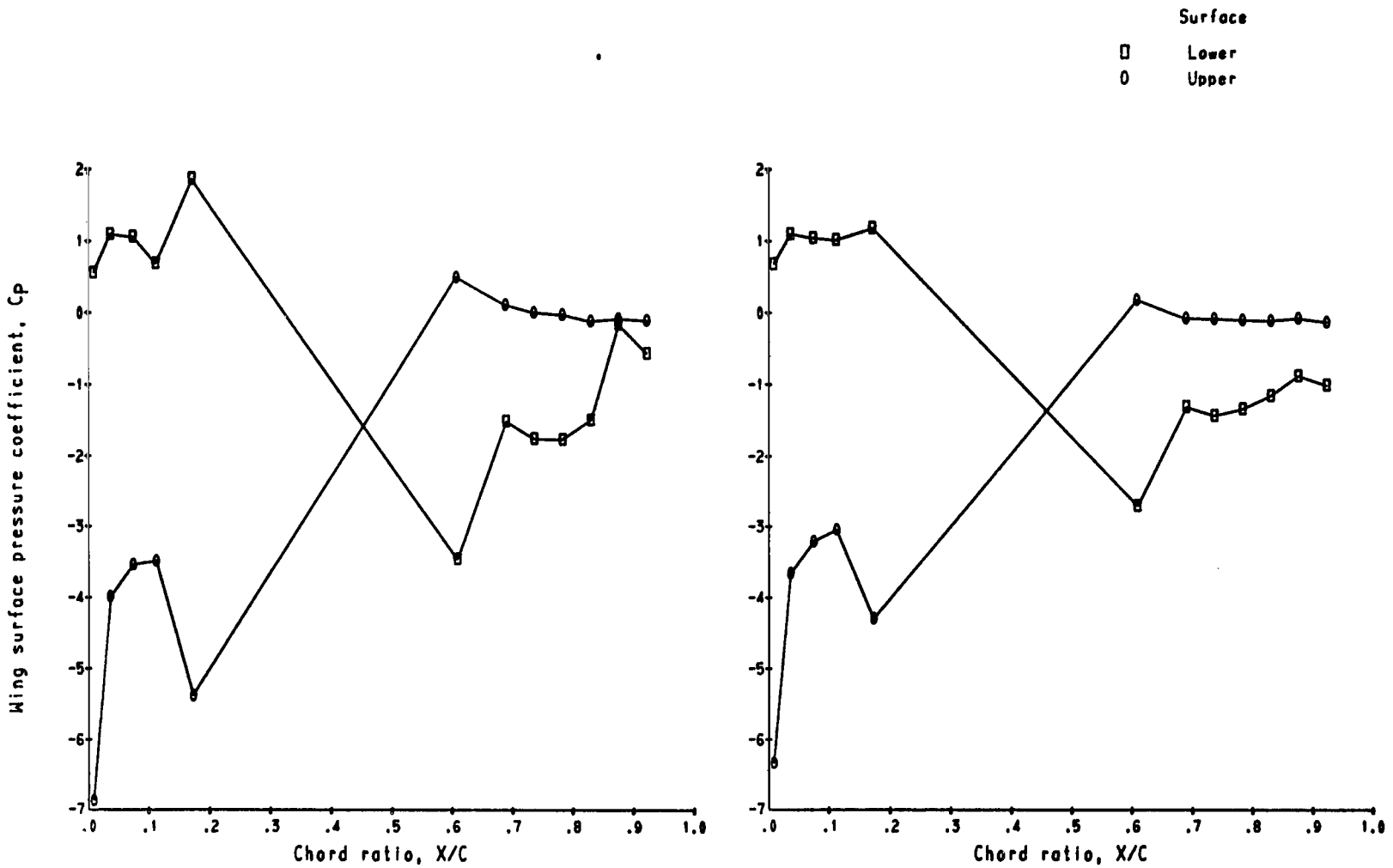

(a) Speed ratio, 0.149.

(b) Speed ratio, 0.193.

Figure 57. - Wing surface pressure coefficient distribution variations with speed ratio. Louvers on; louver angle, 40^{0}; angle of attack, 10^{0}.

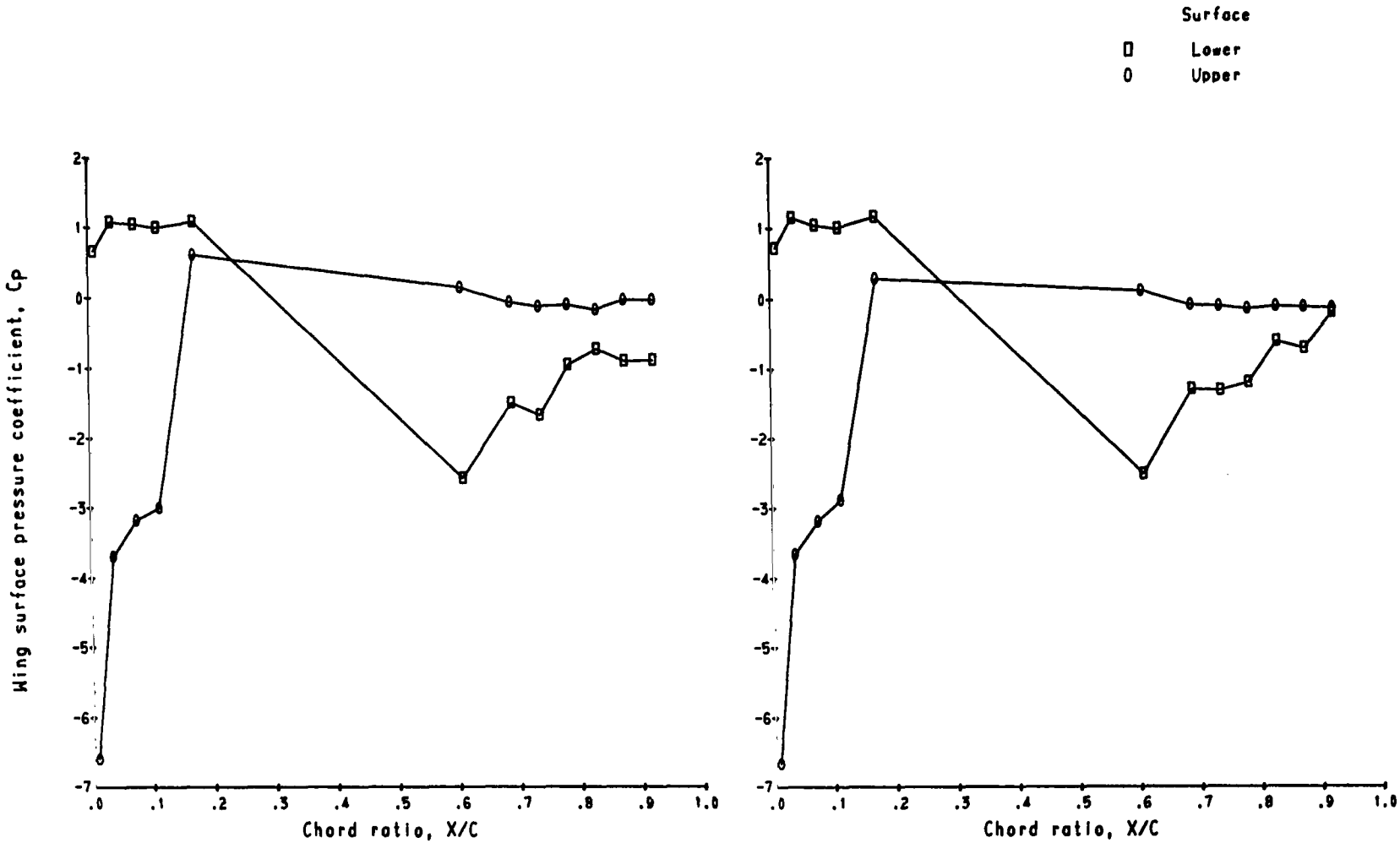

(c) Speed ratio, 0.202.

(d) Speed ratio, 0.210.

Figure 57. - Continued.

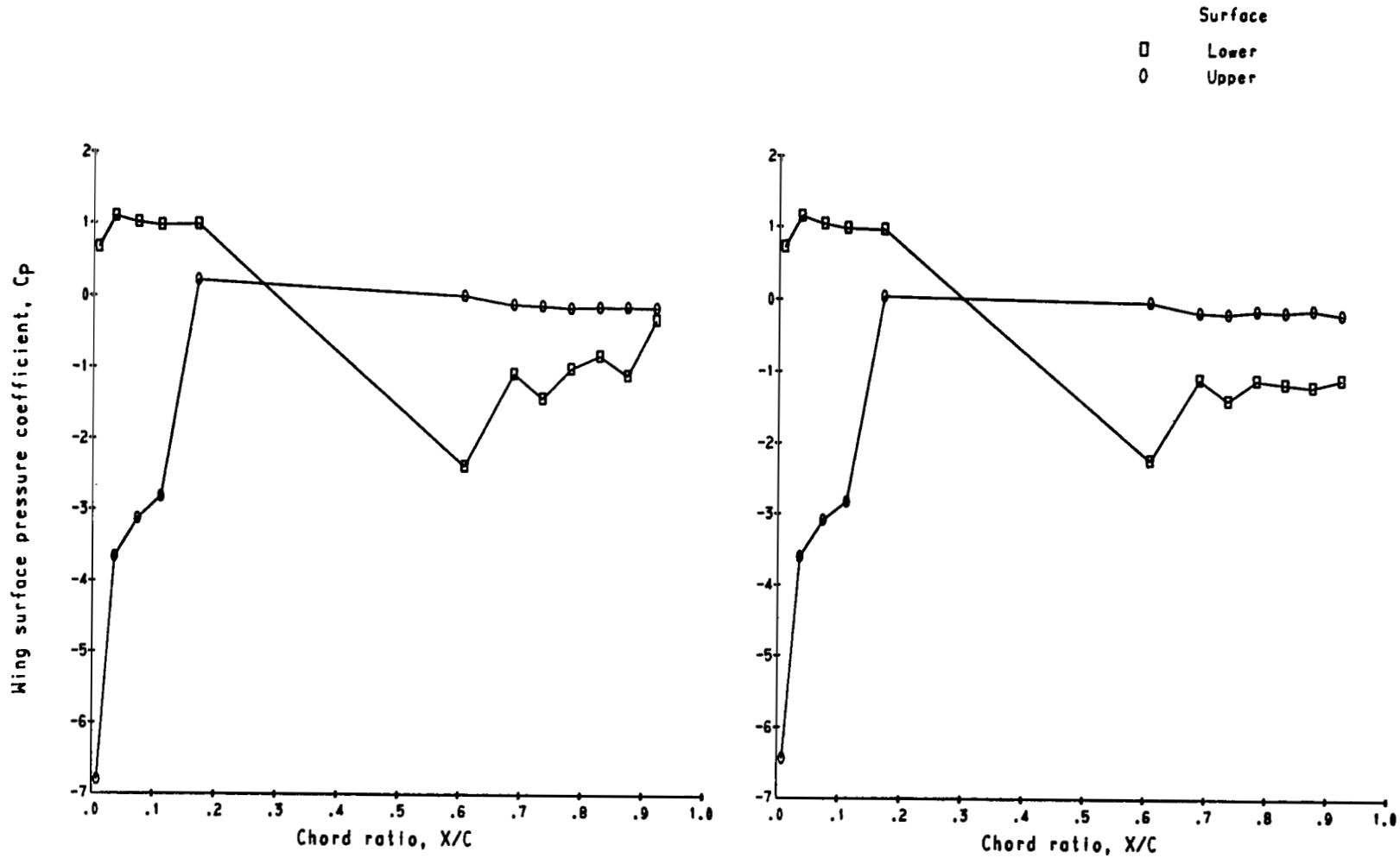

(e) Speed ratio, 0.220.

(f) Speed ratio, 0.230.

Figure 57. - Concluded.

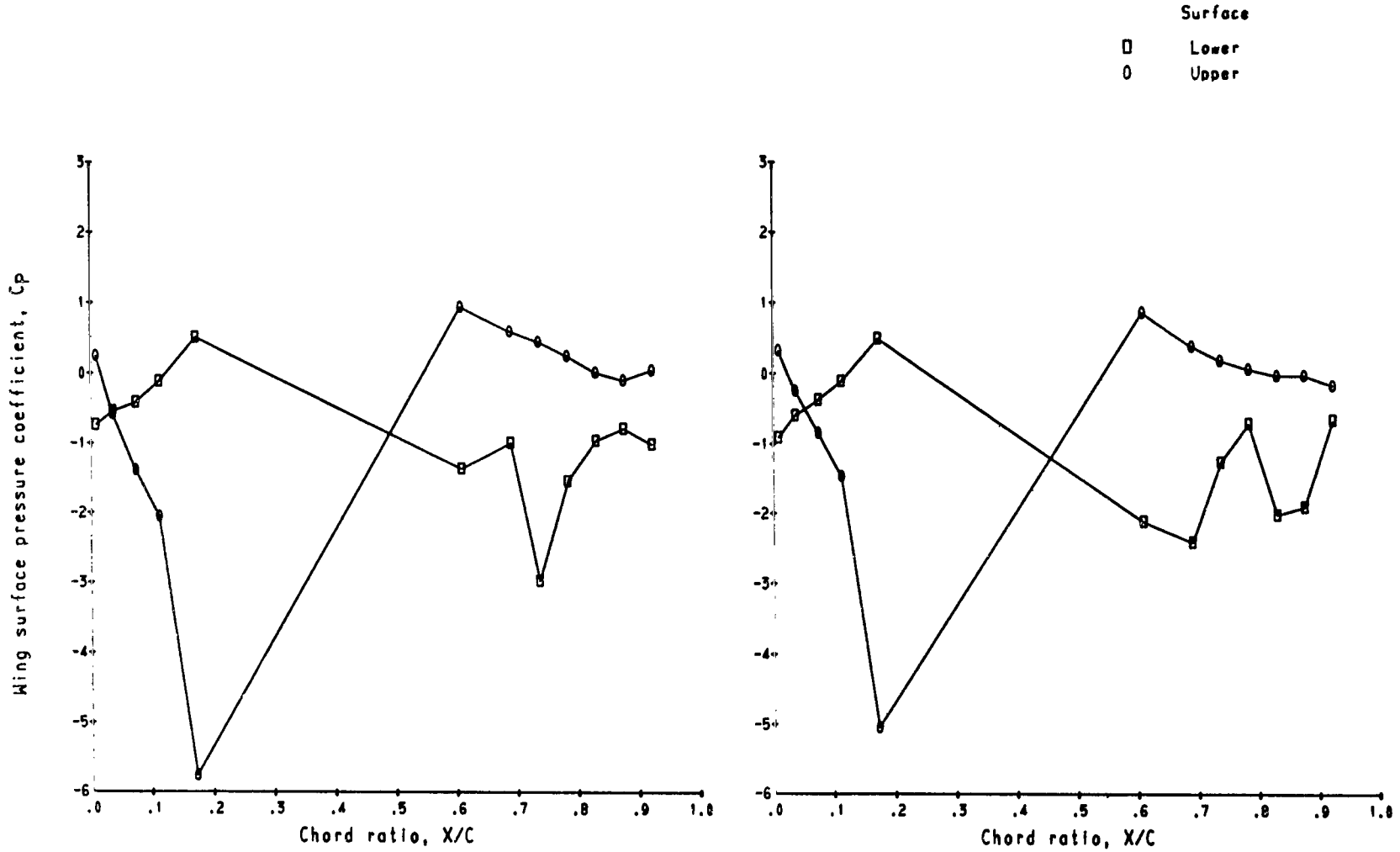

(a) Speed ratio, 0.082.

(b) Speed ratio, 0.120.

Figure 58. - Wing surface pressure coefficient distribution variations with speed ratio. Louvers on; louver angle, -3^{0}; angle of attack, -10^{0}.

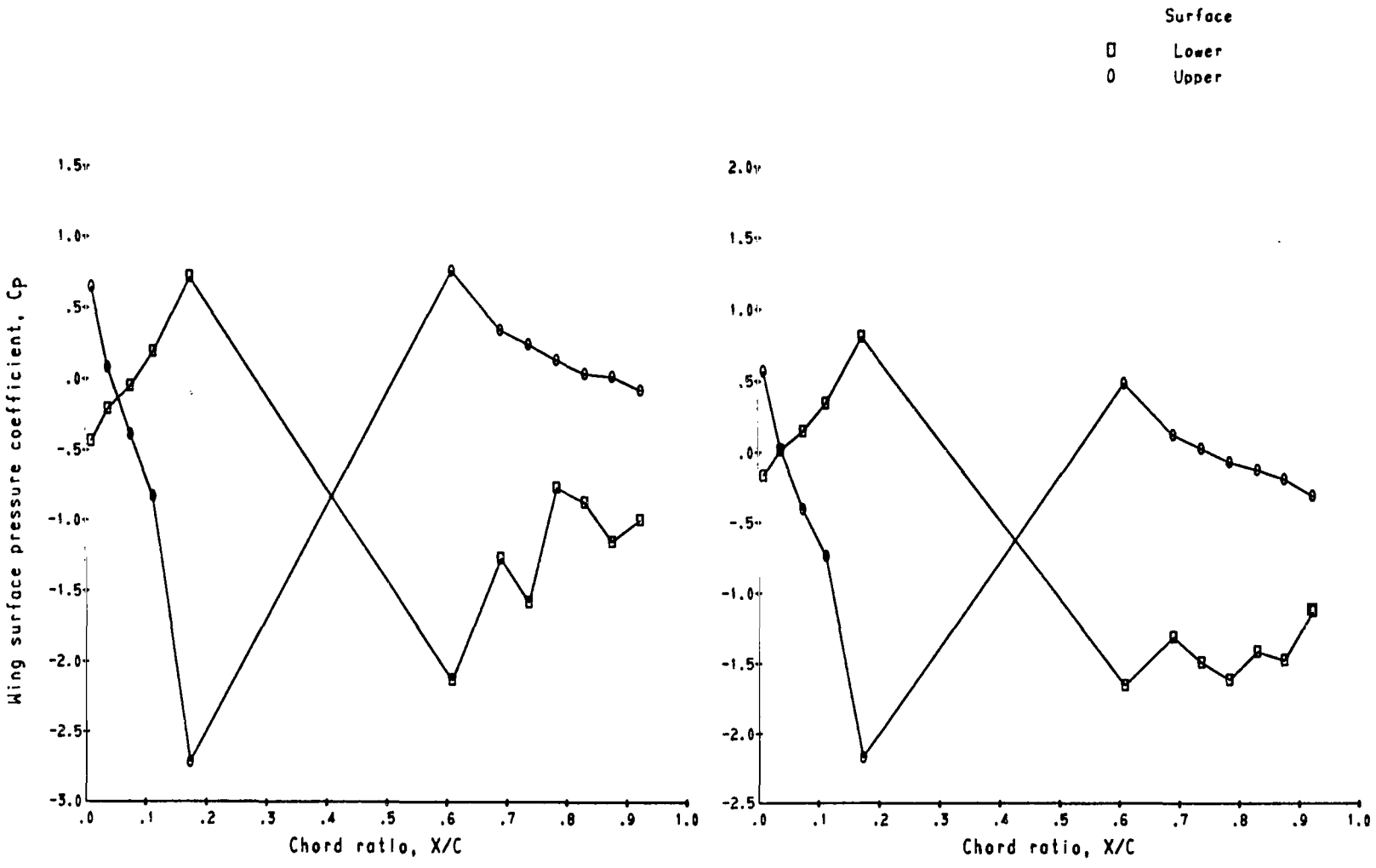

(c) Speed ratio, 0.157.

(d) Speed ratio, 0.200.

Figure 58. - Continued.

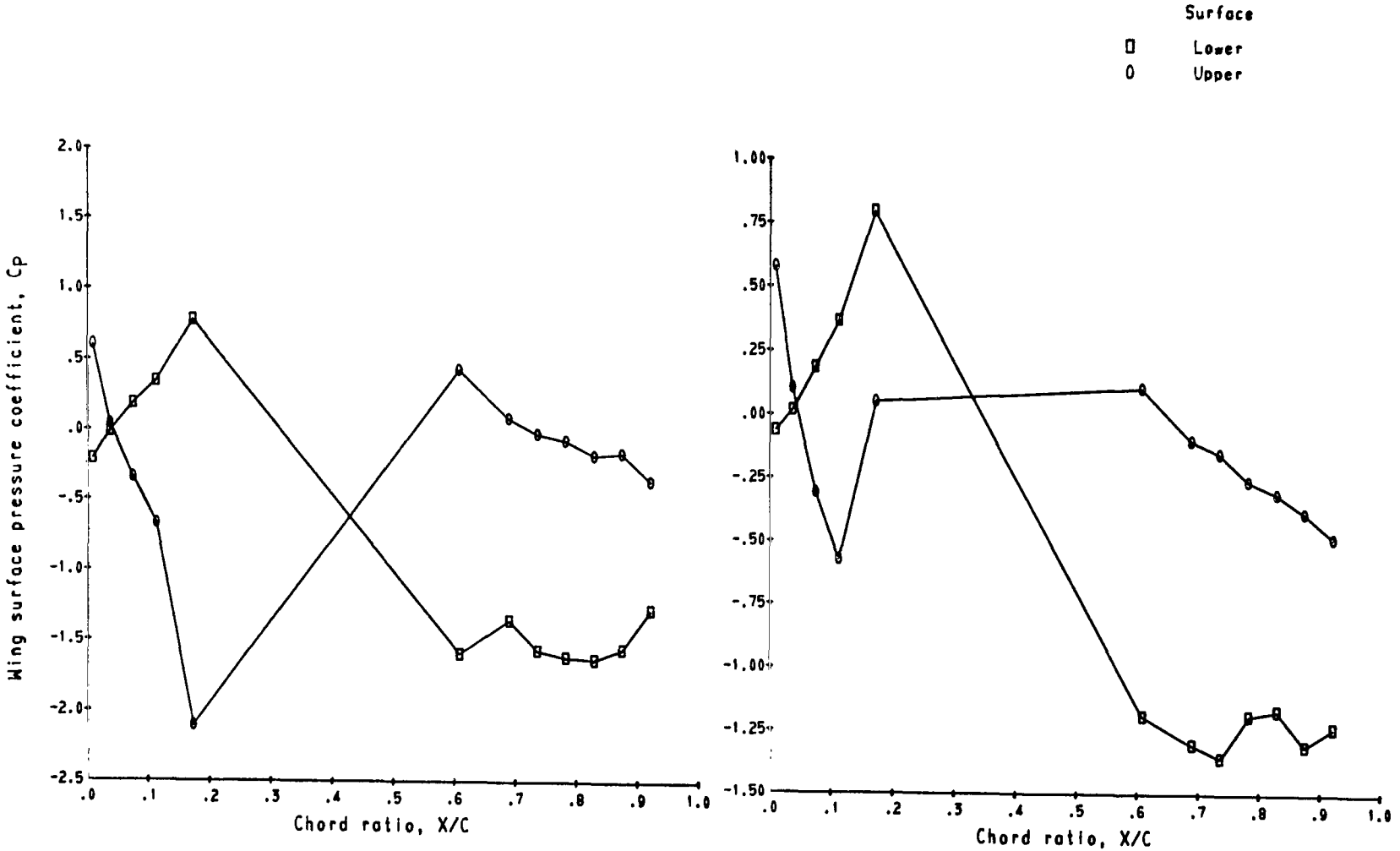

(e) Speed ratio, 0.209.

(f) Speed ratio, 0.304.

Figure 58. - Concluded.

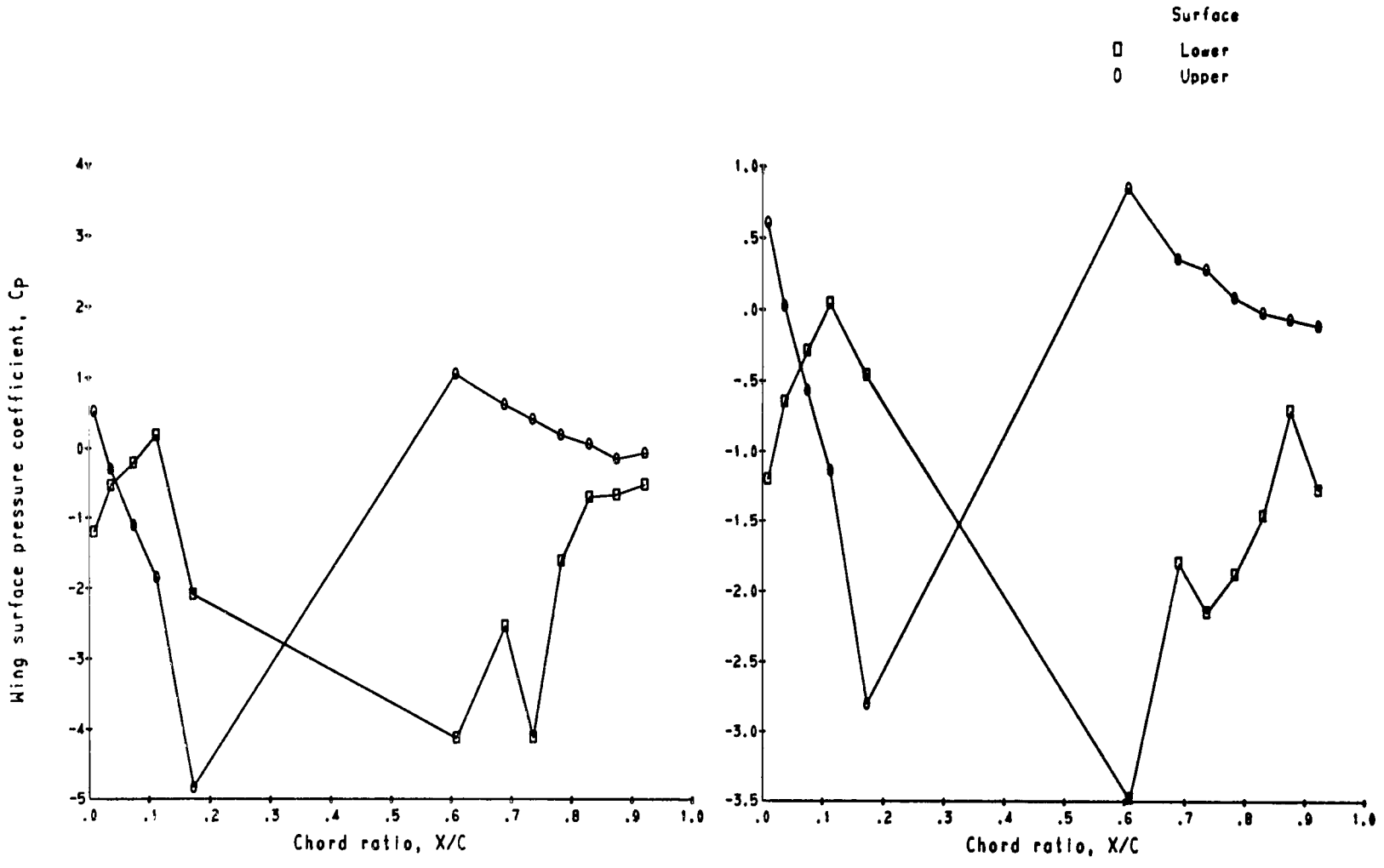

(a) Speed ratio, 0.0845.

(b) Speed ratio, 0.125.

Figure 59. - Wing surface pressure coefficient distribution variations with speed ratio. Louvers on; louver angle, 30^0; angle of attack, -10^0.

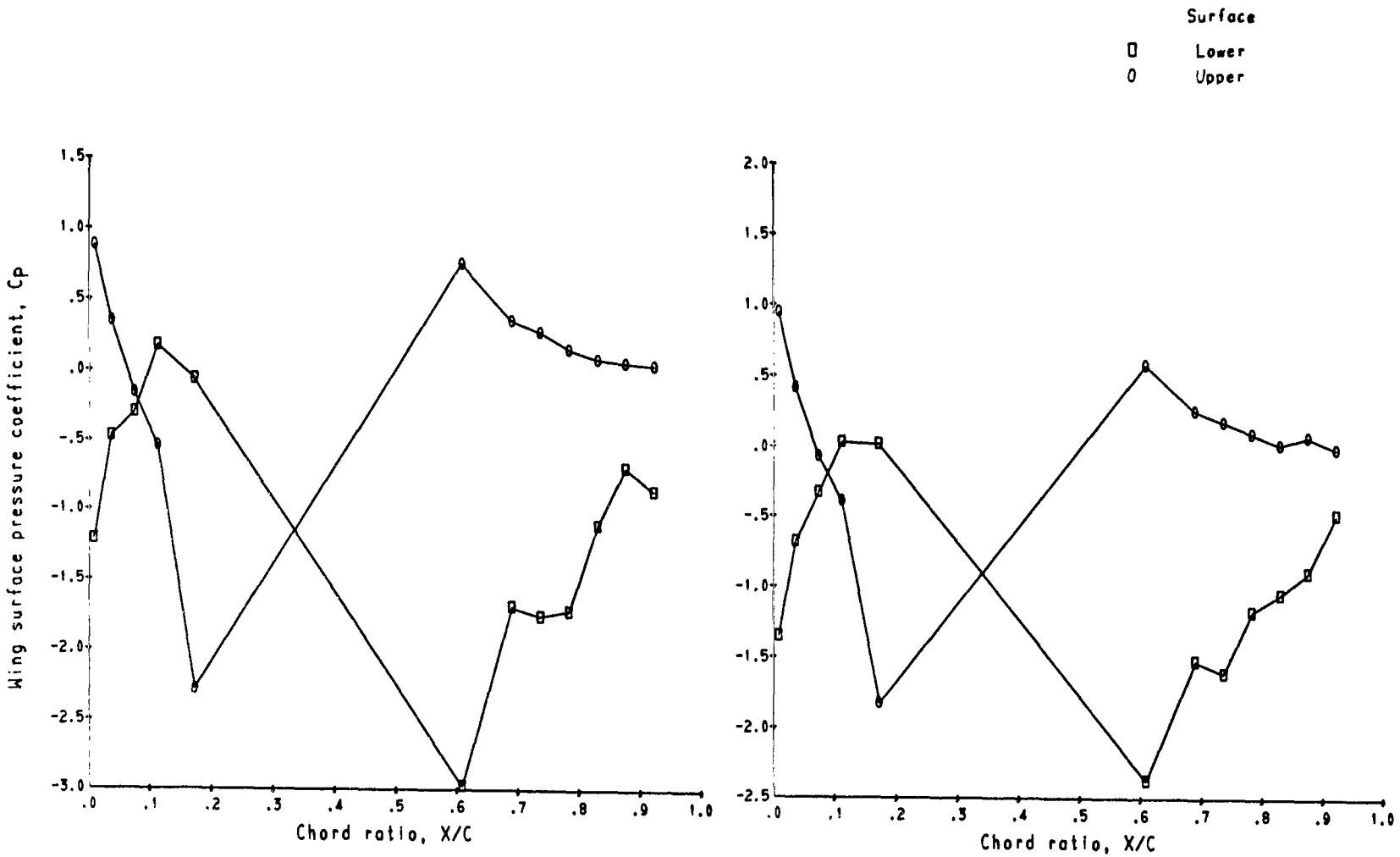

(c) Speed ratio, 0.165.

(d) Speed ratio, 0.202.

Figure 59. - Continued.

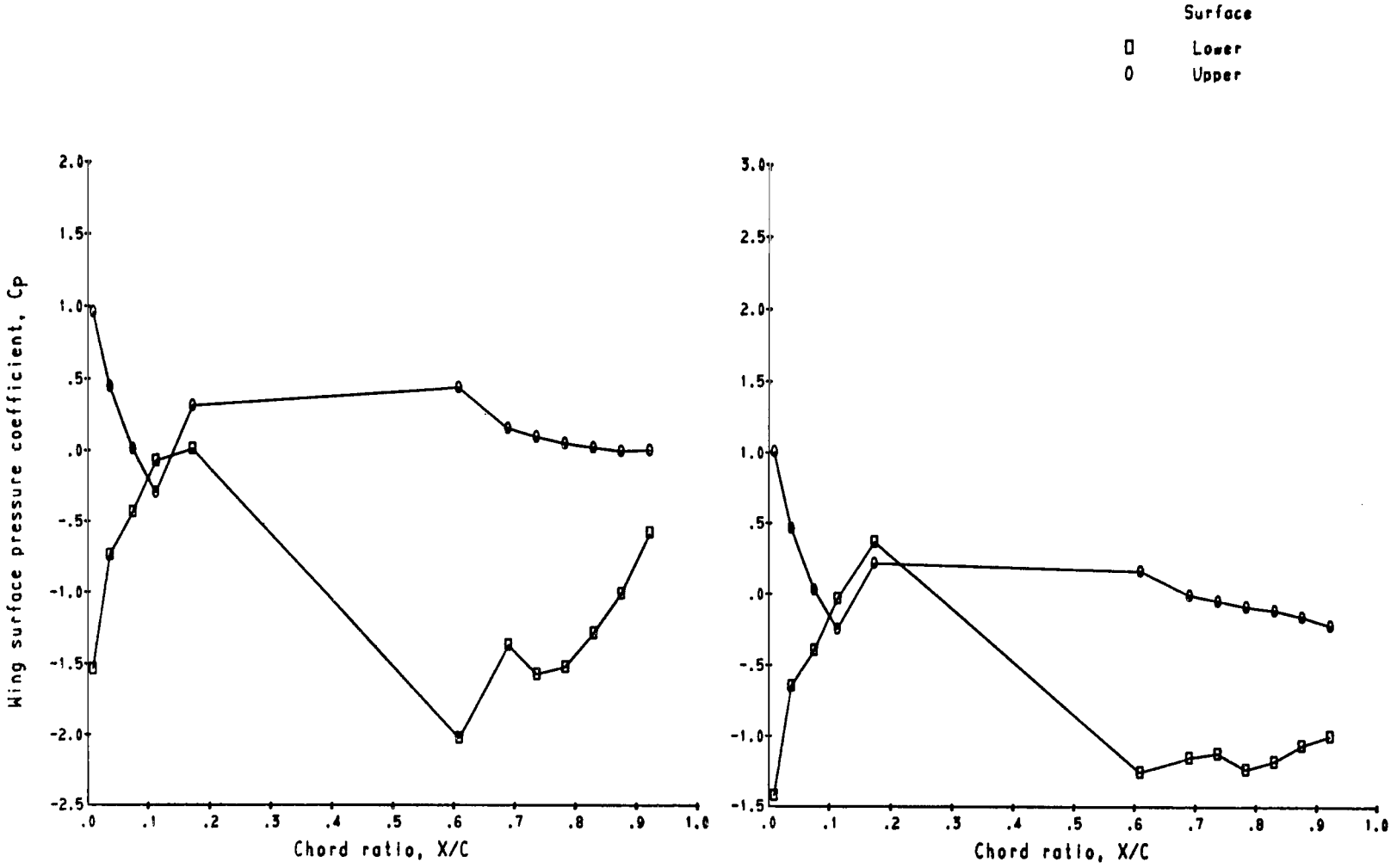

(e) Speed ratio, 0.234.

(f) Speed ratio, 0.336.

Figure 59. - Concluded.

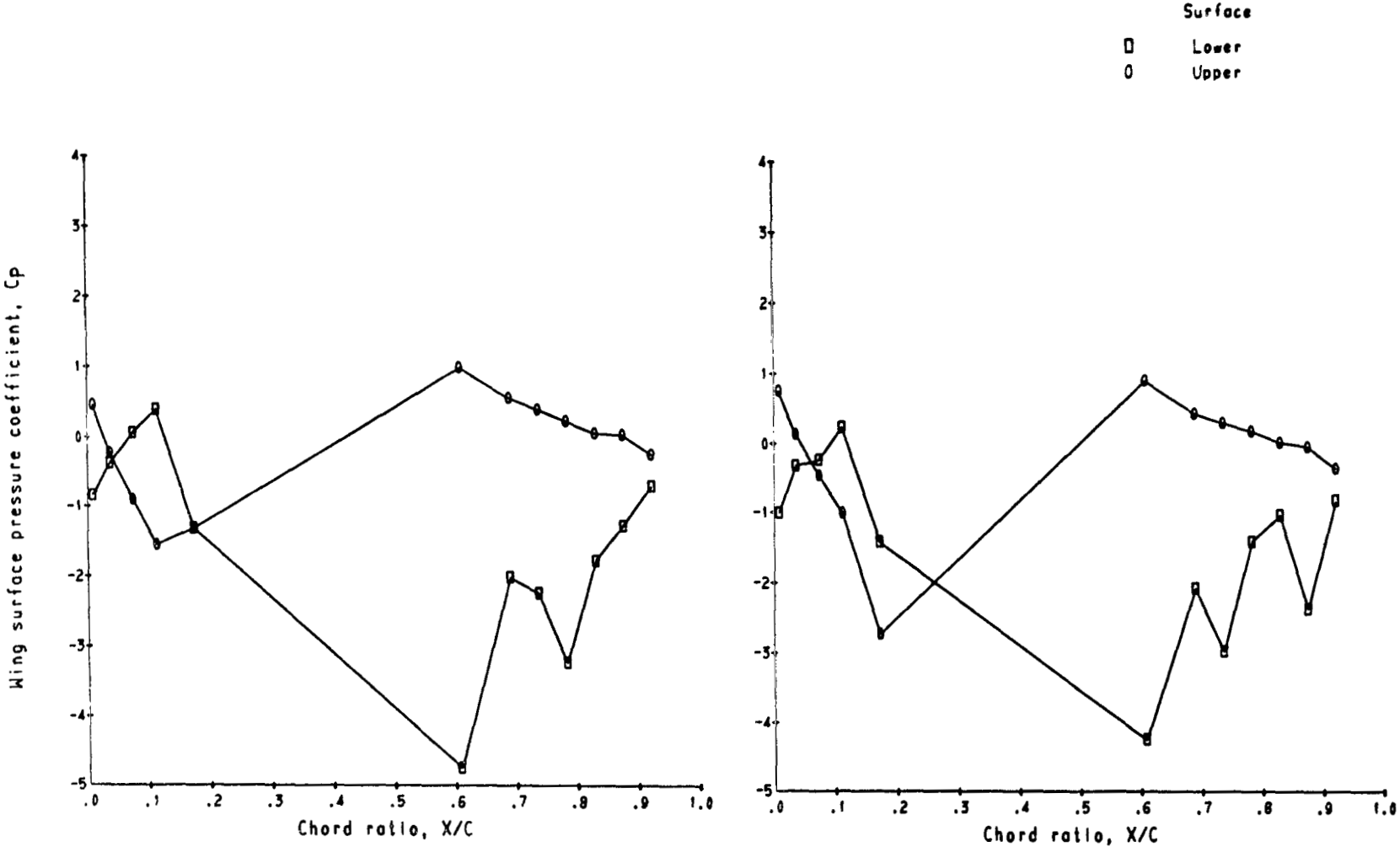

(a) Speed ratio, 0.092.

(b) Speed ratio, 0.122.

Figure 60. - Wing surface pressure coefficient distribution variations with speed ratio. Louvers on; louver angle, 40^{0}; angle of attack, -10^{0}.

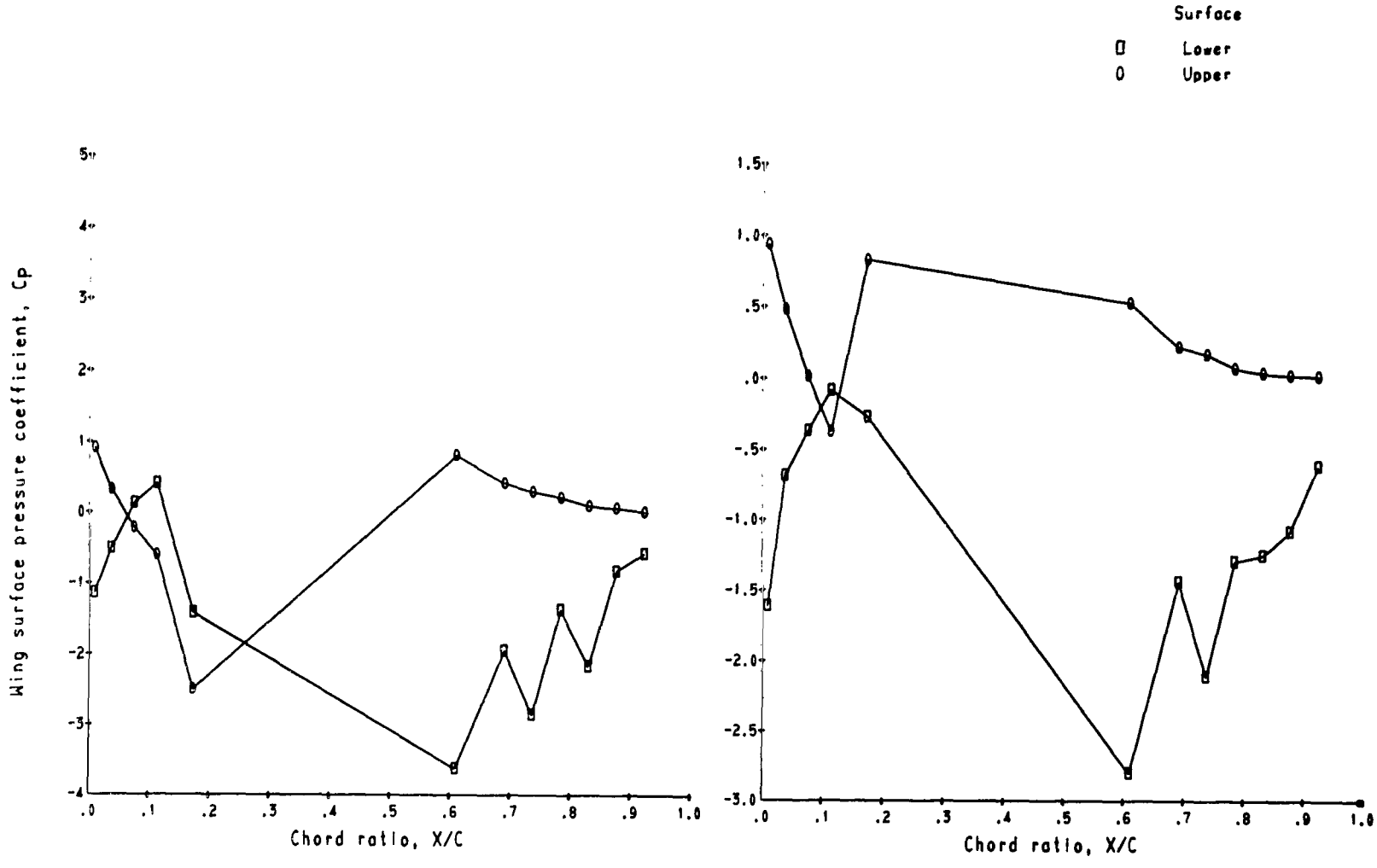

(c) Speed ratio, 0.148.

(d) Speed ratio, 0.202.

Figure 60. - Continued.

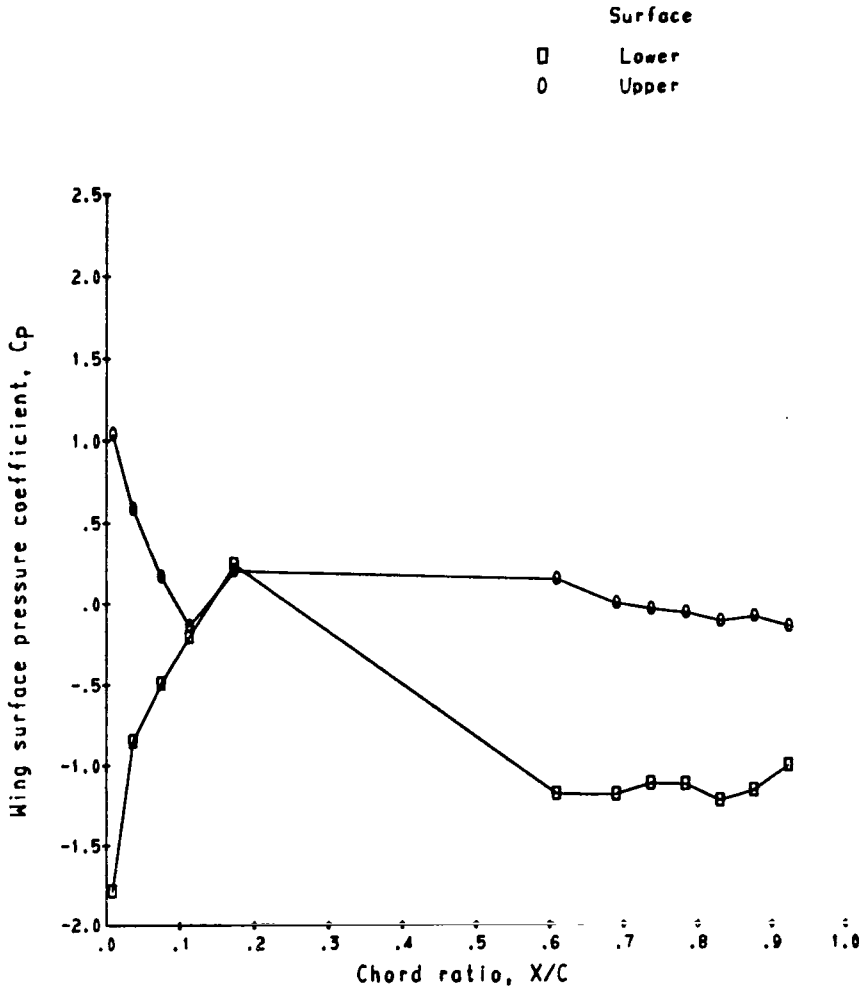

(e) Speed ratio, 0.334.

Figure 60. - Concluded.

NASA-Langley, 1972 —— 28 E-6607

011 001 C1 U 28 720204 S00903DS
DEPT OF THE AIR FORCE
AF WEAPONS LAB (AFSC)
TECH LIBRARY/WLOL/
ATTN: E LOU BOWMAN, CHIEF
KIRTLAND AFB NM 87117

"The aeronautical and space activities of the United States shall be conducted so as to contribute . . . to the expansion of human knowledge of phenomena in the atmosphere and space. The Administration shall provide for the widest practicable and appropriate dissemination of information concerning its activities and the results thereof."

— NATIONAL AERONAUTICS AND SPACE ACT OF 1958

NASA SCIENTIFIC AND TECHNICAL PUBLICATIONS

TECHNICAL REPORTS: Scientific and technical information considered important, complete, and a lasting contribution to existing knowledge.

TECHNICAL NOTES: Information less broad in scope but nevertheless of importance as a contribution to existing knowledge.

TECHNICAL MEMORANDUMS: Information receiving limited distribution because of preliminary data, security classification, or other reasons.

CONTRACTOR REPORTS: Scientific and technical information generated under a NASA contract or grant and considered an important contribution to existing knowledge.

TECHNICAL TRANSLATIONS: Information published in a foreign language considered to merit NASA distribution in English.

SPECIAL PUBLICATIONS: Information derived from or of value to NASA activities. Publications include conference proceedings, monographs, data compilations, handbooks, sourcebooks, and special bibliographies.

TECHNOLOGY UTILIZATION PUBLICATIONS: Information on technology used by NASA that may be of particular interest in commercial and other non-aerospace applications. Publications include Tech Briefs, Technology Utilization Reports and Technology Surveys.

Details on the availability of these publications may be obtained from:

SCIENTIFIC AND TECHNICAL INFORMATION OFFICE

NATIONAL AERONAUTICS AND SPACE ADMINISTRATION

Washington, D.C. 20546